

STABILITY OF STEEL DOME STRUCTURES

by

Cihan Çiftçi

B.S., Civil Engineering, Boğaziçi University, 2007

Submitted to the Institute for Graduate Studies in
Science and Engineering in partial fulfillment of
the requirements for the degree of
Master of Science

Graduate Program in Civil Engineering
Boğaziçi University
June, 2009

STABILITY OF STEEL DOME STRUCTURES

APPROVED BY:

Prof. Gülay Altay, *Ph.D.*

(Thesis Supervisor)

Prof. Semih Tezcan, *Ph.D.*

(Thesis Co-Supervisor)

Prof. Gökhan Baykal, *Ph.D.*Assist. Prof. Hilmi Luş, *Ph.D.*Prof. Zekeriya Polat, *Ph.D.*

DATE OF APPROVAL : 26 / 06 / 2009

ACKNOWLEDGEMENTS

I would like to express my appreciation and gratitude to Prof. Dr. Gülay ALTAY and Prof. Dr. Semih TEZCAN as Co-Supervisors of this Thesis for their guidance, encouragement, continuous support throughout the preparation of this Thesis. I would also like to thank Prof. Zekeriya POLAT, Prof. Gökhan BAYKAL, and Assist. Prof. Hilmi LUŞ for their assistance in developing this Thesis.

I want also to express my extreme pleasure to Prof. Dr. Semih TEZCAN and Dr. Hafez KEYPOUR for their guidance and support in using the computer package program, LUSAS.

Of course, abundantly thanks to my beloved elder-sister Dilek ÇİFTÇİ, to my elder-brothers Kenan ÇİFTÇİ, and Mustafa ÇİFTÇİ and also to my parents for their continuous support and endless love.

ABSTRACT

Basically, the geometric nonlinearity of space structures has been discussed in this Thesis. There are totally three types of nonlinearities, which are a) the geometric nonlinearity which arises from the large nodal deflections and finite changes in the geometry of deformed structure, b) the material nonlinearity, and c) the combination of both the geometric and material nonlinearities.

Linear and nonlinear parts of the tangent stiffness matrices are derived for bar elements in 2-Dimension, and also for truss bar elements in space structures in order to see the effect of the nonlinearity on materials. Furthermore a number of numerical computational techniques have been described, including a) Regular, b) Halved, and c) Mid – Point Incremental Load Procedures, as well as the Newton – Raphson iteration schemes, with modifications of the stiffness matrices at each loading step.

Moreover, in order to investigate the effects of geometric nonlinearity on space structures, a typical steel dome structure is selected, which is analyzed by utilizing the LUSAS package program. Firstly, some pilot test examples are investigated by using the LUSAS program and the solutions are compared with the exact solutions. Secondly, a complete steel lattice dome, with a diameter of 72 meter, has been fully analyzed using the nonlinear Newton – Raphson iteration scheme and the steel structural elements have been designed in accordance with TS 648-Turkish Standard.

ÖZET

Bu tezde temel olarak uzay sistemlerdeki geometrik doğrusalsızlık ele alınmıştır. Genelde üç çeşit doğrusalsızlık bulunmaktadır. Bunlar; a) büyük deformasyonlardan ve de şekli bozulmuş yapıların geometrisindeki sınırlı değişimlerden doğan geometrik doğrusalsızlıklar, b) maddesel doğrusalsızlıklar ve c) geometrik ve maddesel doğrusalsızlıkların birleşimi.

Madde üzerindeki doğrusalsızlık etkisini görmek için teğetsel rijitlik matrislerinin doğrusal ve doğrusal olmayan kısımları, iki boyuttaki ve uzay kafes sistemlerdeki çubuk elemanları için üretilmiştir. Çeşitli nümerik hesap yöntemleri arasında a) Normal, b) Yarı yüklemeli ve c) Orta noktada yüklemeli olmak üzere tüm parça parça yükleme metotları ile, eleman rijitlik matrisi her adımda değiştirilen Newton – Raphson iterasyon metotları ayrı ayrı ele alınmıştır.

Ayrıca uzay sistemler üzerindeki geometrik doğrusalsızlık etkisini incelemek için, tipik bir çelik kubbe yapı seçilmiştir. Bu kubbesel yapı için paket program olarak LUSAS kullanılmıştır. Öncelikle LUSAS kullanılarak bazı test örnekler çözülmüştür ve bu örneklerin çözümleri tam ve gerçek sonuçlar ile karşılaştırılmıştır. Ayrıca 72 metrelik bir çapa sahip olan dantel şeklindeki çelik kubbenin analizinde Newton – Raphson iterasyon yöntemi uygulanmıştır. Çelik yapı elemanları da TS 648-Türk Standartlarına uygun dizayn edilmiştir.

TABLE OF CONTENTS

ACKNOWLEDGEMENTS	iii
ABSTRACT.....	iv
ÖZET.....	v
LIST OF FIGURES.....	x
LIST OF TABLES	xii
LIST OF SYMBOLS.....	xiii
1. INTRODUCTION.....	1
1.1. General Remarks	1
1.2. Nonlinearity.....	3
1.3. Buckling	7
2. THEORY OF NONLINEAR STRUCTURAL ANALYSIS	10
2.1. Method of Nonlinear Analysis	10
2.2. Geometric Nonlinearity.....	12
2.2.1. Incremental Procedure.....	12
2.2.2. Iterative Procedure	13
2.3. Nonlinear Field Problems.....	14
2.4. The Buckling of Lattice Domes under the Simultaneous Concentrated Loads.	15
2.5. Buckling Consideration in the Design and Construction of Space Structures ..	15
2.6. Rapid Progress in Computers	17
3. TANGENT STIFFNESS MATRICES FOR THE BAR ELEMENTS	18
3.1. Tangent Stiffness Matrix of a Truss Bar	19
3.2. Other Form of the Tangent Stiffness Matrix	25
3.3. Tangent Stiffness for a Space Truss System	26
3.4. Tangent Stiffness Matrix for a Space Member.....	31
3.4.1. Linear Part of the Tangent Stiffness Matrix	32

3.4.2. Nonlinear Part of the Tangent Stiffness Matrix	33
4. COMPUTATIONAL TECHNIQUES	34
4.1. About the Computational Techniques	34
4.2. What is Nonlinear Analysis for LUSAS?	34
4.2.1. Geometrically Nonlinear Analysis	37
4.2.2. Nonlinear Mixed Conditions.....	39
4.2.3. Materially Nonlinear Analysis	39
4.3. Incremental Procedures	39
4.3.1. Regular (Basic) Incremental Procedure.....	39
4.3.2. Halved Incremental Procedure.....	41
4.3.3. Midpoint Runge-Kutta Procedure	41
4.4. Iterative Procedures	42
4.4.1. The Newton – Raphson Method	42
4.4.2. The Modified Newton – Raphson Method	44
4.4.3. Mixed Procedure	45
4.5. LUSAS as a Package Program	46
4.5.1. About LUSAS	46
4.5.2. Nonlinear Solution Procedure of LUSAS.....	46
4.5.3. Iterative Procedure	47
4.5.4. Standard Newton – Raphson Method:.....	47
4.5.5. Iterative Acceleration (<i>Line Searches</i>)	48
4.5.6. Separate Iterative Loops	48
4.5.7. Incremental Procedure.....	49
4.5.8. Constrained solution methods (arc-length).....	49
4.5.9. Automatic increment reduction.....	50
5. EXAMPLES OF DOME STRUCTURES	51
5.1. Types of Domes	51

5.2. Significant and Famous Dome Structures in the World	52
6. TEST EXAMPLES	58
6.1. About the Test Examples	58
6.2. The First Illustrative Numerical Example	58
6.3. The Second Illustrative Numerical Example.....	60
6.4. The Third Illustrative Numerical Example	62
6.5. The Fourth Illustrative Example	63
7. NONLINEARITY OF A DOME AS A SPACE STRUCTURE	66
7.1. About the Dome.....	66
7.2. Plan View of the Lattice - Dome	67
7.3. Modeling the Dome with LUSAS	68
7.4. Loading and Constraints	77
7.4.1. Application of TDY-2007 for the Structure	78
7.4.2. Application of TS-498 for the Structure (<i>For Wind Loads</i>).....	82
7.4.3. Application of TS-498 for the Structure (<i>For Snow Loads</i>).....	88
7.4.4. A Single Point Load at the Top Point of the Dome	93
7.5. Nonlinear Solutions for Each Load Case	94
7.5.1. Nonlinear Behavior of a Critical Point for a Single Point Load	94
7.5.2. Nonlinear Behavior for the Dead and Snow Loads.....	94
7.5.3. Nonlinear Behavior for the Dead and Earthquake Loads.....	95
7.5.4. Nonlinear Behavior for the Dead and Wind Loads.....	95
7.6. Local Buckling Control.....	96
7.6.1. Axial Forces of the Members for a Single Point Load at the Top Point	96
7.6.2. Axial Forces of the Members for the Dead and Snow Loads.....	97
7.6.3. Axial Forces of the Members for the Dead and Earthquake Loads	99
7.6.4. Axial Forces of the Members for the Dead and Wind Loads	100
7.7. Surface Cover of the Dome	103

8. CONCLUSIONS AND RECOMMENDATIONS..... 104

9. REFERENCES..... 106

LIST OF FIGURES

Figure 2.1. Incremental loading procedure.....	11
Figure 2.2. Newton – Raphson procedure	11
Figure 2.3. Modified Newton – Raphson procedure.....	11
Figure 2.4. Speed and cost evaluation of computers.....	17
Figure 3.1. A bar element and its axial force, Q	19
Figure 3.2. A space truss system and its axial force, Q	20
Figure 3.3. Angles for the direction of cosine	20
Figure 3.4. A space member with MDOFs.....	20
Figure 4.1. Illustrations of geometrically nonlinear behavior	37
Figure 4.2. Basic incremental procedure	41
Figure 4.3. Halved and Runge – Kutta increments	42
Figure 4.4. Newton – Raphson method	44
Figure 4.5. Modified Newton – Raphson method.....	45
Figure 4.6. Mixed procedure.....	45
Figure 4.7. Nonlinear solution procedure of LUSAS	46
Figure 4.8. Arc – length method	50
Figure 5.1. Shapes of dome types	52
Figure 5.2. An aspect from the Louisiana Superdome	54
Figure 6.1. Two member arch system and the point load.....	58
Figure 6.2. Solution of two member arch system from LUSAS	59
Figure 6.3. Circular arch and the point load	60
Figure 6.4. Solution of circular arch system from LUSAS	60
Figure 6.5. Circular arch and the deformations of the joints	61
Figure 6.6. Parabolic dome and the point load	62
Figure 6.7. Solution of the parabolic dome system from LUSAS	62
Figure 6.8. Arch system with no hinges	64
Figure 6.9. Solution of the parabolic arch system from LUSAS	65
Figure 7.1. An example for lattice dome structures, Panora Alış-Veriş Merkezi.....	66
Figure 7.2. Plan view of the lattice-dome.....	67
Figure 7.3. Rings and the nodes of the dome structure	68

Figure 7.4. Dead and earthquake loads on the points of the dome	82
Figure 7.5. Represented areas for all points of the dome	84
Figure 7.6. Dead and snow loads on the points of the dome	89
Figure 7.7. Single point load at the top point of the dome	93
Figure 7.7. Force vs displacement curve under the single point load at the top point	94
Figure 7.9. Force vs displacement curve under the dead and earthquake load.....	95
Figure 7.10. Force vs displacement curve under the dead load and wind load	95
Figure 7.12. Axial force diagrams of the members under the single point load.....	97
Figure 7.13. Axial force diagrams of the members under the dead and the snow loads..	98
Figure 7.14. Axial force diagrams under the dead and the earthquake loads.....	100
Figure 7.15. Axial force diagrams of the members under the dead and the wind loads ..	101

LIST OF TABLES

Table 1.1. Problem types in finite element method.....	2
Table 1.2. Comparison of geometric and material nonlinearity	5
Table 1.3. Comparison of geometric and material nonlinearity	6
Table 4.1. Nonlinear solution techniques	35
Table 4.2. Comparison of solution techniques.....	36
Table 5.1. General types of dome structures	51
Table 5.2. Largest domes with ranking to the time.....	53
Table 5.3. Dome structures by their materials	54
Table 6.1. Comparison of two different solutions.....	61
Table 6.2. Comparison of two different solutions.....	63
Table 6.3. Values of the factor for the arch system.....	64
Table 7.1. Calculation of nodal coordinates	69
Table 7.2. Coordinates of all points of the dome	70
Table 7.3. Effective ground acceleration coefficient	78
Table 7.4. Spectrum characteristic periods.....	78
Table 7.5. Building importance factor.....	79
Table 7.6. The length and name of the elements	83
Table 7.7. The speed and absorption values for wind loads	83
Table 7.8. Wind loads for all points of the dome.....	87
Table 7.9. Snow pressures with respect to the altitudes and regions	88
Table 7.10. Snow loads for all points of the dome.....	89
Table 7.11. Formulas to calculate the steel weights.....	90
Table 7.12. Total mass and weight for the points due to the materials	92
Table 7.13. Total weights for the rings due to the materials	93
Table 7.14. Section of the members and critical loads under the single point load.....	96
Table 7.15. Section of the members and critical loads under the dead and snow loads ..	97
Table 7.16. Critical loads under the dead and earthquake loads.....	99
Table 7.17. Section of the members and critical loads under the dead and wind loads ..	100
Table 7.18. Sections and properties of the members.....	102

LIST OF SYMBOLS

A	Cross sectional area
A_0	Effective ground acceleration coefficient
$\{d\}$	Nodal displacement vector
d_{CR}	Critical displacement for buckling
$\{D\}_i$	Total displacement of i^{th} cycle
E	Modulus of elasticity
I	Building importance factor
J	Torsion Constant
$[K]$	Tangent stiffness matrix
k_i	Tangent stiffness of i^{th} cycle
k_{ij}	Individual term inside the stiffness matrix
l, m, n	Direction cosines
L	Final length for a cycle
L_0	Initial length
P_{CR}	Critical load for buckling
P_{ext}	External load
P_{int}	Internal load
P_{unb}	Unbalanced load
P_0	Correction load
q	Absorption (Pressure) for TS-498
Q	Compressive force

T_A, T_B	Spectrum characteristic periods
T_n	Natural period for the first mode
u, v, w	Generic displacements at an arbitrary point
ε	Normal strain
ε_e	Effective strain
$\{\varepsilon\}^e$	Elastic strain
$\{\delta\}$	Nodal displacement vector in incremental analysis
δ_0	Correction displacement
σ	Normal stress
DL	Dead Load
LL	Live Load
EL	Earthquake Load
WL	Wind Load

1. INTRODUCTION

1.1. General Remarks

For the last three centuries, linear problems have been a primary concern for structural and soil mechanics because when someone describes nonlinear phenomena, nonlinear equations come with this. These equations render classical methods of mathematical analysis inapplicable. Exact solutions for linear equations have been discovered for over a century. However, any method has not been explored for finding exact solutions to general systems of nonlinear equations yet. The number of available exact solutions for nonlinear differential equations is a mystery.

A nonlinear barrier has been created by the complexities of nonlinear analysis. Recently, this barrier could have been understood by effective use of high speed computers. In spite of the fact that finite element methods can be used for design in structural and soil mechanics, severe tests must be used to prove the accuracy of the proposed computational technique.

It has been understood that nonlinear finite element analysis can be successfully performed and there are several reasons that indicated this. These are the availability of very efficient nonlinear solution algorithms, the experience gained with their application to engineering problems, and the development of improved and high order element characteristics. Nowadays, the barriers to the general solution of nonlinear problems by finite elements have been removed considerably, and this process is successfully applied to nonlinear problems in structural and soil mechanics. It is a well known fact that the finite element methods are the most powerful general tools for the numerical solutions of a various problems encountered in engineering. The stress and deformation analysis of solids and soils, the solution of acoustical and neutron physics, fluid dynamics, biomedical engineering, medical treatment and analyses of various parts and cells of human body are examples of application of this method. For each field of application, the problem may be formulated in any one of the following types:

- Equilibrium problem
- Eigenvalue problem
- Propagation problem

Descriptions of problems in each field of application as shown at one of the categories above are given in Table 1.1. The information in this table is basically extracted from (Desai, *et al.*, 1972).

Table 1.1. Problem types in finite element method

PROPAGATION PROBLEMS	EIGENVALUE PROBLEMS	EQUILIBRIUM PROBLEMS
1. STRUCTURES		
<ul style="list-style-type: none"> • Analysis of bar structures, plates, shells and solids • Torsion of prismatic bars 	<ul style="list-style-type: none"> • Stability of structures • Free vibration of structures, natural mode shapes and frequencies 	<ul style="list-style-type: none"> • Wave propagation • Response of structures to random vibrations (winds, earthquake)
2. SOIL MECHANICS		
<ul style="list-style-type: none"> • Stress analysis • Fill and excavations 	<ul style="list-style-type: none"> • Stability of soil structure • Free vibration of soil media 	<ul style="list-style-type: none"> • Transient seepage • Flow-consolidation
3. HEAT CONDUCTION		
<ul style="list-style-type: none"> • Steady state temperature distribution in solids and fluids 	-----	<ul style="list-style-type: none"> • Transient heat flow in solids and fluids
4. HYDRAULICS		
<ul style="list-style-type: none"> • Potential flow of fluids • Viscous flow of fluids • Steady-State seepage 	<ul style="list-style-type: none"> • Seiche of lakes and harbours, natural periods and modes of oscillation 	<ul style="list-style-type: none"> • Sediment transport • Unsteady fluid flow • Transient seepage

1.2. Nonlinearity

Nonlinearity arises in engineering problems from two main sources. Deformations of the material may be large, when compared with the dimensions of the structure at hand and therefore the equilibrium conditions should be expressed on the deformed geometry. Tension structures, cable bridges, arches, soil structures, retaining systems, settlement problems are this entire category. Problems of this type are called Geometrically Nonlinearity problems, in which only the force deformation characteristics of the medium are nonlinear, while the stress strain relationship of the material remains purely elastic.

There is a second category however, in which the nonlinear relationship is primarily due to the elasto-plastic material behavior or due to the hyperelastic efforts of some form. Nonlinear response may be associated also with temporal effects, such as viscoplastic behavior or dynamic transient phenomena. Nonlinearities arising from the stress strain characteristics of material or from the time and rate dependence loading are called Material Nonlinearity. Creep of metals and plastics as well as consolidation problems in soil mechanics fall into this category.

It is quite likelihood that both of these two different nonlinearities may occur within the context of one problem, it would be therefore, appropriate to classify nonlinear problems into three categories as follows:

- Geometric nonlinearity: It arises from nonlinear behavior in the kinematical equations, in other words, from finite changes in the geometry of the deforming body.
- Material nonlinearity: It arises from the nonlinearities in the constitutive equations of the material, or from nonlinearities in the time dependence of the strains.
- Combined geometric and material nonlinearity

Computationally these categories are somewhat superficial since, the mathematical techniques and solution algorithms are almost the same in all categories.

In the first category the stress strain equations are assumed to be linear but nonlinearity may arise both from nonlinear strain displacement relations, such as the case in very thin plates, and from finite changes in geometry such as the case in stability of arches and domes. In other words, the geometric nonlinearity encompasses either large strains or large displacements. And thus the Eulerian Equations are appropriate to use for this geometric nonlinearity problems.

An important subclass of geometrically nonlinear problems is the case of small or infinitesimal strains but large and finite displacements. An example of this subclass is the elastic postbuckling behavior of structures.

The second category, material or physical nonlinearity alone, is easy to define. Although the displacements and strains are small the stresses are not linearly proportional to strains. The changes in geometry are considered to be infinitesimal and the linear strain displacement relations are used in finite element property derivations.

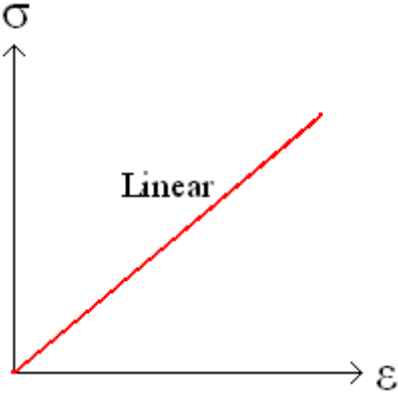
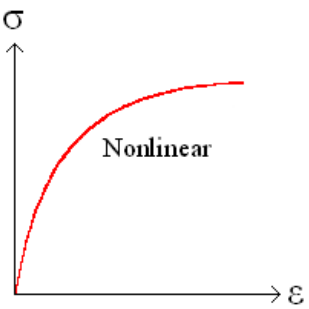
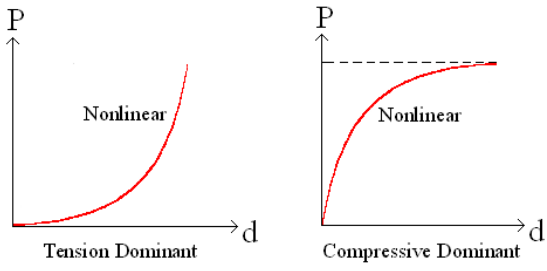
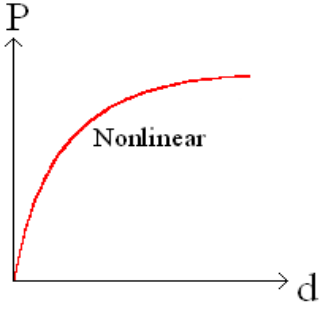
The third and the most general and famous category of nonlinear problems is the combined geometric and material nonlinearity, not only the constitutive behavior is nonlinear, but also the strains are large. Soft soil layers, rubberlike materials fall into this category.

The basic differences existing in the geometric and material nonlinearities are also summarized in Table 1.2 and Table 1.3.

Table 1.2. Comparison of geometric and material nonlinearity

Parameter	Geometric Nonlinearity	Material Nonlinearity
General Field of Study	Structural Mechanics	Soil and Rock Mechanics
Displacements	Finite	Infinitesimal
Equilibrium	Eulerian <i>(Deformed state coordinates are used)</i>	Lagrangian <i>(Undeformed state coordinates are used)</i>
Changes in Geometry	Considered	Neglected
Strains Displacements Relations	Tensor Notation: $\varepsilon_{jk} = \frac{1}{2}(u_{k,j} + u_{j,k} + u_{i,j} + u_{i,k})$	Tensor Notation: $\varepsilon_{jk} = \frac{1}{2}(u_{k,j} + u_{j,k})$
	Engineering Notation: $\varepsilon_x = \frac{\partial u}{\partial x} + \frac{1}{2} \left[\left(\frac{\partial u}{\partial x} \right)^2 + \left(\frac{\partial v}{\partial x} \right)^2 + \left(\frac{\partial w}{\partial x} \right)^2 \right]$ $\varepsilon_{xy} = \frac{1}{2} \left[\left(\frac{\partial u}{\partial y} + \frac{\partial v}{\partial x} \right) + \left(\frac{\partial u}{\partial x} \frac{\partial u}{\partial y} + \frac{\partial v}{\partial x} \frac{\partial v}{\partial y} + \frac{\partial w}{\partial x} \frac{\partial w}{\partial y} \right) \right]$	Engineering Notation: $\varepsilon_x = \frac{\partial u}{\partial x}$ $\varepsilon_{xy} = \frac{1}{2} \left(\frac{\partial u}{\partial y} + \frac{\partial v}{\partial x} \right)$

Table 1.3. Comparison of geometric and material nonlinearity

Parameter	Geometric Nonlinearity	Material Nonlinearity
Yield Criteria	Not needed	Essential
Flow Rule	Not needed	Essential
Constitutive Law		
Force Deflection Relation		
Examples	<ul style="list-style-type: none"> Thin plate bending $\left(\text{Deflections} > \frac{1}{2} \text{thickness} \right)$ Stability of arches, domes, etc. Suspension bridges, hanging roofs 	<ul style="list-style-type: none"> All metals strained beyond elastic limit Elasto-plastic behavior in structural and soil mechanics Any material with nonlinear constitutive law

1.3. Buckling

In engineering, buckling is a failure mode characterized by a sudden failure of a structural member subjected to high compressive stresses, where the actual compressive stress at the point of failure is less than the ultimate compressive stresses that the material is capable of withstanding. This mode of failure is also described as failure due to elastic instability. Mathematical analysis of buckling makes use of an axial load eccentricity that introduces a moment, which does not form part of the primary forces to which the member is subjected.

The ratio of the effective length of a column to the least radius of gyration of its cross section is called the *slenderness ratio* (sometimes expressed with the Greek letter lambda, λ). This ratio affords a means of classifying columns. All the following are approximate values used for convenience.

- A short steel column is one whose slenderness ratio does not exceed 50; an intermediate length steel column has a slenderness ratio ranging from about 50 to 200, while a long steel column may be assumed to have a slenderness ratio greater than 200.
- A short concrete column is one having a ratio of unsupported length to least dimension of the cross section not greater than 10. If the ratio is greater than 10, it is a long column (sometimes referred to as a slender column).
- Timber columns may be classified as short columns if the ratio of the length to least dimension of the cross section is equal to or less than 10. The dividing line between intermediate and long timber columns cannot be readily evaluated. One way of defining the lower limit of long timber columns would be to set it as the smallest value of the ratio of length to least cross sectional area that would just exceed a certain constant K of the material. Since K depends on the modulus of elasticity and the allowable compressive stress parallel to the grain, it can be seen that this arbitrary limit would vary with the species of the timber. The value of K is given in most structural handbooks.

If the load on a column is applied through the center of gravity of its cross section, it is called an axial load. A load at any other point in the cross section is known as an eccentric

load. A short column under the action of an axial load will fail by direct compression before it buckles, but a long column loaded in the same manner will fail by buckling (bending), the buckling effect being so large that the effect of the direct load may be neglected. The intermediate-length column will fail by a combination of direct compressive stress and bending.

In 1757, mathematician Leonhard Euler derived a formula that gives the maximum axial load that a long, slender, ideal column can carry without buckling. An ideal column is one that is perfectly straight, homogeneous, and free from initial stress. The maximum load, sometimes called the critical load, causes the column to be in a state of unstable equilibrium; that is, any increase in the load, or the introduction of the slightest lateral force, will cause the column to fail by buckling. The formula derived by Euler for columns with no consideration for lateral forces is given below. However, if lateral forces are taken into consideration the value of critical load remains approximately same.

$$F = \frac{\pi^2 EI}{(KL)^2} \quad (1.1)$$

K = column effective length factor, whose value depends on the conditions of end support of the column, as follows.

For both ends pinned (hinged, free to rotate), $K = 1.0$.

For both ends fixed, $K = 0.50$.

For one end fixed and the other end pinned, $K = 0.699\dots$

For one end fixed and the other end free to move laterally, $K = 2.0$.

Examination of this formula reveals the following interesting facts with regard to the load-bearing ability of slender columns.

- Elasticity and not compressive strength of the materials of the column determines the critical load.
- The critical load is directly proportional to the second moment of area of the cross section.

- The boundary conditions have a considerable effect on the critical load of slender columns. The boundary conditions determine the mode of bending and the distance between inflection points on the deflected column. The closer together the inflection points are, the higher the resulting capacity of the column.

The strength of a column may therefore be increased by distributing the material so as to increase the moment of inertia. This can be done without increasing the weight of the column by distributing the material as far from the principal axes of the cross section as possible, while keeping the material thick enough to prevent local buckling. This bears out the well-known fact that a tubular section is much more efficient than a solid section for column service.

Another bit of information that may be gleaned from this equation is the effect of length on critical load. For a given size column, doubling the unsupported length quarters the allowable load. The restraint offered by the end connections of a column also affects the critical load. If the connections are perfectly rigid, the critical load will be four times that for a similar column where there is no resistance to rotation (hinged at the ends).

Since the moment of inertia of a surface is its area multiplied by the square of a length called the radius of gyration, the above formula may be rearranged as follows. Using the Euler formula for hinged ends, and substituting $A \cdot r^2$ for I , the following formula results.

$$\sigma = \frac{F}{A} = \frac{\pi^2 E}{(l/r)^2} \quad (1.2)$$

where F/A is the allowable stress of the column, and l/r is the slenderness ratio.

Since structural columns are commonly of intermediate length, and it is impossible to obtain an ideal column, the Euler formula on its own has little practical application for ordinary design. Issues that cause deviation from the pure Euler strut behavior include imperfections in geometry in combination with plasticity/non-linear stress strain behavior of the column's material. Consequently, a number of empirical column formulae have been developed to agree with test data, all of which embody the slenderness ratio. For design, appropriate safety factors are introduced into these formulas.

2. THEORY OF NONLINEAR STRUCTURAL ANALYSIS

2.1. Method of Nonlinear Analysis

To express a brief summary of the numerical solution techniques will be presented. There are elementally three schemes employed on the literature as illustrated in Fig 2.1, Fig. 2.2, and Fig. 2.3 for one dimensional case. They are that:

- Incremental loading procedure
- Newton – Raphson procedure
- Modified Newton – Raphson procedure

In the *Incremental Loading Procedure*, the external loads are applied at a sequence of increments and a merely linear elastic analysis is performed for each increment. At the end of each incremental cycle however, the geometry is modified, the material features are modified, and thus the tangent stiffness is modified normally. A refined approach is to consider the stresses and strains of the previous cycle as the “*initial stresses*” of the subsequent cycle.

In the *Newton – Raphson Procedure*, initially, the full external loads are applied and a linear analysis is performed for each increment. By utilizing the calculated strains, a set of internal nodal forces are developed, which are checked and controlled compared with the external joint loads. The differences between the external and internal nodal forces at each node;

$$P_{unb} = P_{ext} - P_{int} \quad (2.1)$$

are applied as the external joint loads of the second cycle of analysis. In the second cycle of analysis, the tangent stiffness properties correspond to the largest stage of the material properties and state of stress.

If however, the initial constant stiffness matrices are used until the analysis cycles, instead of the tangent stiffness matrices, the name of this method is the *Modified Newton – Raphson Method*, as illustrated in Fig. 2.3.

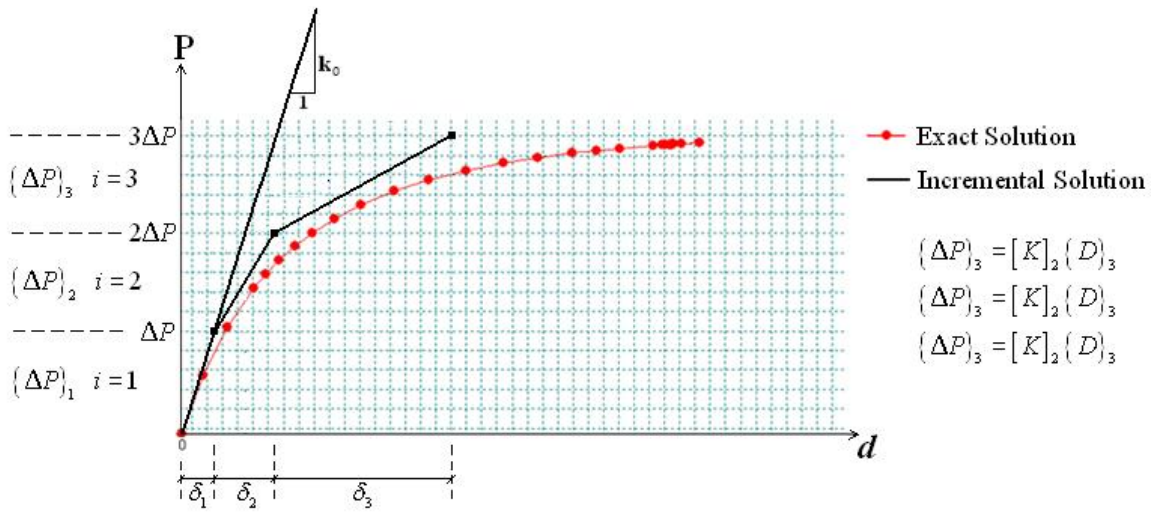


Figure 2.1. Incremental loading procedure

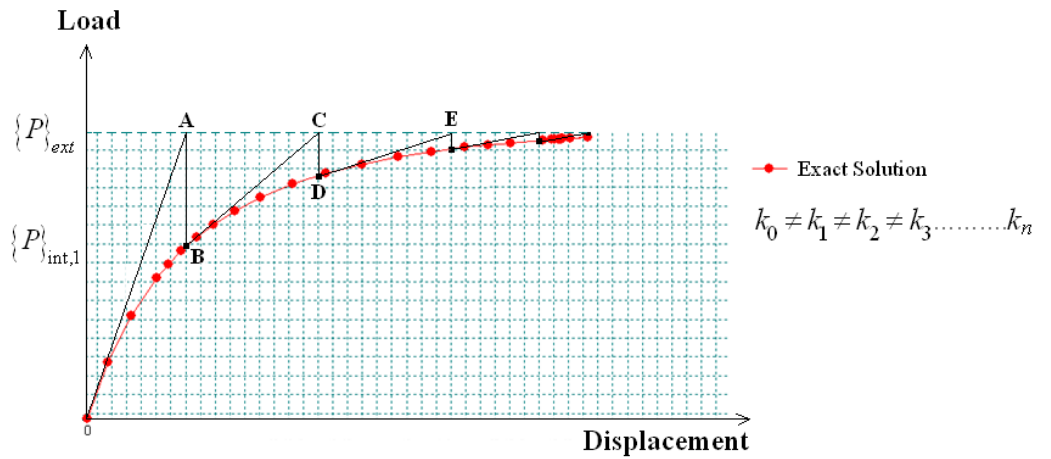


Figure 2.2. Newton – Raphson procedure

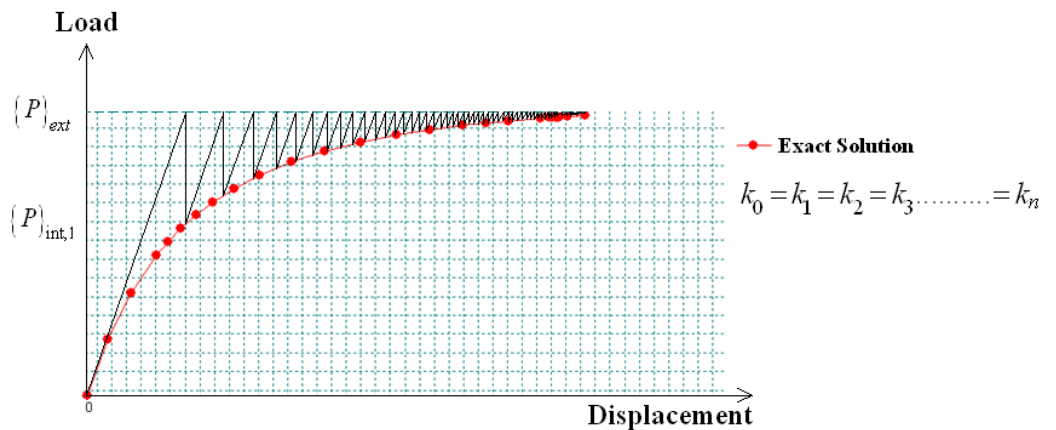


Figure 2.3. Modified Newton – Raphson procedure

2.2. Geometric Nonlinearity

2.2.1. Incremental Procedure

To use the incremental procedure has been very famous and popular since especially 1960s by considering applications of the finite element methods to a class of geometrically nonlinear problems thanks to certain researchers such as (Turner *et al.*, 1960). In this procedure, the nonlinear behavior is determined by solving a sequence of linear problems in which corrective the tangent stiffness matrices are used to update the geometry at the end of each cycle.

(Turner, 1959) and (Argyris, 1959) apparently discussed such incremental procedures as early as 1959, and (Greene, 1960) employed geometric stiffness matrices in an unpublished memorandum dealing with the instability of beam columns. Similar work was reported by (Ortega, 1969). In 1962 an extension of their earlier work was presented by (Turner *et al.*, 1964) and by (Argyris *et al.*, 1964) which were subsequently published in 1964. (Gallagher and Padlog, 1963) discussed a procedure for linearized stability analysis.

Geometric stiffness matrices were also used to calculate large displacements of finite element models by (Argyris-a, 1964), (Argyris-b, 1965), and (Argyris-c, 1966) and moreover in the first Dayton conference on matrix method in structural mechanics in (Przemieniecki *et al.*, 1966), and (Martin, 1966) reviewed the work on geometrically nonlinear problems up to that time, and presented geometric stiffness matrices for a number of structural elements. Martin's paper was published in 1966 along with his summary report on the subject (Martin, 1966). The general formulas for computing geometric stiffness matrices were subsequently presented by (Oden, 1966), and (Przemieniecki, 1967).

Numerous researchers have used incremental procedures and geometric stiffness matrices to study both stability and large displacements of complex structures. These include studies of the stability of thin plates by (Hartz, 1965), (Kapur, 1965), (Kapur and Hartz, 1966), (Felippa, 1966), (Anderson *et al.*, 1968), (Kawai and Ohtsubo, 1969), and (Hicks, 1967); stability of thin shells by (Gallagher, 1966), (Gallagher *et al.*, 1967), (Navaratna *et al.*, 1967), (Navaratna, 1967), and (Bakus and Mello, 1969); large deflection of the plates by (Murray, 1967), (Murray and Wilson, 1969); large deflections of thin shells by (Stricklin *et al.*, 1968), (Stricklin *et al.*, 1969), (Wempner, 1969), (Mallett and Marcal, 1968), (Yaghmai,

1968), and (Yao, 1968). Problems of dynamic stability of plates and beams have been considered by (Hutt, 1968), and (Brown et.al, 1968). Surveys of methods and previous work and finite element applications to geometrically nonlinear problems have recently been contributed by (Martin, 1969), and (Kawai, 1969).

2.2.2. Iterative Procedure

The Newton – Raphson method has been used by a number of investigators to solve nonlinear structural problems. (Walker and Hall, 1968) used this method to study large deflections of beams, and (Brebbia and Conner, 1969) recently used this method successfully to study stability and geometrically nonlinear behavior of arbitrary shells. Brebbia and Conner refer to the incremental formulations used by (Wissmann, 1966), (Felippa, 1966), and (Argyris, 1966) as a one step Newton – Raphson Method and the incremental loading procedures described previously. They employ a mixed procedure wherein incremental loading is used for three steps and then Newton – Raphson method is introduced to provide successive corrections.

Similar iterative procedures have been discussed in connection with nonlinear frame analysis by (Tezcan and Mahapatra, 1969), (Corner *et al.*, 1968), (Zarghamee and Shah, 1968), (Poskitt, 1967), and (Prasad, 1969). Tezcan and Mahapatra presented explicit forms of tangent stiffness matrices for plane and space frame members, which have been successfully employed for the geometrically nonlinear two and three dimensional structures, including the stability problems. (Thompson and Walker, 1969), (Walker, 1968) have used the Newton-Raphson method as well as perturbation and incremental step-by-step techniques to study stability and large deflections, including branching analysis of finite element models of structural systems.

According to (Tezcan and Ovunc, 1966), an iteration procedure is presented to determine buckling loads of plane and space structures taking into account nonlinear behavior. The basic idea in this procedure is to perform a standard linear analysis under the action of given set of external loads and then calculate the member end forces using the deformed geometry. If the member end forces at a joint are not in equilibrium with the given

external loads, the out of balance forces are applied on to deformed geometry to yield another set of deformations and forces. If the new forces do not satisfy the joint equilibrium, the linear analysis continues with the latest geometry and with the latest out of balance forces. This procedure is repeated until equilibrium is reached at every joint. The original external loads are gradually increased and the equilibrium status is established in each time by following the process. The magnitude of the external loads causing divergence in the unbalanced forces, in other works, producing excessive deformations at the joints, is considered as the buckling load of the system.

2.3. Nonlinear Field Problems

More general finite elements formulations of problems of nonlinear continua have been also considered. These include studies of nonlinear viscoelasticity (Oden, 1967), and (Oden, 1969) coupled thermoelasticity (Oden *et al.*, 1969), nonlinear heat conduction (Aguire *et al.*, 1969), finite thermoelasticity (Oden, 1969), fluid dynamics (Oden *et al.*, 1969), materials with microstructure (Oden *et al.*, 1969), and thermomechanically simple materials with memory (Oden and Ramirez, 1969). The development of general finite element formulations, valid for any choice of reference coordinates, of heat conduction and motion of nonlinear thermomechanical materials is discussed in the paper (Oden and Ramirez, 1969).

Incremental Analysis of large deformations of elastoplastic materials, with emphasis on shells of revolution, is examined by (Yaghmai, 1968), and applications of the finite elements method to the analysis of nonlinear thermoviscoelastic solid is considered by (Dong *et al.*, 1968). A survey and extension of finite element formulations of problems of finite deformation and irreversible thermodynamics of nonlinear continua including of both solid and fluids, has recently been given by (Oden, 1969).

A comprehensive treatment is given by (Naylor *et al.*, 1981), for the application of the finite element method in geotechnical engineering. (Simo, 1991), presented very general proofs of unconditional stability based on contractivity of the operators with areas for implicit integrators, midpoint rule for heat conduction, midpoint rule for static plasticity and viscoplasticity.

2.4. The Buckling of Lattice Domes under the Simultaneous Concentrated Loads

Triangular lattice domes are, in effect, warped; three dimensional trusses, due to the assumed perfectly frictionless member connections, and when a system of point loads are applied to the nodes of the frame, two types of stability problems are that:

- Bar stability problems with solutions given by the Euler critical load,
- Snap-Through problems

When a system of compressive loads is applied to the joints of a framed, triangulated dome with straight members, two distinct stability problems may arise as the loads are gradually increased.

- If the members located in the neighborhood of the loaded joints are slender, high ratio of effective length to minimum radius of gyration, some of them may buckle in the manner of axially loaded columns. This behavior constitutes the bar stability problem, the solution is given by the Euler critical load.
- As the bar lengths decrease with increasing number of members, the framework around any particular joint becomes flatter, as the angles of intersection of adjoining bars grow closer to 180°. When the applied forces are slowly increased, the deflections of the loaded joints, coupled with the deformations of the surrounding ones, tend to flatten the framework even further, until a configuration is reached beyond which a loaded joint becomes unstable. More increasing of the load would cause this joint to snap-through, and the dome's surface would develop a more or less circular depression or dimple. And moreover this subject have been reported by (Krivoshapko, 2002), (Yamada *et al.*, 1997), (Carpenter *et al.*, 1966), (Aguilar and Huang, 1966).

2.5. Buckling Consideration in the Design and Construction of Space Structures

Buckling is a serious problem that should be considered in the design and construction of large doubly curved space structures. The past investigations of existing structures indicate that certain designs have a marginal factor of safety against buckling.

Several investigators suspect that inadequate resistance to buckling contributed to the past failure of several structures such as the dome roofs in Bucharest, Rumania, and Fargo, North Dakota, and the failure of the sandwich dome on the Saturn Booster.

Considerable research and analysis on the stability of shell and shell-like structures has been performed in past years (Buchert-a, 1965), (Buchert-b, 1965), (Wright, 1965), (Kloppel and Roos, 1956), (Crawford and Schwartz, 1965). However the present analysis of these structures leaves much to be desired, the professional engineer can use the results available to design a safe, structurally efficient, economic doubly curved shell-like structure.

The stability analysis of a shell-like doubly curved structure such as braced dome, single or double layer grid, stressed skin system, and sandwich type should include consideration of the following factors:

- General buckling,
- Local buckling,
- Edge conditions,
- Yield strain of the materials,
- Deviation from a perfect surface.

As a result of past research and testing, equations have been derived to allow the designer estimate the critical buckling loads for the general and local buckling. Although quantitative theoretical equations are not available for the effects of the edge conditions, yield strain, and imperfections; certain general design guides can be stated that will minimize the effects of these important factors.

Three types of buckling could occur in this type of dome such as member buckling, local buckling, and general buckling. Member buckling is similar to column or arch type buckling that occurs in a many civil engineering structures. Local buckling occurs in a local area and consists of the buckling of more than one member. General buckling occurs over a considerable portion of the structure and results in a general failure or collapse of the dome. And moreover this subject have been reported by (Darooka and Jensen, 2001), (Kitipornchai *et al.*, 2004), and (Buchert, 1966).

2.6. Rapid Progress in Computers

There are two basic reasons in preferring mathematical modeling to the experimental testing. One of them is that the computational powers of computers have been drastically improved for the last forty years. The second one is that the cost per unit computation has been intensely decreased as shown in Fig. 2.4.

As a matter of fact, the computational power of the oldest computer ENIAC in 1945 was approximately 100 flops (floating point operation per second) and it has been increased to 80000 flops at an IBM-7090 computer in 1960. Today, the CRAY4 computer for example, has one billion flops high computational speeds. It is easily seen that along a time period of about fifty years, the computational speeds of the computers have been increased by ten million times (Hughes, 1987) and (Hughes and Belytschko, 1992).

In opposite to this increase in speed, the cost of computation has been decreased by about thousand folds within the same time period as shown in Figure 2.4. An inflation factor of approximately four is assumed to occur in the computer prices between the years 1966 and 1990.

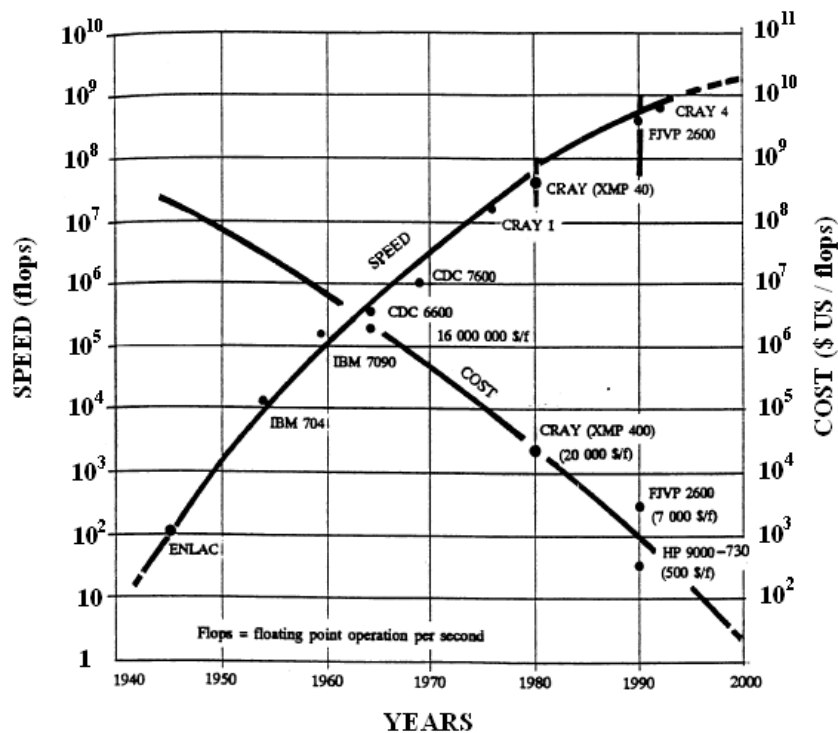


Figure 2.4. Speed and cost evaluation of computers

3. TANGENT STIFFNESS MATRICES FOR BAR ELEMENTS

In this chapter of the Thesis, the geometric nonlinearity tangent stiffness matrices of the bar elements will be derived. For the bar elements, the Taylor expansion method will be used while for the finite elements and strain energy concept will be applied. In deriving the tangent stiffness matrices for one dimensional bars, the Taylor expansion method is the most convenient. With the omission of the second and higher order derivatives, the change in the value of a continuous function P_i , with n independent parameters $u_1, u_2, u_3, \dots, u_n$ is

$$\Delta P_i = \frac{\partial P_i}{\partial u_1} \Delta u_1 + \frac{\partial P_i}{\partial u_2} \Delta u_2 + \frac{\partial P_i}{\partial u_3} \Delta u_3 + \dots + \frac{\partial P_i}{\partial u_n} \Delta u_n \tag{3.1}$$

in which, P_i represents any particular member end-force and $u_1, u_2, u_3, \dots, u_n$ represent the deformations along the specified n degrees of freedom, in the global coordinate system.

$$\{\Delta P\}_i = \left[\frac{\partial P_i}{\partial u_j} \right] \{\Delta u_i\} \tag{3.2}$$

Then if this formula, which is above, is compared with the formula which is below,

$$\{F\} = [K]\{d\} \tag{3.3}$$

As a result, the partial derivative of the P_i with respect to the u_j is equal to the stiffness matrix K in the global coordinate system.

$$[K_{i,j}] = \left[\frac{\partial P_i}{\partial u_j} \right] \tag{3.4}$$

$$[K]_{xyz} = \begin{bmatrix} \frac{\partial P_1}{\partial u_1} & \frac{\partial P_1}{\partial u_2} & \frac{\partial P_1}{\partial u_3} & \dots & \frac{\partial P_1}{\partial u_n} \\ \frac{\partial P_2}{\partial u_1} & \frac{\partial P_2}{\partial u_2} & \frac{\partial P_2}{\partial u_3} & \dots & \frac{\partial P_2}{\partial u_n} \\ \frac{\partial P_3}{\partial u_1} & \frac{\partial P_3}{\partial u_2} & \frac{\partial P_3}{\partial u_3} & \dots & \frac{\partial P_3}{\partial u_n} \end{bmatrix} \tag{3.5}$$

Once the algebraic expressions of the member end-forces $P_1, P_2, P_3, \dots, P_n$ in terms of $u_1, u_2, u_3, \dots, u_n$ are known in the deformed geometry, the tangent stiffness matrix of a bar element may be obtained simply by taking the partial derivatives of the end-forces with respect to each one of the end-displacements.

3.1. Tangent Stiffness Matrix of a Truss Bar

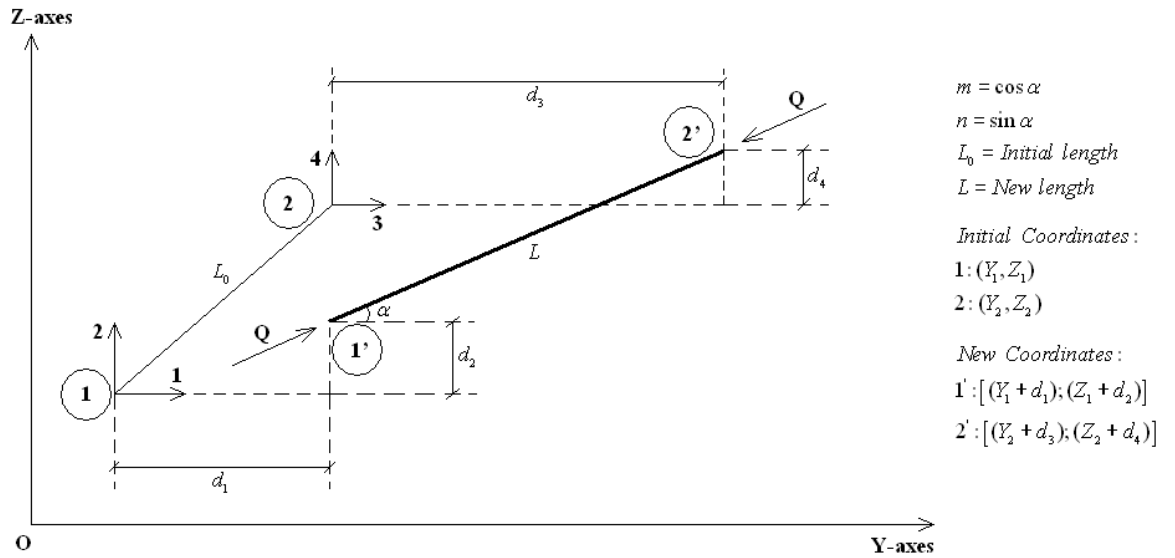


Figure 3.1. A bar element and its axial force, Q

$$Q = A\sigma \quad (3.6)$$

$$\sigma = E\varepsilon \quad (3.7)$$

$$Q = A(E\varepsilon) = AE \frac{\Delta L}{L_0} = AE \frac{L_0 - L}{L_0} \quad (3.8)$$

$$m = \frac{\Delta Y}{L} = \frac{1}{L} [(Y_2 + d_3) - (Y_1 + d_1)] = \frac{u}{L} \quad (3.9)$$

$$m = \cos \alpha \quad (3.10)$$

$$n = \frac{\Delta Z}{L} = \frac{1}{L} [(Z_2 + d_4) - (Z_1 + d_2)] = \frac{v}{L} \quad (3.11)$$

$$n = \sin \alpha \quad (3.12)$$

$L \leq L_0$, due to the compressive axial force, Q

The new coordinate for the point 1:

$$Y = Y_1 + d_1 \quad (3.13)$$

$$Z = Z_1 + d_2 \quad (3.14)$$

The new coordinate for the point 2:

$$Y = Y_2 + d_3 \quad (3.13)$$

$$Z = Z_2 + d_4 \quad (3.14)$$

The new length:

$$L = \sqrt{[(Y_2 + d_3) - (Y_1 + d_1)]^2 + [(Z_2 + d_4) - (Z_1 + d_2)]^2} \quad (3.15)$$

$$L = \sqrt{u^2 + v^2} \quad (3.16)$$

First of all, in order to determine and form the axial force vector, the angle α , which is between the horizontal axes and the new bar element, is used by the values of sine and cosine of the angle.

$$\{Q\} = \begin{Bmatrix} Q_1 \\ Q_2 \\ Q_3 \\ Q_4 \end{Bmatrix} = \begin{Bmatrix} Q_1 \\ Q_2 \\ -Q_1 \\ -Q_2 \end{Bmatrix} = \begin{Bmatrix} Q \cos \alpha \\ Q \sin \alpha \\ -Q \cos \alpha \\ -Q \sin \alpha \end{Bmatrix} = \begin{Bmatrix} \frac{AE}{L_0} \left(\frac{L_0 - L}{L} \right) [(Y_2 + d_3) - (Y_1 + d_1)] \\ \frac{AE}{L_0} \left(\frac{L_0 - L}{L} \right) [(Z_2 + d_4) - (Z_1 + d_2)] \\ -\frac{AE}{L_0} \left(\frac{L_0 - L}{L} \right) [(Y_2 + d_3) - (Y_1 + d_1)] \\ -\frac{AE}{L_0} \left(\frac{L_0 - L}{L} \right) [(Z_2 + d_4) - (Z_1 + d_2)] \end{Bmatrix} \quad (3.17)$$

To determine k_{11} ;

$$k_{11} = \frac{\partial Q_1}{\partial d_1} \quad (3.18)$$

$$k_{11} = \frac{\partial}{\partial d_1} \left\{ \frac{AE}{L_0} \left(\frac{L_0}{L} - 1 \right) \left[(Y_2 + d_3) - (Y_1 + d_1) \right] \right\} \quad (3.19)$$

$$k_{11} = \frac{\partial}{\partial d_1} \left\{ \frac{AE}{L_0} \left(L_0 \frac{u}{L} - u \right) \right\} = \frac{\partial}{\partial d_1} \frac{AE}{L_0} \left(L_0 \frac{u}{\sqrt{u^2 + v^2}} - u \right) \quad (3.20)$$

Remember that:

$$(\sqrt{u})' = \frac{u'}{2\sqrt{u}} \quad (3.21)$$

$$\frac{\partial u}{\partial d_1} = u' = -1 \quad (3.22)$$

$$(\sqrt{u^2 + v^2})' = \frac{2uu'}{2\sqrt{u^2 + v^2}} \quad (3.22)$$

$$m = \frac{u}{L} = \frac{u}{\sqrt{u^2 + v^2}} \quad (3.23)$$

$$k_{11} = \frac{AE}{L_0} \left[L_0 \frac{u' \sqrt{u^2 + v^2} - u \frac{2uu'}{2\sqrt{u^2 + v^2}}}{u^2 + v^2} - u' \right] \quad (3.24)$$

$$k_{11} = \frac{AE}{L_0} \left[L_0 \frac{(-1)L - \frac{u^2}{L}}{L^2} + 1 \right] \quad (3.25)$$

$$k_{11} = \frac{AE}{L_0} \left[L_0 \frac{-L + m^2 L}{L^2} + 1 \right] \quad (3.26)$$

$$k_{11} = \frac{AE}{L_0} \left[L_0 \frac{m^2 - 1}{L} + 1 \right] \quad (3.27)$$

Add to the last equation $+m^2 - m^2$,

$$k_{11} = \frac{AE}{L_0} \left[m^2 + \frac{L_0}{L} m^2 - m^2 - \frac{L_0}{L} + 1 \right] \quad (3.28)$$

$$k_{11} = \frac{AE}{L_0} m^2 + \frac{AE}{L_0} \left[\left(1 - \frac{L_0}{L} \right) - m^2 \left(1 - \frac{L_0}{L} \right) \right] \quad (3.29)$$

$$k_{11} = \frac{AE}{L_0} m^2 - \frac{AE}{L_0} \left[(1 - m^2) \left(\frac{L_0 - L}{L} \right) \right] \quad (3.30)$$

$$k_{11} = \frac{AE}{L_0} m^2 - \frac{AE}{L_0} (L_0 - L) \frac{1 - m^2}{L} \quad (3.31)$$

Remember that:

$$Q = \frac{AE}{L_0} (L_0 - L) \quad (3.32)$$

$$k_{11} = \frac{AE}{L_0} m^2 - \frac{Q}{L} (1 - m^2) \quad (3.33)$$

In order to get the k_{22} of the tangent stiffness matrix by analogy only m is replaced by n ;

$$k_{22} = \frac{AE}{L_0} n^2 - \frac{Q}{L} (1 - n^2) \quad (3.34)$$

To determine k_{21} ;

$$k_{21} = \frac{\partial Q_2}{\partial d_1} \quad (3.35)$$

$$k_{21} = \frac{\partial}{\partial d_1} \left\{ \frac{AE}{L_0} \left(\frac{L_0 - L}{L} \right) [(Z_2 + d_4) - (Z_1 + d_2)] \right\} \quad (3.36)$$

$$k_{21} = \frac{\partial}{\partial d_1} \left\{ \frac{AE}{L_0} \left(L_0 \frac{v}{L} - v \right) \right\} = \frac{\partial}{\partial d_1} \frac{AE}{L_0} \left(L_0 \frac{v}{\sqrt{u^2 + v^2}} - v \right) \quad (3.37)$$

Remember that:

$$(\sqrt{u})' = \frac{u'}{2\sqrt{u}} \quad (3.38)$$

$$\frac{\partial u}{\partial d_1} = u' = -1 \quad (3.39)$$

$$v \text{ is not a function of } d_1, \Rightarrow \frac{\partial v}{\partial d_1} = v' = 0 \quad (3.40)$$

$$\left(\frac{1}{\sqrt{u^2 + v^2}} \right)' = \frac{2uu'}{u^2 + v^2} \quad (3.41)$$

$$m = \frac{u}{L} = \frac{u}{\sqrt{u^2 + v^2}} \quad (3.42)$$

$$m^2 = \frac{u^2}{u^2 + v^2} \quad (3.43)$$

$$n = \frac{v}{L} = \frac{v}{\sqrt{u^2 + v^2}} \quad (3.44)$$

$$k_{21} = \frac{AE}{L_0} \left[vL_0 \frac{-2uu'}{u^2 + v^2} - 0 \right] \quad (3.45)$$

$$k_{21} = \frac{AE}{L_0} \left[vL_0 \frac{u}{L^2} - 0 \right] \quad (3.46)$$

$$k_{21} = \frac{AE}{L_0} \left[L_0 \frac{v}{L} \frac{m}{L} \right] \quad (3.47)$$

$$k_{21} = \frac{AE}{L_0} \left[L_0 \frac{mn}{L} \right] \quad (3.48)$$

Add to the last equation $+mn - mn$,

$$k_{21} = \frac{AE}{L_0} \left[mn + \frac{L_0}{L} mn - mn \right] \quad (3.49)$$

$$k_{21} = \frac{AE}{L_0} mn - \frac{AE}{L_0} (L_0 - L) \frac{-mn}{L} \quad (3.50)$$

Remember that:

$$Q = \frac{AE}{L_0} (L_0 - L) \quad (3.51)$$

$$k_{21} = \frac{AE}{L_0} mn - \frac{Q}{L} (-mn) \quad (3.52)$$

By the symmetry in the tangent stiffness matrix,

$$k_{21} = k_{12} = \frac{AE}{L_0} mn - \frac{Q}{L} (-mn) \quad (3.53)$$

Let us make up the general stiffness matrix for the bar elements under the axial force Q;

$$[K]_i = \frac{AE}{L_0} \begin{bmatrix} m^2 & mn & -m^2 & -mn \\ mn & n^2 & -mn & -n^2 \\ -m^2 & -mn & m^2 & mn \\ -mn & -n^2 & mn & n^2 \end{bmatrix} - \frac{Q}{L} \begin{bmatrix} 1-m^2 & -mn & -(1-m^2) & mn \\ -mn & 1-n^2 & mn & -(1-n^2) \\ -(1-m^2) & mn & 1-m^2 & -mn \\ mn & -(1-n^2) & -mn & 1-n^2 \end{bmatrix} \quad (3.54)$$

3.2. Other Form of the Tangent Stiffness Matrix

$$Q = \frac{AE}{L_0}(L_0 - L) \quad (3.55)$$

Q represents the compressive axial force, therefore sign of the force, Q is positive. If it is a tensile axial force, then it will be negative.

$$k_{11} = \frac{AE}{L_0}m^2 - \frac{Q}{L}(1 - m^2) \quad (3.56)$$

$$k_{11} = \frac{AE}{L_0}m^2 - \frac{AE}{L_0} \frac{L_0 - L}{L}(1 - m^2) \quad (3.57)$$

$$k_{11} = \frac{AE}{L_0}m^2 - \frac{AE}{L_0} \frac{L_0 - L}{L} + \frac{AE}{L_0} \frac{L_0}{L}m^2 - \frac{AE}{L_0} \frac{L}{L}m^2 \quad (3.58)$$

$$k_{11} = \frac{AE}{L}m^2 - \frac{AE}{L} \frac{L_0 - L}{L_0} = \frac{AE}{L}(m^2 - \varepsilon) \quad (3.59)$$

$$[K]_t = \frac{AE}{L} \begin{bmatrix} m^2 - \varepsilon & mn & -m^2 + \varepsilon & -mn \\ mn & n^2 - \varepsilon & -mn & -n^2 + \varepsilon \\ -m^2 + \varepsilon & -mn & m^2 - \varepsilon & mn \\ -mn & -n^2 + \varepsilon & mn & n^2 - \varepsilon \end{bmatrix} \quad (3.60)$$

3.3. Tangent Stiffness for a Space Truss System

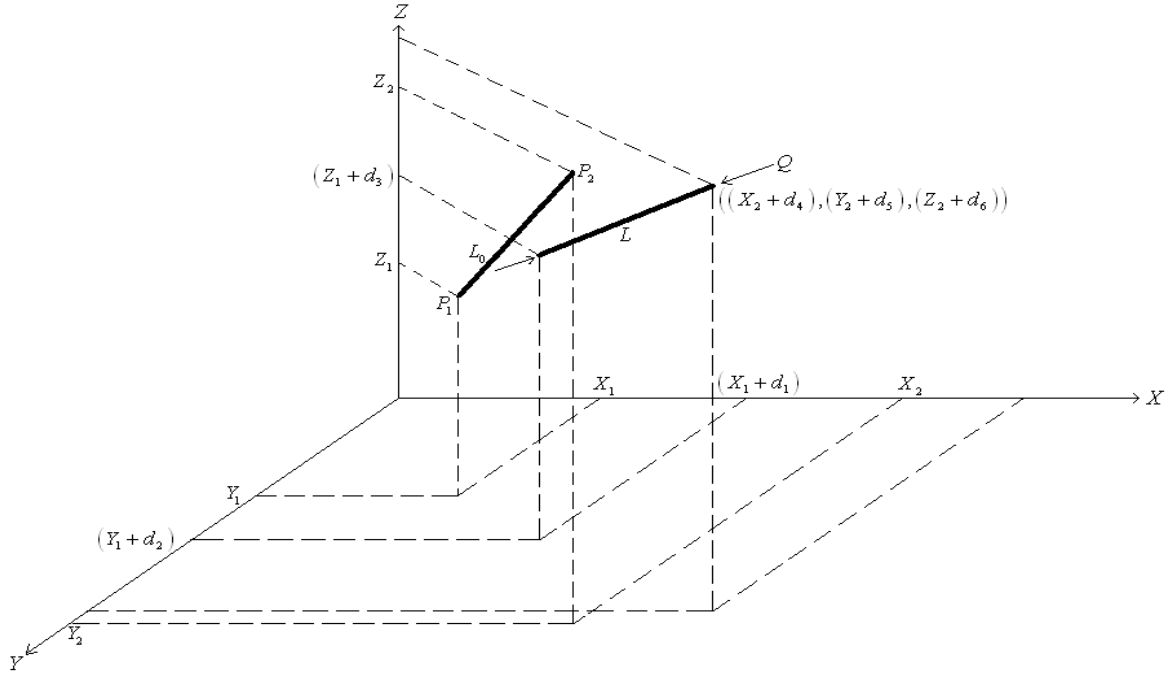


Figure 3.2. A space truss system and its axial force, Q

$$Q = A\sigma \quad (3.61)$$

$$\sigma = E\varepsilon \quad (3.62)$$

$$Q = A(E\varepsilon) = AE \frac{\Delta L}{L_0} = AE \frac{L_0 - L}{L_0} \quad (3.63)$$

$$l = \frac{\Delta X}{L} = \frac{[(X_2 + d_4) - (X_1 + d_1)]}{L} = \frac{u}{L} \quad (3.64)$$

$$m = \frac{\Delta Y}{L} = \frac{[(Y_2 + d_5) - (Y_1 + d_2)]}{L} = \frac{v}{L} \quad (3.65)$$

$$n = \frac{\Delta Z}{L} = \frac{[(Z_2 + d_6) - (Z_1 + d_3)]}{L} = \frac{w}{L} \quad (3.66)$$

$L \leq L_0$, due to the compressive axial force, Q

The new coordinate for the point 1:

$$X = X_1 + d_1 \quad (3.67)$$

$$Y = Y_1 + d_2 \quad (3.68)$$

$$Z = Z_1 + d_3 \quad (3.69)$$

The new coordinate for the point 2:

$$X = X_2 + d_4 \quad (3.70)$$

$$Y = Y_2 + d_5 \quad (3.71)$$

$$Z = Z_2 + d_6 \quad (3.72)$$

The new length:

$$L = \sqrt{[(X_2 + d_4) - (X_1 + d_1)]^2 + [(Y_2 + d_5) - (Y_1 + d_2)]^2 + [(Z_2 + d_6) - (Z_1 + d_3)]^2} \quad (3.73)$$

$$L = \sqrt{u^2 + v^2 + w^2} \quad (3.74)$$

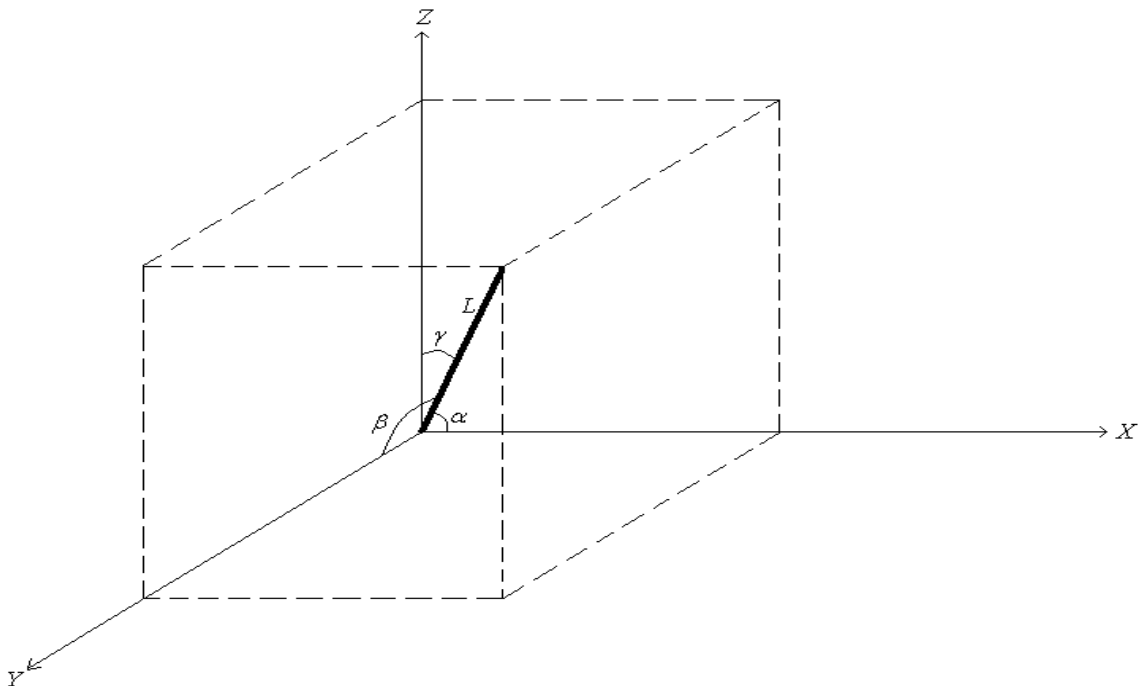


Figure 3.3. Angles for the direction of cosine

The direction cosines formulas:

$$\cos \alpha = \frac{\Delta X}{L}, \quad \cos \beta = \frac{\Delta Y}{L}, \quad \cos \gamma = \frac{\Delta Z}{L} \quad (3.75)$$

$$\cos^2 \alpha + \cos^2 \beta + \cos^2 \gamma = 1 \quad \left(\frac{\Delta X^2 + \Delta Y^2 + \Delta Z^2}{L^2} = \frac{L^2}{L^2} = 1 \right) \quad (3.76)$$

If the Length, L is considered as a vector;

$$L = L(\cos \alpha)i + L(\cos \beta)j + L(\cos \gamma)k \quad (3.77)$$

$$L = L_x i + L_y j + L_z k \quad (3.78)$$

$$Q = Q_x i + Q_y j + Q_z k \quad (3.79)$$

$$Q_x = Q \cos \alpha = Q \frac{\Delta X}{L} = Q \frac{((X_2 + d_4) - (X_1 + d_1))}{L} = Ql \quad (3.80)$$

$$Q_y = Q \cos \beta = Q \frac{\Delta Y}{L} = Q \frac{((Y_2 + d_5) - (Y_1 + d_2))}{L} = Qm \quad (3.81)$$

$$Q_z = Q \cos \gamma = Q \frac{\Delta Z}{L} = Q \frac{((Z_2 + d_6) - (Z_1 + d_3))}{L} = Qn \quad (3.82)$$

$$\{Q\} = \begin{Bmatrix} Q_1 \\ Q_2 \\ Q_3 \\ Q_4 \\ Q_5 \\ Q_6 \end{Bmatrix} = \begin{Bmatrix} Q_1 \\ Q_2 \\ Q_3 \\ -Q_1 \\ -Q_2 \\ -Q_3 \end{Bmatrix} = \begin{Bmatrix} \frac{AE}{L_0} \left(\frac{L_0 - L}{L} \right) [(X_2 + d_4) - (X_1 + d_1)] \\ \frac{AE}{L_0} \left(\frac{L_0 - L}{L} \right) [(Y_2 + d_5) - (Y_1 + d_2)] \\ \frac{AE}{L_0} \left(\frac{L_0 - L}{L} \right) [(Z_2 + d_6) - (Z_1 + d_3)] \\ -Q_1 \\ -Q_2 \\ -Q_3 \end{Bmatrix} \quad (3.83)$$

To determine k_{11} ;

$$k_{11} = \frac{\partial Q_1}{\partial d_1} \quad (3.84)$$

$$k_{11} = \frac{\partial}{\partial d_1} \left\{ \frac{AE}{L_0} \left(\frac{L_0}{L} - 1 \right) \left[(X_2 + d_4) - (X_1 + d_1) \right] \right\} \quad (3.85)$$

$$k_{11} = \frac{\partial}{\partial d_1} \left\{ \frac{AE}{L_0} \left(L_0 \frac{u}{L} - u \right) \right\} = \frac{AE}{L_0} \frac{\partial}{\partial d_1} \left(L_0 \frac{u}{\sqrt{u^2 + v^2 + w^2}} - u \right) \quad (3.86)$$

Remember that:

$$(\sqrt{u})' = \frac{u'}{2\sqrt{u}} \quad (3.87)$$

$$\frac{\partial u}{\partial d_1} = u' = -1 \quad (3.88)$$

$$\left(\sqrt{u^2 + v^2 + w^2} \right)' = \frac{2uu'}{2\sqrt{u^2 + v^2 + w^2}} \quad (3.89)$$

$$l = \frac{u}{L} = \frac{u}{\sqrt{u^2 + v^2 + w^2}} \quad (3.90)$$

$$l^2 = \frac{u^2}{u^2 + v^2 + w^2} \quad (3.91)$$

$$k_{11} = \frac{AE}{L_0} \left[L_0 \frac{u' \sqrt{u^2 + v^2 + w^2} - u \frac{2uu'}{2\sqrt{u^2 + v^2 + w^2}}}{u^2 + v^2 + w^2} - u' \right] \quad (3.92)$$

$$k_{11} = \frac{AE}{L_0} \left[L_0 \frac{(-1)L + \frac{u^2}{L}}{L^2} + 1 \right] \quad (3.93)$$

$$k_{11} = \frac{AE}{L_0} \left[L_0 \frac{-L + l^2 L}{L^2} + 1 \right] \quad (3.94)$$

$$k_{11} = \frac{AE}{L_0} \left[L_0 \frac{l^2 - 1}{L} + 1 \right] \quad (3.95)$$

Add to the last equation $+l^2 - l^2$,

$$k_{11} = \frac{AE}{L_0} \left[l^2 + \frac{L_0}{L} l^2 - l^2 - \frac{L_0}{L} + 1 \right] \quad (3.96)$$

$$k_{11} = \frac{AE}{L_0} l^2 + \frac{AE}{L_0} \left[\left(1 - \frac{L_0}{L} \right) - l^2 \left(1 - \frac{L_0}{L} \right) \right] \quad (3.97)$$

$$k_{11} = \frac{AE}{L_0} l^2 - \frac{AE}{L_0} \left[(1 - l^2) \left(\frac{L_0 - L}{L} \right) \right] \quad (3.98)$$

$$k_{11} = \frac{AE}{L_0} l^2 - \frac{AE}{L_0} (L_0 - L) \frac{1 - l^2}{L} \quad (3.99)$$

$$k_{11} = \frac{AE}{L_0} l^2 - \frac{Q}{L} (1 - l^2) \quad (3.100)$$

$$k_{22} = \frac{\partial Q_2}{\partial d_2} \quad (3.101)$$

$$k_{33} = \frac{\partial Q_3}{\partial d_3} \quad (3.102)$$

$$k_{21} = \frac{\partial Q_2}{\partial d_1} = k_{12} = \frac{\partial Q_1}{\partial d_2} \quad (3.103)$$

$$k_{31} = \frac{\partial Q_3}{\partial d_1} = k_{13} = \frac{\partial Q_1}{\partial d_3} \quad (3.104)$$

$$k_{32} = \frac{\partial Q_3}{\partial d_2} = k_{23} = \frac{\partial Q_2}{\partial d_3} \quad (3.105)$$

$$[k] = \frac{AE}{L_v} \begin{bmatrix} l^2 & lm & ln & -l^2 & -lm & -ln \\ lm & m^2 & mn & -lm & -m^2 & -mn \\ ln & mn & n^2 & -ln & -mn & -n^2 \\ -l^2 & -lm & -ln & l^2 & lm & ln \\ -lm & -m^2 & -mn & lm & m^2 & mn \\ -ln & mn & -n^2 & ln & mn & n^2 \end{bmatrix} - \frac{Q}{L} \begin{bmatrix} 1-l^2 & -lm & -ln & l^2-1 & lm & ln \\ -lm & 1-m^2 & -mn & lm & m^2-1 & mn \\ -ln & -mn & 1-n^2 & ln & mn & n^2-1 \\ l^2-1 & lm & ln & 1-l^2 & -lm & -ln \\ lm & m^2-1 & mn & -lm & 1-m^2 & -mn \\ ln & mn & n^2-1 & -ln & -mn & 1-n^2 \end{bmatrix} \quad (3.106)$$

3.4. Tangent Stiffness Matrix for a Space Member

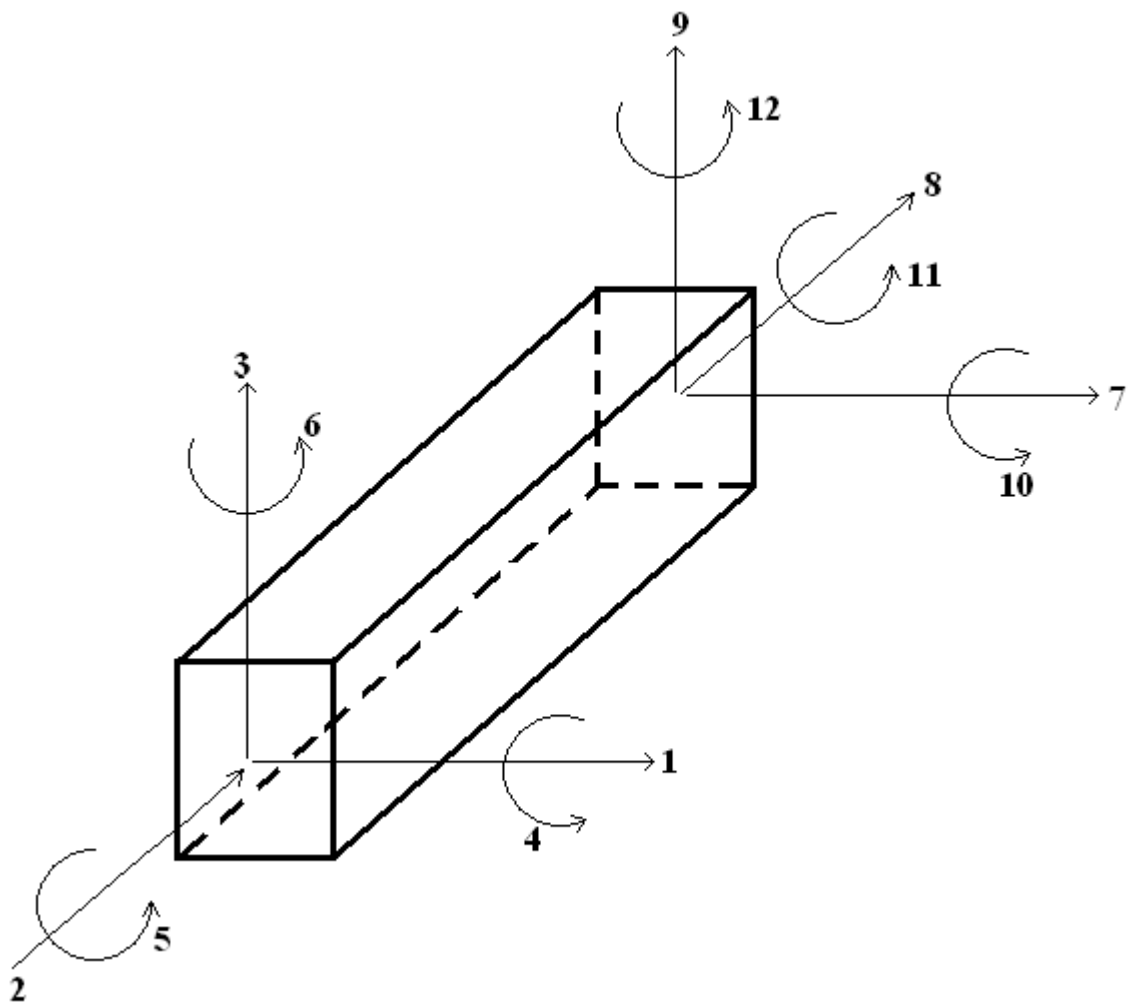


Figure 3.4. A space member with MDOFs

At the figure above, totally 12 degree of freedoms are separately shown on an example of a space member. Therefore the tangent stiffness matrix should be by 12x12. Moreover, there are two parts of the tangent stiffness matrix for a space member. The first one is the linear-part, the other one is the nonlinear part of the tangent stiffness. If these parts are shown separately:

3.4.1. Linear Part of the Tangent Stiffness Matrix Relative to Member Axes

$$k_l = \begin{bmatrix} H & . & . & . & . & -G & -H & . & . & . & . & -G \\ . & S & . & . & . & . & . & -S & . & . & . & . \\ . & . & D & C & . & . & . & . & -D & C & . & . \\ . & . & C & A & . & . & . & . & -C & B & . & . \\ . & . & . & . & T & . & . & . & . & . & -T & . \\ -G & . & . & . & . & E & G & . & . & . & . & F \\ -H & . & . & . & . & G & H & . & . & . & . & G \\ . & -S & . & . & . & . & . & S & . & . & . & . \\ . & . & -D & -C & . & . & . & . & D & -C & . & . \\ . & . & C & B & . & . & . & . & -C & A & . & . \\ . & . & . & . & -T & . & . & . & . & . & T & . \\ -G & . & . & . & . & F & G & . & . & . & . & E \end{bmatrix}$$

$$\begin{aligned} A &= \frac{4EI_x s_{1x}}{L} & E &= \frac{4EI_z s_{1z}}{L} \\ B &= \frac{2EI_x s_{2x}}{L} & F &= \frac{2EI_z s_{2z}}{L} & S &= \frac{AE}{L} \\ C &= \frac{A+B}{L} & G &= \frac{E+F}{L} & T &= \frac{GJ}{L} \\ D &= \frac{2C-Q}{L} & H &= \frac{2G+Q}{L} \end{aligned} \quad (3.107)$$

$Q = \text{Axial force (Compressive positive)}$

For compression members:

$$s_1 = \frac{\rho (\sin \rho - \rho \cos \rho)}{4(2 - 2 \cos \rho - \rho \sin \rho)} \quad (3.108)$$

$$s_2 = \frac{\rho (\rho - \sin \rho)}{2(2 - 2 \cos \rho - \rho \sin \rho)} \quad (3.109)$$

3.4.2. Nonlinear Part of the Tangent Stiffness Matrix Relative to Member Axes

$$k_{nl} = \frac{Q}{L} \begin{bmatrix} c & . & . & . & . & -d & -c & . & . & . & . & -d \\ . & . & . & . & . & . & . & . & . & . & . & . \\ . & . & c & d & . & . & . & . & -c & d & . & . \\ . & . & d & a & . & . & . & . & -d & b & . & . \\ . & . & . & . & . & . & . & . & . & . & . & . \\ -d & . & . & . & . & a & d & . & . & . & . & . \\ -c & . & . & . & . & d & c & . & . & . & . & . \\ . & . & . & . & . & . & . & . & . & . & . & . \\ . & . & -c & -d & . & . & . & . & c & -d & . & . \\ . & . & d & b & . & . & . & . & -d & a & . & . \\ . & . & . & . & . & . & . & . & . & . & . & . \\ -d & . & . & . & . & . & . & . & . & . & . & a \end{bmatrix}$$

$$a = \frac{2L^2}{15} \quad c = \frac{6}{5} \quad b = \frac{-L^2}{30} \quad d = \frac{L}{10} \quad (3.110)$$

Q = Axial force (Compressive Negative)

4. COMPUTATIONAL TECHNIQUES

4.1. About the Computational Techniques

All materials have the nonlinearity when they are subjected to a force or a deflection. At the before of the invention of the computers all people, engineers, have an obligation to accept that all systems have linear solution. But after the coming of the computers in our life and business we can easily think about the nonlinear solutions. Because some iterative or incremental procedures are required in order to get any nonlinear solution from any system since actually, the nonlinear analysis is obtained by means of repetitious linear analysis. And these procedures are applicable thanks to the computers which can calculate lots of equations in very short time.

In this chapter, the computational techniques existing in nonlinear analysis are summarized.

4.2. What is Nonlinear Analysis for LUSAS?

Linear Finite Element Analysis assumes that all materials are linear elastic in behavior and that deformations are small enough to not significantly affect the overall behavior of the structure. Obviously, this description applies to very few situations in the real world, but with a few restrictions and assumptions linear analysis will suffice for the majority of engineering applications.

What do we look for, therefore, in our problem to indicate that a nonlinear finite element analysis is required?

- Gross changes in geometry
- Permanent deformations
- Structural cracks
- Buckling
- Stresses greater than the yield stress
- Contact between component parts

Three types of nonlinear analysis may be modeled using LUSAS:

- Geometric Nonlinearity e.g. large deflection or rotation, large strain, non-conservative loading.
- Mixed Nonlinearity e.g. lift-off supports, general contact, compression load transfer, dynamic impact.
- Material Nonlinearity e.g. plasticity, fracture/cracking, damage, creep, volumetric crushing, rubber material.

Table 4.1. Nonlinear solution techniques

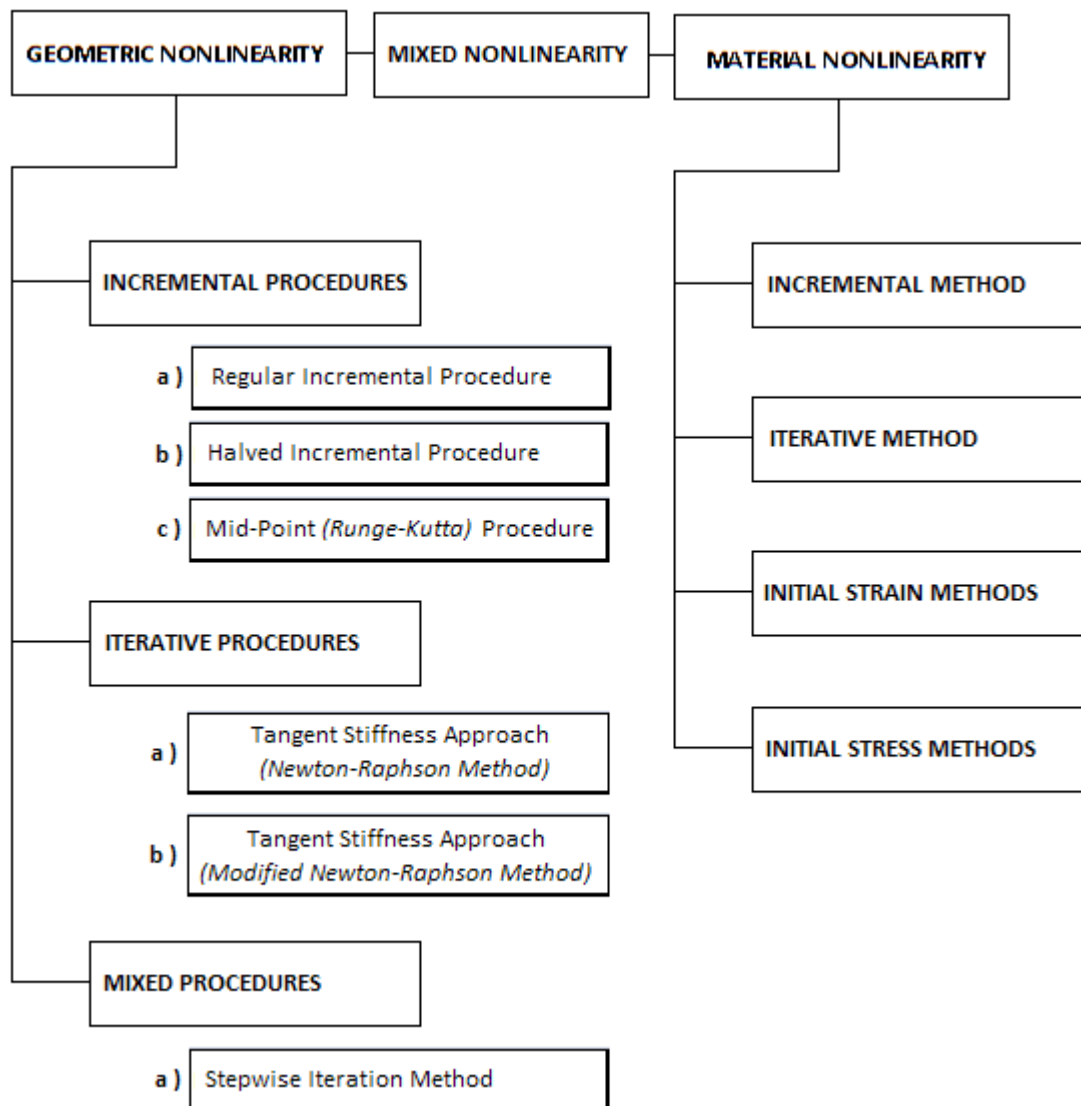


Table 4.2. Comparison of solution techniques

INCREMENTAL PROCEDURES	
Advantages	Disadvantages
1. “ <i>Incremental theory</i> ”, (<i>Flow Theory</i>) of plasticity is conveniently used in incremental procedures	1. There is a tendency of always deviating from the true solution. To avoid this, a mixed procedure may be necessary.
2. Very general applicable to all types of nonlinearity, except <i>work-softening</i> materials, for the method fails.	2. Number of increments is initially unknown. Thus it is difficult to estimate the number of increments and therefore the degree of the accuracy is unknown.
3. Useful results are produced at each of the intermediate steps of loading.	3. More time consuming than the iterative solutions, because all matrices must be updated in each cycle.
-----	4. Not applicable to <i>work-softening</i> materials.
ITERATIVE PROCEDURES	
Advantages	Disadvantages
1. Less time consuming than the incremental procedure.	1. The efficient “ <i>Incremental Theory</i> ” of plasticity may not be applicable, but instead “ <i>the total strain theory</i> ”, (<i>Deformation Theory</i>) of plasticity should be used, which by the way has many doubtful assumptions.
2. The results normally converge to the exact solution.	2. There is no assurance to converge to the exact solution.
3. Loads are constant in each successive cycle of analysis.	3. Not applicable to “ <i>dynamic problems</i> ” or path dependent hysteretic materials.
4. Easier to use, easier to code in the computers.	4. Displacements, stresses and strains are determined for only the total load. No information is obtained for the intermediate steps of loading.
5. Convenient for the bi modular materials with different modulus of elasticity in tension and compression. $E_t \neq E_c$	
6. When combined with “ <i>Chord Modulus</i> ” approach, it becomes very successful for materials with <i>strain softening</i> .	

4.2.1. Geometrically Nonlinear Analysis

Geometric nonlinearities arise from significant changes in the structural configuration during loading. Common examples of geometric nonlinearity are plate structures which develop membrane behavior, or the geometric bifurcation of truss or shell structures. The changing applications of loads or boundary conditions are also geometrically nonlinear effects. The figure below shows two simple structural examples which serve as good illustrations of geometrically nonlinear behavior.

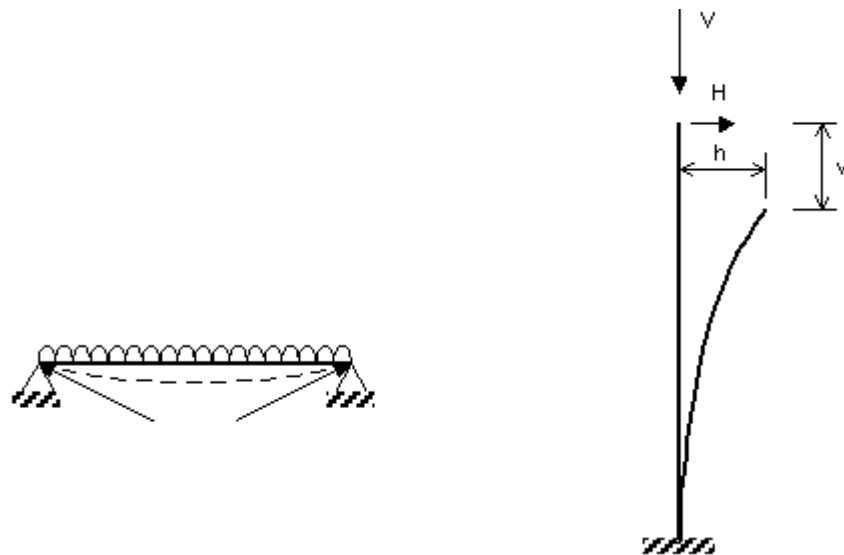


Figure 4.1. Illustrations of geometrically nonlinear behavior

For the simply supported beam (above left), the linear solution would predict the familiar simply supported bending moment and zero axial force. In reality as the beam deforms its length increases and an axial component of force is introduced.

For the loaded strut (above right), the linear solution would fail to consider the progressive eccentricity of the vertical load on the bending moment diagram. In both these cases depending on how large the deflections were, serious errors could be introduced if the effects of nonlinear geometry were neglected.

In LUSAS geometric nonlinearity is accounted for using four basic formulations:

- Total Lagrangian
- Updated Lagrangian
- Eulerian
- Co-rotational

In the Lagrangian formulations all variables are referred to a reference configuration. This will be the undeformed configuration in what is termed Total Lagrangian, or the configuration at the last converged solution in what is termed Updated Lagrangian. A Lagrangian approach tends to be preferred in structural problems where it is required to monitor the path of a particular particle through space. It is thus termed a referential or material description. The derivation which follows applies to both Total and Updated versions except where the differences are highlighted. The limits of integration are carried out over the undeformed configuration for the Total approach and the configuration at the last converged solution for the Updated approach.

In the Eulerian formulation all variables are referred to the deformed configuration. In the past this has been preferred for fluid problems where it is required to monitor the path of fluid through a particular control volume and not the path of one particle in its entirety. It is thus termed a spatial description. For structural problems its use has been limited as the deformed configuration is unknown. The formulation used in LUSAS is not Eulerian in the strictest sense but the term is used to avoid confusion with the Lagrangian description.

In the co-rotational formulation all strains are computed in a local frame which follows the element as it deforms. This approach is generally applicable, but is especially useful when used to formulate elements with rotational degrees of freedom. At present, this formulation is available for one beam element and for all 2D and 3D continuum elements including the solid composite elements.

4.2.2. Nonlinear Mixed Conditions

Deformation dependent boundary condition models account for the modifications to the external restraints resulting from lift-off, or smooth or frictional contact during the process within an analysis. Within LUSAS node on node may be accounted for using joint elements and arbitrary contact may be accounted for using slidelines. Consider the simple example shown in the figure 4.1 in which the structure and its supporting surface can resist being pushed together, but not being pulled apart. The required contact condition may be imposed by using joint elements to connect between the structure and the rigid support, and specifying a nonlinear contact joint model incorporating large, and zero local stiffnesses in compression and tension respectively.

4.2.3. Materially Nonlinear Analysis

Materially nonlinear effects arise from a nonlinear constitutive model (that is, progressively disproportionate stresses and strains). Common examples of nonlinear material behavior are the plastic yielding of metals, the ductile fracture of granular composites such as concrete or time-dependent behavior such as creep.

LUSAS incorporates a variety of nonlinear constitutive models, covering the behavior of the more common engineering materials. Details of these material models and their applicability to each LUSAS element are described in About Material Properties which should be read in conjunction with the Element Reference Manual.

4.3. Incremental Procedures

4.3.1. Regular (Basic) Incremental Procedure

The external loads are subdivided into equal or sometimes unequal divisions and each load increment is applied onto the system and a perfectly linear analysis is performed.

The displacements, stresses, and strains of each cycle are superimposed in order to obtain the total displacements, stresses, and strains. The regular incremental procedure is illustrated in Fig. 4.2. It is seen that in each cycle of analysis, a new updated stiffness matrix is used corresponding to the state of stress and material properties of the previous cycle. The governing equations are that:

Loads:

$$\{P\} = \sum_{i=1}^m \{\Delta P\}_i \quad (4.1)$$

(m is the number of increments)

Stiffness Equation:

$$[K]_{i-1} \{D\}_i = \{\Delta P\}_i \quad (4.2)$$

Total Displacements:

$$\{D\} = \sum_{i=1}^m \{D\}_i \quad (4.3)$$

The calculated force displacement curve is slightly different than the true force-displacement curve because of a small deviation from the exact solution as a result of piecewise linearization. The stiffness matrix in each cycle is based on the tangent moduli corresponding to the effective strains of the previous cycle. In fact, the proper “the tangent stiffness matrix” is used in each successive cycle. The constitutive law may be prescribed either in digital form or in functional form. It may be determined by the following testing methods:

- Uniaxial Testing
- Triaxial Testing
- Equivalent Stress-Strain Curve

4.3.2. Halved Incremental Procedure

The accuracy may be improved taking smaller load increments. For instance, in each load step half of the load increment is taken and the tangent stiffness matrix may be updated in the second half. At first, the analysis proceeds along the line A to H. Then with the updated tangent stiffness at half point H, the analysis proceeds along to H to C. The accuracy will be improved by moving the solution from B to C, but the number of load cycles will be doubled. This is illustrated in Fig. 4.3.

4.3.3. Midpoint Runge-Kutta Procedure

As already illustrated in Fig. 4.3, after the tangent stiffness matrix is updated at half point H, the full value of incremental load ΔP is applied at the beginning point A using the updated stiffness; therefore the linear analysis proceeds along the line A to D.

Here again two cycles of analysis are needed within each load increment. But the accuracy is much better than the previously described the basic increment and the halved increment procedures.

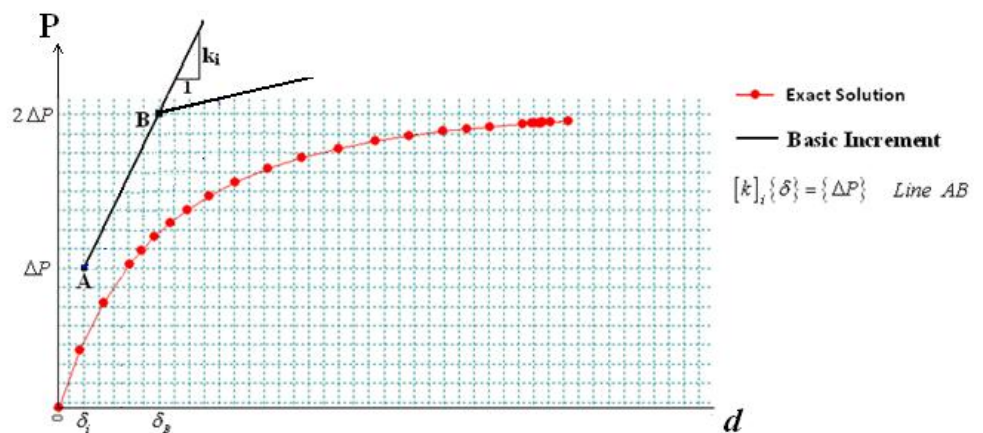


Figure 4.2. Basic incremental procedure

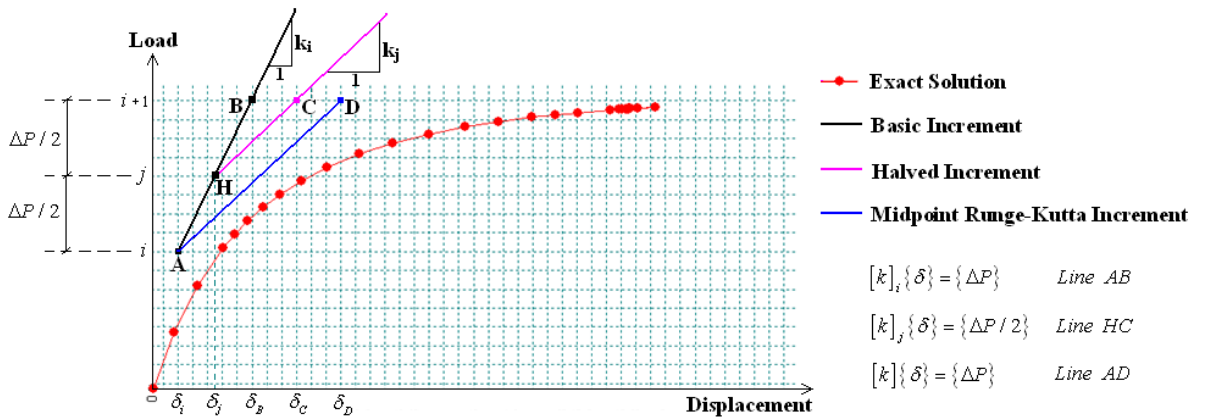


Figure 4.3. Halved and Runge – Kutta increments

4.4. Iterative Procedures

4.4.1. The Newton – Raphson Method

A sequence of analysis is repeated under the full unbalanced nodal nodes. Because we perform a linear analysis in each iteration, equilibrium is not necessarily satisfied between the given external loads and the calculated internal nodal forces.

Normally the linear iteration cycles for the compressive type (concave down) nonlinearity procedure deflections less than the true values. Therefore the internal strains and the resulting nodal forces will be less than the true values. Therefore the external loads will be larger than the internal loads. After each iteration the differences between the external loads and the internal calculated loads will be regarded as the unbalanced loads and these unbalanced loads will be used in the next step to compute in additional increment of displacements. This process will be repeated until the maximum unbalanced loads anywhere in the structure become less than a tolerable value.

The Newton – Raphson process is illustrated in Fig. 4.4. Initially the external loads are applied in the 1st cycle of linear analysis

$$[K]_0 \{D\}_1 = \{P\}_{ext} - \{0\} \tag{4.4}$$

Strains at the centroid of each element are calculated by

$$\{\varepsilon\}_1 = [G]\{d\}_1 \quad (4.5)$$

These strains are regarded as the initial strains $\{\varepsilon_0\}$ for the subsequent step and therefore, the equivalent nodal forces $\{P\}_0$ acting onto the elements are calculated corresponding to these initial strains from

$$\{P\}_{int,1} = \left(\int_V [G][D] dV \right) \{\varepsilon\}_1 \quad (4.6)$$

where, the material matrix is dependent on the state of stress of the previous cycle

$$[D] = [D(\sigma_{i-1})] = [D]^{ep} \quad (4.7)$$

These nodal forces are then superimposed at each node with those of the adjoining elements and a set of (fixed end reactions) internal nodal forces is obtained. The unbalanced nodal loads for the second cycle of analysis therefore, are

$$\{P\}_{unb,2} = \{P\}_{ext} - \{P\}_{int,1} \quad (4.8)$$

The next step is to modify the stiffness matrix of each element to accommodate the initial stresses and yielding conditions, if any. The new stiffness matrix is called the tangent stiffness matrix, which contains in it, the stresses of the previous cycle and the new material elastic constants. It is expected that the second cycle of linear analysis will proceed along the line B to C, tangent to the nonlinear force-deflection curve.

The closer the tangent stiffness matrix to the true value, faster is the convergence. But in each step there is a need for the calculation of a new tangent stiffness matrix. The total stresses and strains are obtained by superimposing algebraically the respective values of each cycle as;

$$\{\varepsilon\} = \sum \{\varepsilon\}_i \quad (4.9)$$

$$\{\sigma\} = \sum \{\sigma\}_i \quad (4.10)$$

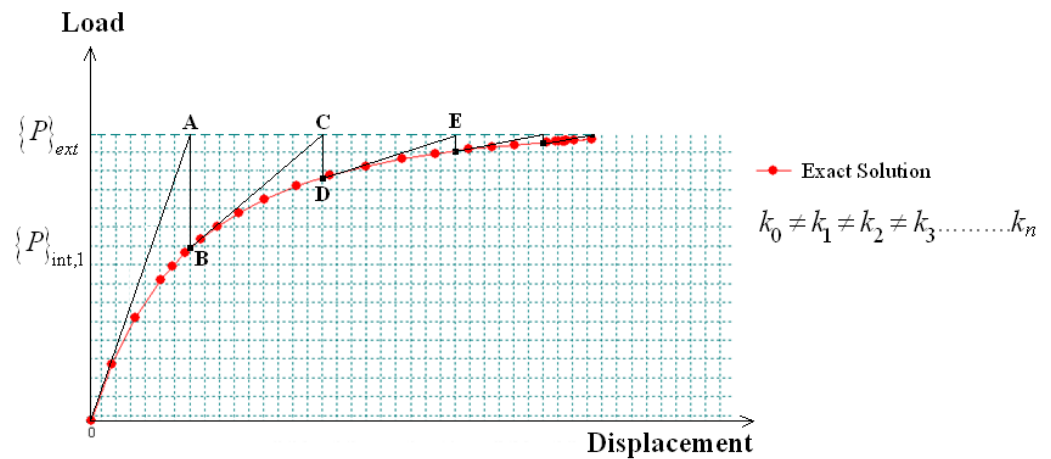


Figure 4.4. Newton – Raphson method

4.4.2. The Modified Newton – Raphson Method

In order to avoid the need for calculating the tangent stiffness matrix in each step, a constant stiffness, equal to the initial stiffness K_i is used throughout the iteration, as illustrated in Fig.4.5. Normally the tangent stiffness requires to invert a matrix and complicated numerical integration techniques. Thus a considerable saving is achieved in computations of stiffness calculations, if the stiffness matrix is assumed to remain constant. But with the availability of explicit forms of tangent stiffness matrices, there is practically no necessity any more to employ the Modified Newton – Raphson Method.

The number of iteration cycles in the modified procedure is substantially more than the regular Newton – Raphson Method, because the stiffness matrices will no longer be tangent to the nonlinear force–deflection curve.

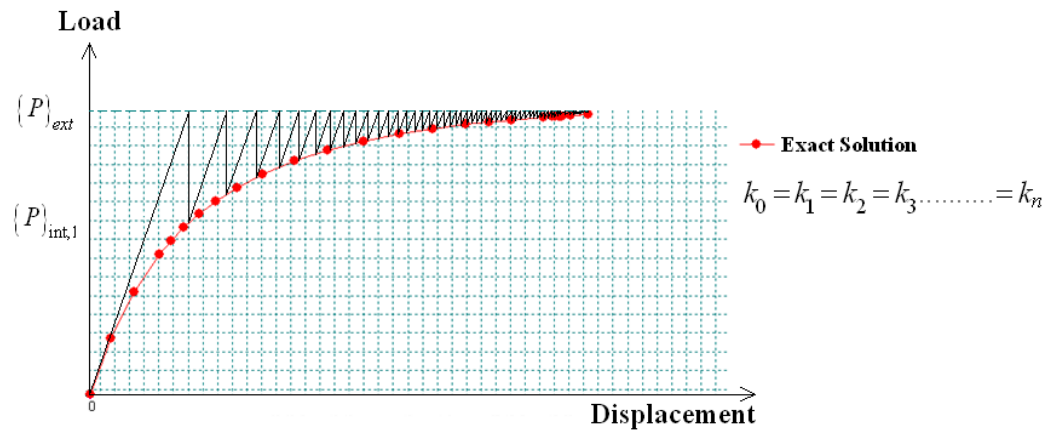


Figure 4.5. Modified Newton – Raphson method

4.4.3. Mixed Procedure

In order to benefit from the advantages of both the incremental and iterative procedures, the step-iteration or the mixed procedure is utilized as illustrated in Fig.4.6. It minimizes the disadvantages of each procedure.

In each load increment, an iterative solution procedure is used. The computational efforts are increased, but a higher accuracy is obtained than the pure incremental or pure iterative methods.

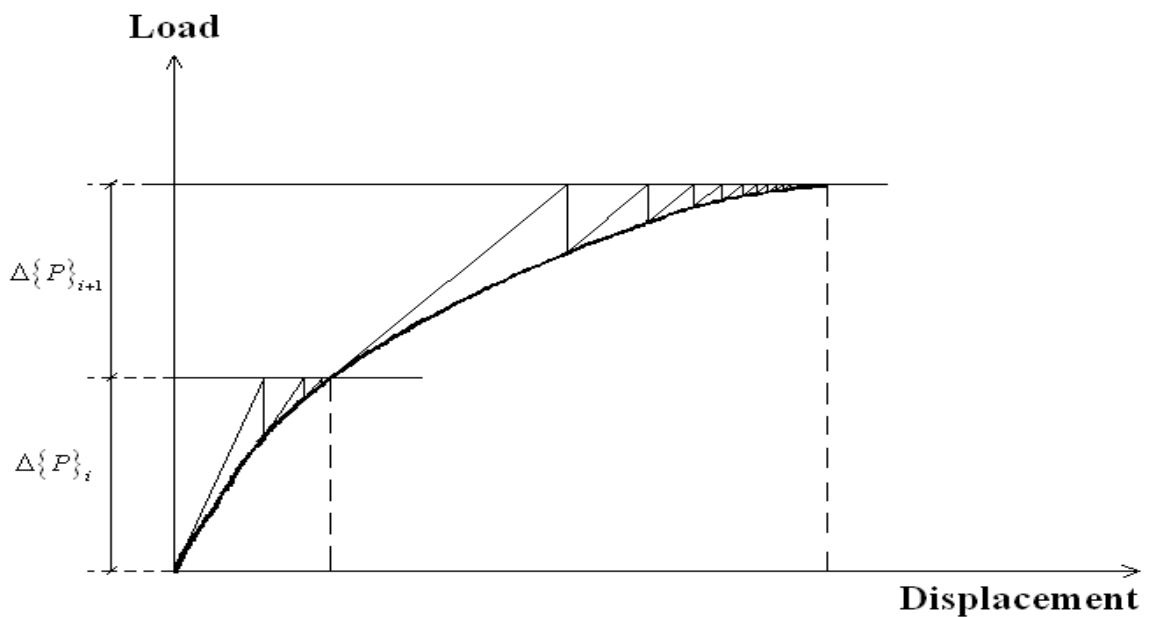


Figure 4.6. Mixed procedure

4.5. LUSAS as a Package Program

4.5.1. About LUSAS

Finite element methods are commonly utilized in the world by lots of investigators and researchers from lots of departments such as, especially, civil engineering, mechanical engineering, aircraft engineering, dentistry, and biomedical engineering and so on...LUSAS is famous and familiar one of them. Therefore in the Chapter 5 and 6 the LUSAS is chosen as a package program in order to use and gain the nonlinear solutions from the test samples and the dome structure. As it is known that LUSAS is a computer program and so its mathematical calculations and the secrets, which are hidden behind the interface of the program, are very significant.

4.5.2. Nonlinear Solution Procedure of LUSAS

For nonlinear analysis, since it is no longer possible to directly obtain a stress distribution which equilibrates a given set of external loads, a solution procedure is usually adopted in which the total required load is applied in a number of increments.

Within each increment a linear prediction of the nonlinear response is made, and subsequent iterative corrections are performed in order to restore equilibrium by the elimination of the residual or 'out of balance' forces.

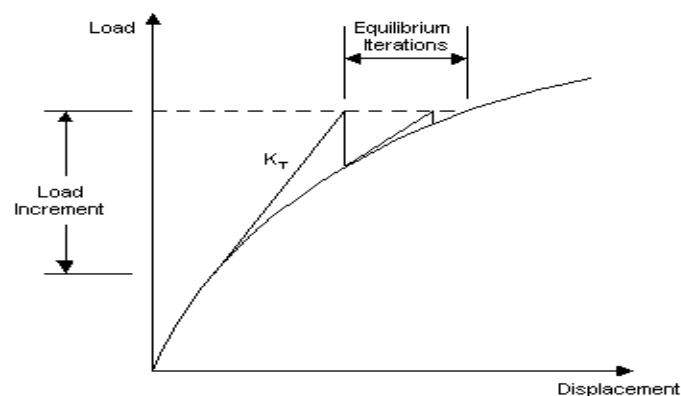


Figure 4.7. Nonlinear solution procedure of LUSAS

The iterative corrections are referred to some form of convergence criteria which indicates to what extent an equilibrate state has been achieved. **Such a solution procedure is therefore commonly referred to as an incremental-iterative (or predictor-corrector) method shown in the figure above. In LUSAS, the nonlinear solution is based on the Newton-Raphson procedure.** The details of the solution procedure are controlled using the Nonlinear Control properties assigned to load case.

For the analysis of nonlinear problems, the solution procedure adopted may be of significance to the results obtained. In order to reduce this dependence, wherever possible, nonlinear control properties incorporate a series of generally applicable default settings, and automatically activated facilities.

4.5.3. Iterative Procedure

In LUSAS the incremental-iterative solution is based on Newton-Raphson iterations. In the Newton-Raphson procedure an initial prediction of the incremental solution is based on the “*tangent stiffness*” from which incremental displacements and their iterative corrections may be derived.

4.5.4. Standard Newton – Raphson Method

In the standard Newton-Raphson procedure each iterative calculation is always based upon the current tangent stiffness. For finite element analysis, this involves the formation (and factorization) of the tangent stiffness matrix at the start of each iteration.

Although the standard Newton-Raphson method generally converges rapidly, the continual manipulation of the stiffness matrix is often expensive. The need for a robust yet inexpensive procedure therefore leads to the development of the family of modified Newton-Raphson methods.

4.5.5. Iterative Acceleration (*Line Searches*)

A slow convergence rate may be significantly improved by employing an iterative acceleration technique. In cases of severe and often localized nonlinearity, encountered typically in materially nonlinear or contact problems, some form of acceleration may be a prerequisite to convergence.

In LUSAS, iterative acceleration may be performed by applying line searches. In essence, the line search procedure involves extra optimization iterations, in which the potential energy associated with the residual forces at each iterative step, are minimized. Line search application is controlled via parameters on the Iteration section of the Nonlinear Control properties.

The selection of line search parameters is problem dependent and largely a matter of experience. However, a maximum of 3 to 5 line search iterations with a tolerance of 0.3 to 0.8 is usually sufficient. (The closer the tolerance is to unity, the more slack the minimum energy requirement)

4.5.6. Separate Iterative Loops

In problems where both material and contact nonlinearities are present convergence difficulties can arise when evaluating material nonlinearities in configurations where the contact conditions are invalid because the solution is not in equilibrium. To avoid this situation contact equilibrium can be established using elastic properties from the previous load increment before the material nonlinearity is resolved. The option to define separate iterative loops is defined on advanced solution strategy dialog which can be found on the nonlinear control form.

4.5.7. Incremental Procedure

For the Newton-Raphson solution procedures it is assumed that a displacement solution may be found for a given load increment and that, within each load increment, the load level remains constant. Such methods are therefore often referred to as constant load level incrementation procedures. For instance, in the analysis of the dome structure of the Chapter 6, the constant load level incrementation is chosen as 50.

However, where limit points in the structural response are encountered (for example in the geometrically nonlinear case of snap-through failure) constant load level methods will, at best, fail to identify the load shedding portion of the curve and, at worst, fail to converge at all past the limit point. The solution of limit point problems therefore leads to the development of alternative methods, including displacement incrementation and constrained solution methods.

4.5.8. Constrained solution methods (arc-length)

Constrained methods differ from constant level methods in that the load level is not required to be constant within an increment. In fact the load and displacement levels are constrained to follow some pre-defined path.

In LUSAS two forms of arc-length method have been implemented:

- Crisfield's modified arc-length procedure in which the solution is constrained to lie on a spherical surface defined in displacement space. For the one degree of freedom case this becomes a circular arc.
- Rheinboldt's arc-length algorithm which constrains the largest displacement increment (defined by the predictor) to remain constant for that particular increment.

The use of the arc-length method has the following advantages over constant load level methods:

- Improved convergence characteristics
- Ability to detect and negotiate limit points

In LUSAS, control of arc-length solution procedures is via the Incrementation section of the Nonlinear Control properties. If required, the solution may be started under constant load control, and automatically switched to arc-length control based on a specified value of the current stiffness parameter (defined as the scaled inner product of displacements and loads). The required stiffness parameter for automatic conversion to arc-length control is input in the Incrementation section of Nonlinear Control properties.

Where limit points are encountered, LUSAS will automatically determine the sign of the next load increment by the sign of the determinant of the stiffness matrix. This is a reliable method in most cases; however, it will often fail in the vicinity of bifurcation points when negative eigenvalues may cause premature unloading. In such cases the load reversal criteria may be optionally changed to be dependent on the sign of the current stiffness parameter. This method is better at coping with bifurcation points, but will always fail when a snap-back situation is encountered.

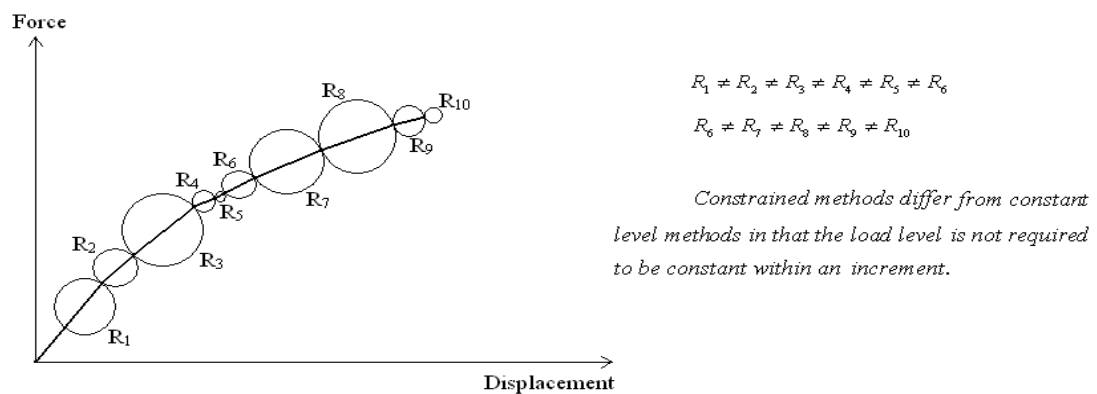


Figure 4.8. Arc – length method

4.5.9. Automatic increment reduction

Where an increment has failed to converge within the specified maximum number of iterations it will be automatically reduced and re-applied. This will be repeated according to values specified in the step reduction section (Advanced dialog) until the maximum number of reductions has been tried. In a final attempt to achieve a solution the load increment is then increased to try and step over a difficult point in the analysis. If after this the solution has still failed to converge to the solution terminated.

5. EXAMPLE DOME STRUCTURES

5.1. Types of Domes

About the sorts of the dome shapes, it can be said that there are remarkably 4 types of dome shapes. These different dome shapes are generally used in everywhere. These are:

- Schwedler Domes
 - With Diagonals
 - No Diagonals
- Lattice Domes
- Lamella Domes
- Geodesic Domes

According to the paper (Richter *et al.*, 1975), the strength of these dome types are different in each other compared with their weight. This dome geometry comparison is that:

Table 5.1. General types of dome structures (Richter *et al.*, 1975)

	DOMES TYPES				
	Schwedler Domes		Lattice Domes	Lamella Domes	Geodesic Domes
	Diagonal	No Diag.			
Dome Weight (kg)	4500	4500	4500	4500	4500
Number of Nodes	61	61	61	61	61
Maximum Unbalanced Load (kg/m ²)	205	90	147	205	293
Relative Strength	70%	30%	50%	70%	100%
Deflection with under the Unbalanced Load	3.9 cm.	45 cm.	4.2 cm.	2.2 cm.	2.2 cm.
All domes are the same overall size; that is, 30 meters in diameter and in a spherical radius and all are 43 meters high.					
All four are completely triangulated space-truss configurations.					

The geodesic dome type is commonly used in all over the world because of some advantages such as its high strength and light-weight property. But in this Thesis, the lattice dome shape is selected to research in Chapter 7.

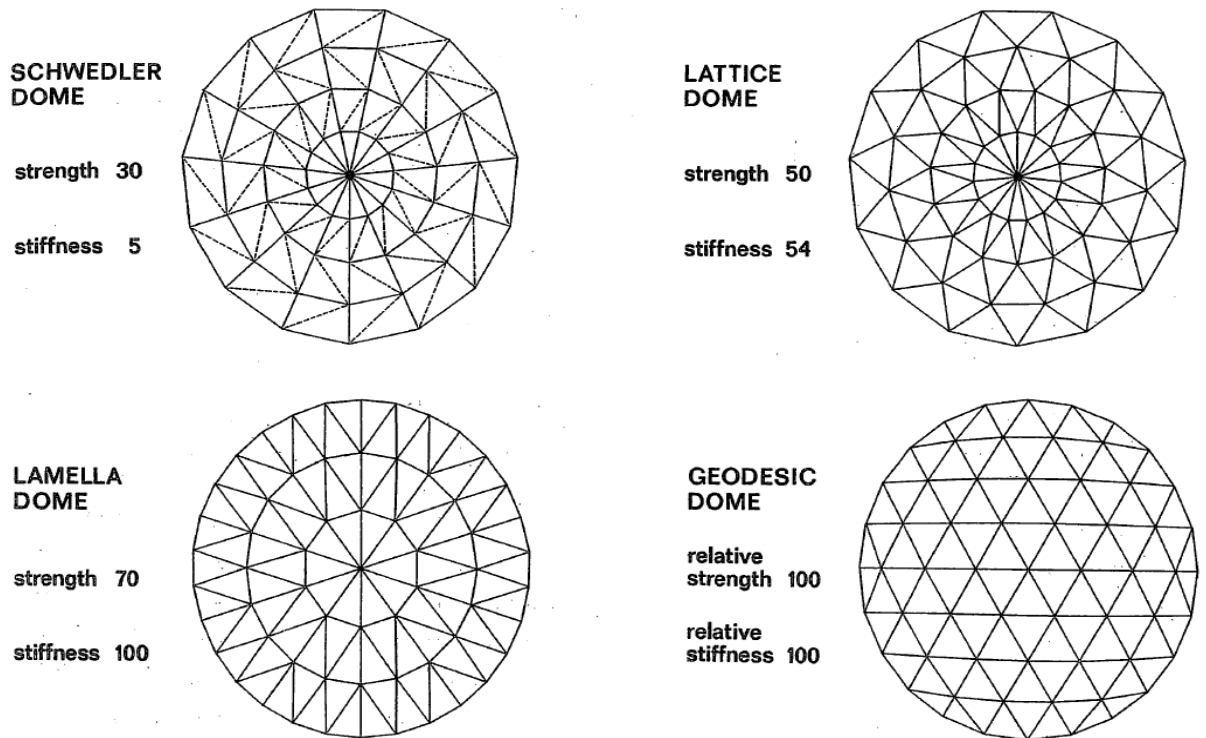


Figure 5.1. Shapes of dome types

5.2. Significant and Famous Dome Structures in the World

Until now lots of dome structures have been built in the world. Their materials consist of not only concrete but also steel. Some of them could succeed to be live into our era. Below is a list of buildings that have held the title of the largest dome compared with the held record times of the structures:

Table 5.2. Largest domes with ranking to the time

Dates	Diameter	Name	Location	Builders
1stc.BC– 19 BC	21.5 m	Temple of Mercury	Baiae, Italy	Roman Empire
128–1436	43.4 m	Pantheon	Rome, Italy	Roman Empire
1436–1881	45 m	The Duomo	Florence, Italy	City state of Florence
1881–1902	46.9 m	Devonshire Royal Hospital	Buxton, UK	Cotton Famine Relief Fund
1902–1913	59.45 m	West Baden Springs Hotel	West Baden, Indiana, USA	Lee Wiley Sinclair
1913–1930	65.0 m	Centennial Hall	Breslau, Poland	Deutsches Reich
1930–1957	65.8 m	Leipzig Market Hall	Leipzig, Germany	Deutsches Reich
1957–1965	109 m	Belgrade Fair - Hall 1	Belgrade, Serbia	Belgrade Fair
1965–1975	195.5 m	Reliant Astrodome	Housto, Texas, USA	H.A. Lott, Inc.
1975–1992	207 m	Louisiana Superdome	New Orleans, USA	City State of New Orleans
1992 – <i>present</i>	256.0 m	Georgia Dome	Atlanta, Georgia, USA	Georgia World Congress Center Authority

From the above table the *Louisiana Superdome* in New Orleans, USA was built from the structural steel frame and due to this property it is like our lattice dome structure which is searched in the Chapter 7. An aspect from its picture and some properties of the Louisiana Superdome are that:

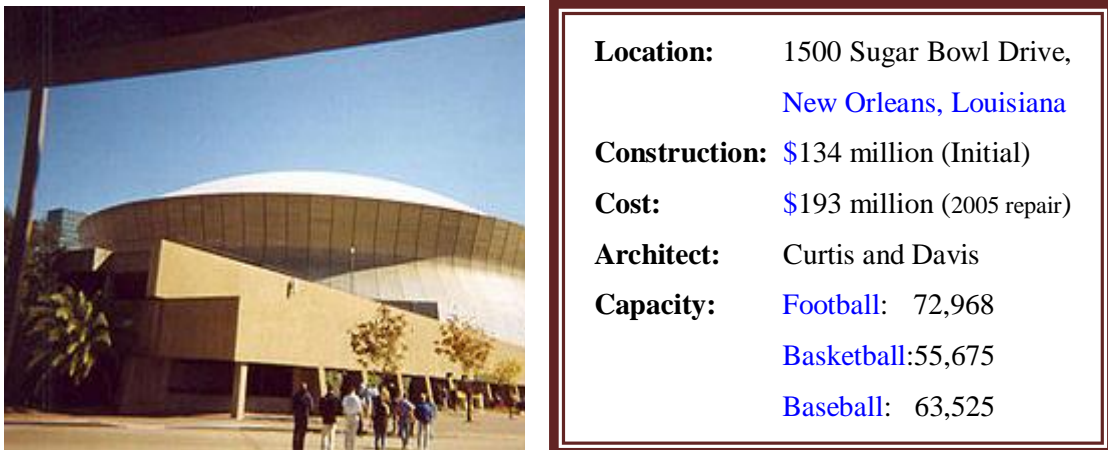


Figure 5.2. An aspect from the Louisiana Superdome

Of course, a dome structure may have different kinds of the materials such as stone, concrete, masonry, wood, cast iron, steel and reinforced concrete and so on... Below is a list of buildings that have held the title of the largest dome in terms of their structure:

Table 5.3. Dome structures by their materials

Material	Diameter	Name	Location	Builder
Stone	14.5 m	Treasury - Atreus	Mycenae, Greece	City of Mycenae
	15.0 m	Western Thermae	Gerasa, Jordan	Roman Empire
Concrete	6.52 m	Stabiae Thermae	Pompeii, Italy	Roman Empire
	21.5 m	Temple Mercury	Baiae, Italy	Roman Empire
	43.4 m	Pantheon	Rome, Italy	Roman Empire
Masonry	11.5 m	Red Hall	Pergamon, Turkey	Roman Empire
	23.85 m	Zeus Temple	Pergamon, Turkey	Roman Empire
	24.15 m	Rotunda – George	Thessaloniki, Greece	Roman Empire
	31.5 m	Hagia Sophia	Istanbul, Turkey	Byzantine Empire
	45 m	The Duomo	Florence, Italy	City of Florence
Wood	20.40 m	Dome of the Rock	Jerusalem, Israel	Umayyad Empire
	36.0 m	St. Blaise's Abbey	St. Blaise, Germany	Pierre M. d'Ixnard
	153.0 m	Walkup Skydome	Flagstaff, Arizona, USA	Northern Arizona University

Table 5.4. Dome structures by their materials (Cont.)

Material	Diameter	Name	Location	Builder
Wood	161.5 m	Tacoma Dome	Tacoma, Washington, USA	City of Tacoma, WA
	163.4 m	Superior Dome	Marquette, Michigan, USA	State of Mich./Northern Michigan Uni.
Cast iron	29.0 m	US Capitol dome	Washington D.C., USA	USA
Steel	59.45 m	West Baden Springs Hotel	West Bade, Indiana, USA	Lee Wiley Sinclair
	195.5 m	Relian Astrodome	Houston, Texas, USA	H.A. Lott, Inc.
	207 m	Louisiana Superdome	New Orleans, USA	City State of New Orleans
Reinforced Concrete	65.0 m	Centennial Hall	Breslau, Poland	Deutsches Reich
	65.8 m	Leipzig Hall	Leipzig, Germany	Deutsches Reich
	100.6 m	Palazzo dello Sport	Rome, Italy	1960 Summer Olympics
	121.9 m	Assembly Hall	Champaign, Illinois, USA	Uni. of Illinois Urbana- Champaign
	134.1 m	Norfolk Scope	Norfolk, Virginia, USA	City of Norfolk
	201.0 m	Kingdome	Seattle, Washington, USA	King County, Washington

If it is wanted that the famous steel dome structures, which are listed in Table 5.4., are shown from outside and inside:



Figure 5.3. An aspect of the outside view of West Baden Springs Hotel



Figure 5.4. An aspect of the inside view of West Baden Springs Hotel



Figure 5.5. An aspect of the inside view of Relian Astrodome



Figure 5.6. An aspect of the outside view of Relian Astrodome

6. TEST EXAMPLES

6.1. About the Test Examples

The aim of this Chapter of the Thesis is to test solution the skills of usage of the computer program (LUSAS) and to control with the exact solutions. Totally there are three different test samples and their separately solutions and errors or the similarity compared with the exact solutions by using the LUSAS as a package program in this Chapter.

6.2. The First Illustrative Numerical Example

In this part of the test examples, the stability of the pin-connected two member arch system shown in Fig. 6.1 is investigated by using the computer program, LUSAS. And for this problem (*two member arch system*), the properties of the two member arch system are that:

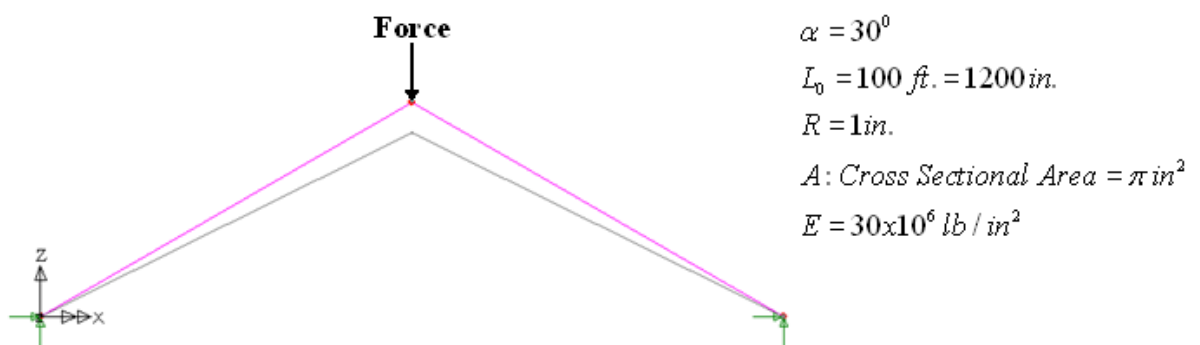


Figure 6.1. Two member arch system and the point load

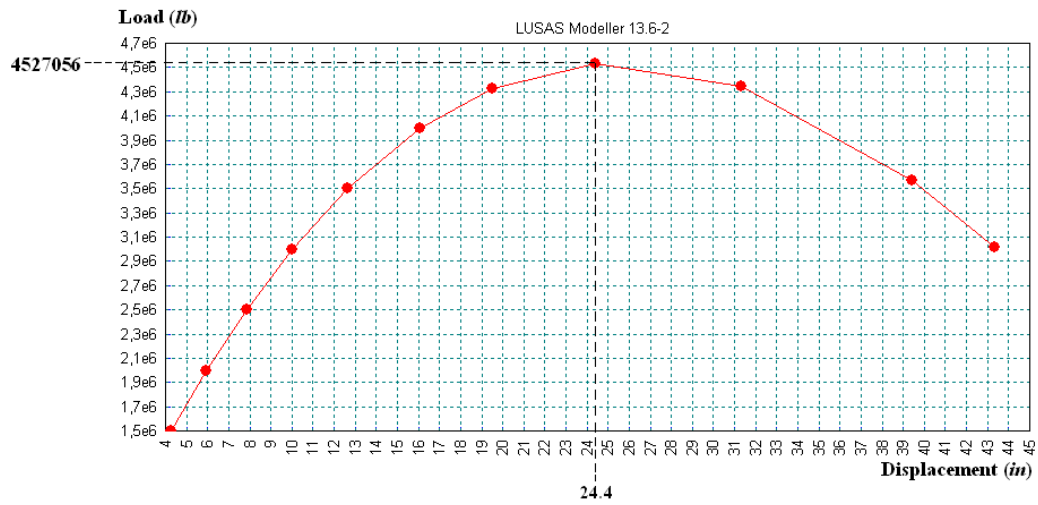


Figure 6.2. Solution of two member arch system from LUSAS

According to the LUSAS;

$$P_{\max.} = \frac{(4527056 \text{ lb.})}{2(\pi \text{ in}^2)(30 \times 10^6 \text{ lb/in}^2)}$$

$$\frac{P_{CR}}{2AE} = 0.024$$

$$d_{CR} = 24.4 \text{ in.}$$

According to the Paper (Tezcan and Ovunc, 1966);

$$\frac{P_{CR}}{2AE} = 0.0276$$

$$d_{CR} = 22.6 \text{ in.}$$

6.3. The Second Illustrative Numerical Example

In this test example of a circular arch, with a concentrated load P acting at the crest is shown in Fig. 6.4. is investigated by using the computer program, LUSAS. And for this problem (*Non-linear Buckling of a Circular Arch*), the properties of the circular arch system are that:

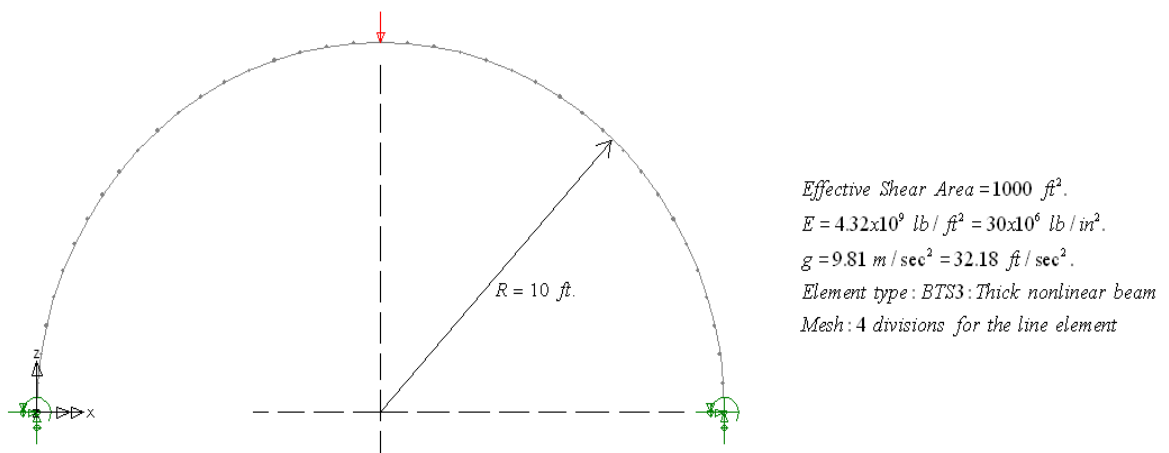


Figure 6.3. Circular arch and the point load

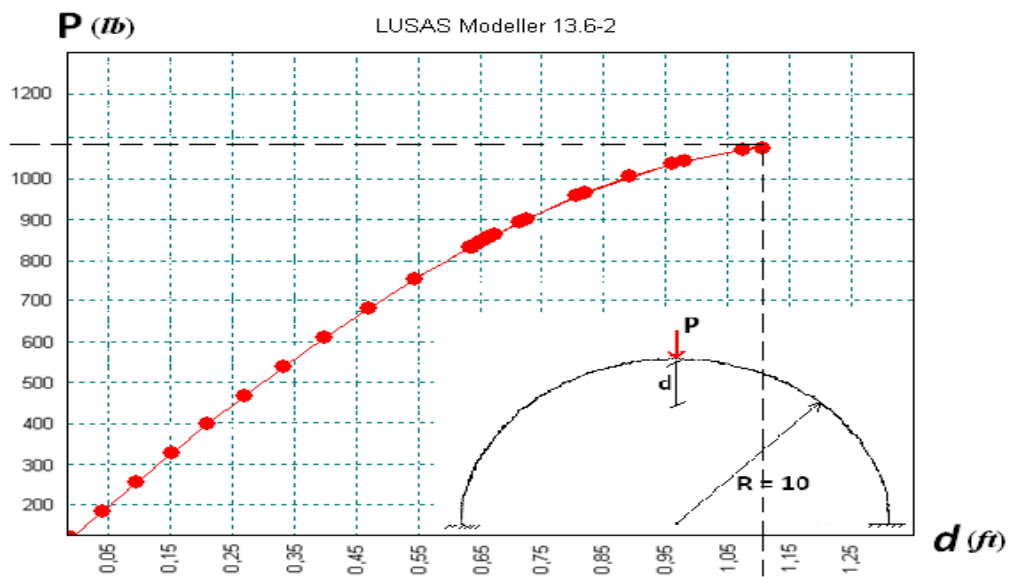


Figure 6.4. Solution of circular arch system from LUSAS

According to the LUSAS;

$$P_{CR} = 1066.79 \text{ lb.}$$

$$d_{CR} = 1.12 \text{ ft.}$$

According to the Paper (Tezcan and Ovunc, 1966);

$$P_{CR} = 956 \text{ lb.}$$

$$d_{CR} \cong 0.908 \text{ ft.}$$

Table 6.1. Comparison of two different solutions

Displacement Values From the LUSAS				
Directions	Point 1	Point 3	Point 4	Point 6 (Top)
X direction (ft.)	0	-0.3931	-0.2502	0
Y direction (ft.)	0	0.1082	-0.0668	-0.9363
Z direction (rad.)	0	0.0049	-0.1447	0

Displacement Values From the Paper (Tezcan and Ovunc, 1966)				
Directions	Point 1	Point 3	Point 4	Point 6 (Top)
X direction (ft.)	0	-0.3902	-0.2394	0
Y direction (ft.)	0	0.1094	-0.0520	-0.9083
Z direction (rad.)	0	0.0050	-0.1412	0

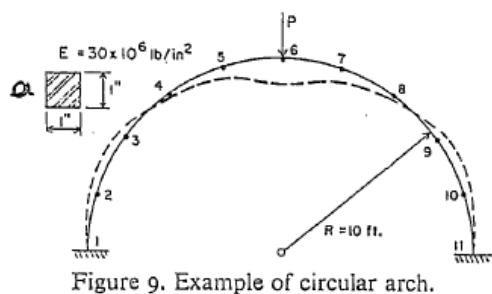


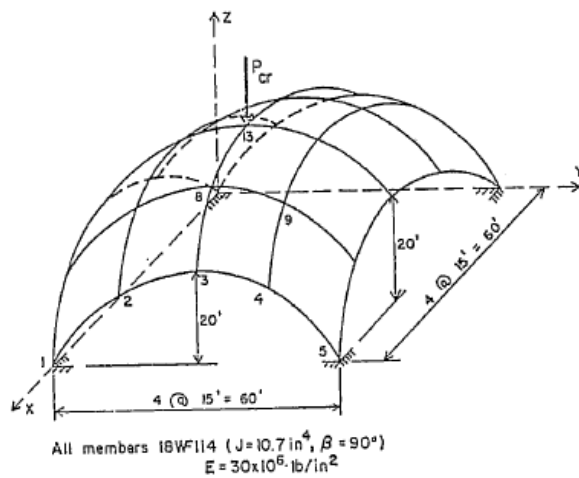
Figure 9. Example of circular arch.

	Joint numbers			
	1	3	4	6
$P = 940 \text{ lb}$				
Deformations				
$\delta_1 \text{ ft}$	0	-0.3902	-0.2394	0
$\delta_2 \text{ ft}$	0	0.1094	-0.0520	-0.9083
$\delta_3 \text{ rad}$	0	0.0050	-0.1412	0

Figure 6.5. Circular arch and the deformations of the joints (Tezcan and Ovunc, 1966)

6.4. The Third Illustrative Numerical Example

In this test example of a parabolic dome, which has a concentrated load P acting at its top point is shown in Fig. 6.7. is investigated by using the computer program, LUSAS. And for this problem (*Non-linear Buckling of a Parabolic Dome*), the properties of the circular arch system are that:



- $A = 0.17 \text{ ft}^2$.
- $I_{xx} = 15.9 \times 10^{-3} \text{ ft}^4$.
- Torsion Constant, $J = 0.517 \times 10^{-3} \text{ ft}^4$.
- Effective Shear Area = 1000 ft^2 .
- $E = 4.32 \times 10^9 \text{ lb/ft}^2 = 30 \times 10^6 \text{ lb/in}^2$.
- Element type: *BTS3* = thick nonlinear beam
- Mesh: 4 divisions for the line element

Figure 6.6. Parabolic dome and the point load (Tezcan and Ovunc, 1966)

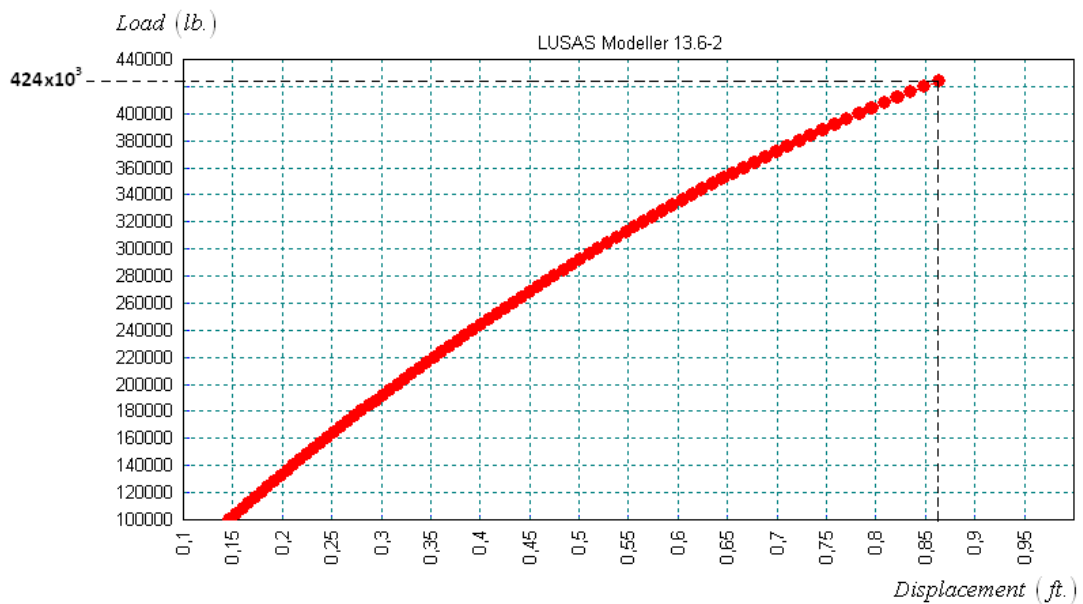


Figure 6.7. Solution of the parabolic dome system from LUSAS

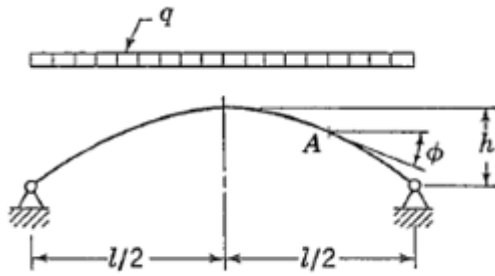
Table 6.2. Comparison of two different solutions

Displacement Values From the LUSAS				
Directions	Point 3	Point 8	Point 9	Point 13 (Top)
X direction (ft.)	0.3008	0,0074	0.0311	0
Y direction (ft.)	0	0	0.0311	0
Z direction (rad.)	-0.1037	-0,5651	-0.4049	-0.8633
Displacement Values From the Paper (Tezcan and Ovunc, 1966)				
Directions	Point 3	Point 8	Point 9	Point 13 (Top)
X direction (ft.)	0.3906	0.0799	0.0420	0
Y direction (ft.)	0	0	0.0420	0
Z direction (rad.)	-0.0084	-0.3469	-0.2376	-0.5603

6.5. The Fourth Illustrative Example

According to the book whose name is *Theory of Elastic Stability*, if an arch system is under a uniformly distributed load, for the buckling case the arch's critical load can be expressed by the formula below:

$$q_{cr} = \gamma_4 \frac{EI}{l^3} \quad (6.1)$$



q_{cr} = The critical Load,

γ_4 = The Constant value from the Table 6.3.

l = The length of the span for the arch system.

q = Uniformly distributed load

Figure 6.8. Arch system with no hinges (Timoshenko *et al.*, 1961)

Table 6.3. Values of the factor for the arch system (Timoshenko *et al.*, 1961)

$\frac{h}{l}$	No hinges γ_4	One hinge γ_4	Two hinges γ_4	Three hinges γ_4
0.1	60.7	33.8	28.5	22.5
0.2	101	59	45.4	39.6
0.3	115	46.5	46.5
0.4	111	96	43.9	43.9
0.5	97.4	38.4	38.4
0.6	83.8	80	30.5	30.5
0.8	59.1	59.1	20.0	20.0
1.0	43.7	43.7	14.1	14.1

In this test sample, the properties of the problem are that:

$$h = 8 \text{ m.}$$

$$l = 20 \text{ m.}$$

$$A = 1 \text{ m}^2 \text{ (Cross sectional area : } 1 \times 1_{\text{square}} \text{)}$$

$$I = \frac{1}{12} (1 \text{ m.}) (1 \text{ m}^3) = 0.0833 \text{ m}^4$$

$$\Rightarrow \frac{h}{l} = 0.4, \quad \Rightarrow \gamma_4 = 111$$

$$E = 200 \times 10^6 \text{ kN / m}^2$$

$$\Rightarrow q_{cr} = \gamma_4 \frac{EI}{l^3} = 111 \frac{(200 \times 10^6 \text{ kN / m}^2)(0.0833 \text{ m}^4)}{(20 \text{ m})^3} = 231157.5 \text{ kN / m}.$$

In this test example, the data are applied by using the computer program, LUSAS. According to the program, the load displacement graph is that:

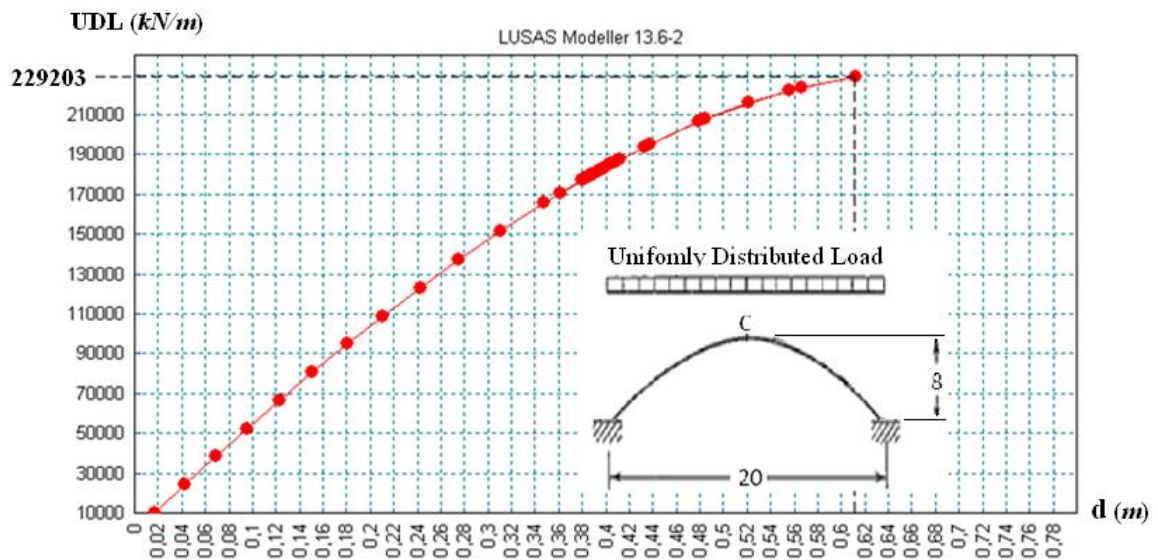


Figure 6.9. Solution of the parabolic arch system from LUSAS

Error:

$$E = \frac{\{q_{cr}\}_T - \{q_{cr}\}_L}{\{q_{cr}\}_T} = \frac{231157.5 - 229203}{231157.5} = 0.84 \times 10^{-2} = 0.84\%$$

7. NONLINEARITY OF A DOME AS A SPACE STRUCTURE

7.1. About the Dome

This lattice dome structure is a kind of space structures whose elements are steel bars and have different sections. It is covered by using the flexi glass because of the strong and lightweight materials. Moreover all supports are pinned.

About the physical properties of the dome is that its height is exactly 30 m. The diameter of the dome is approximately 72 m. And so this structure is the largest dome in Turkey and it has a good place in the list of the largest domes in the world.

To refer to the goal of using the dome is that it may be used for lots of different aims such as sports activities, concert and theater areas, cultural activities, great organizations, and botanic parks and so on...

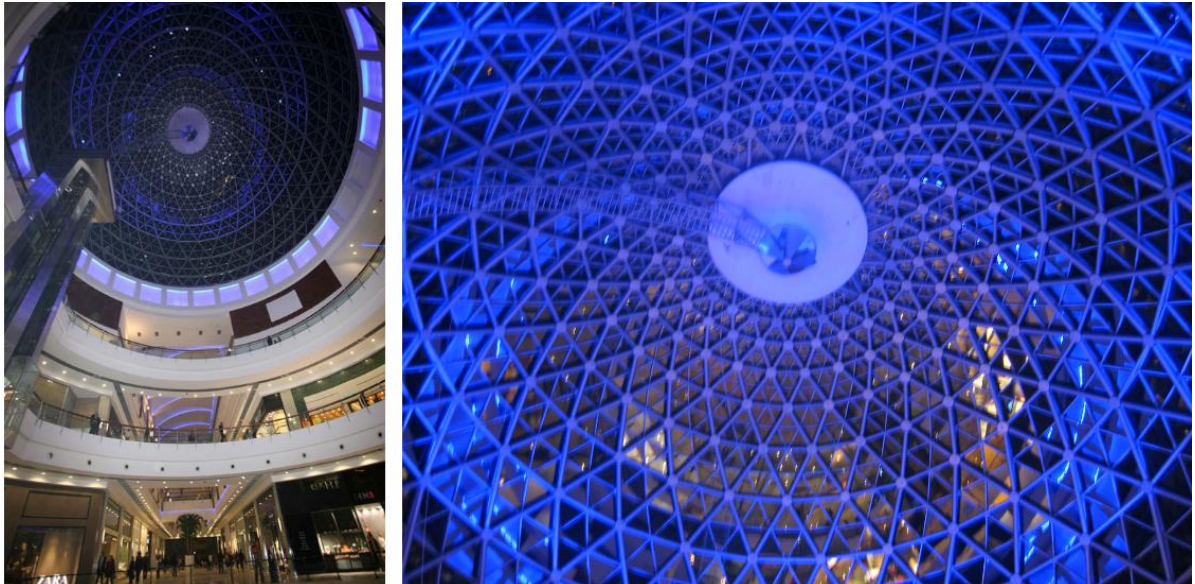


Figure 7.1. An example for lattice dome structures, Panora Alış-Veriş Merkezi, Ankara

7.2. Plan View of the Lattice - Dome

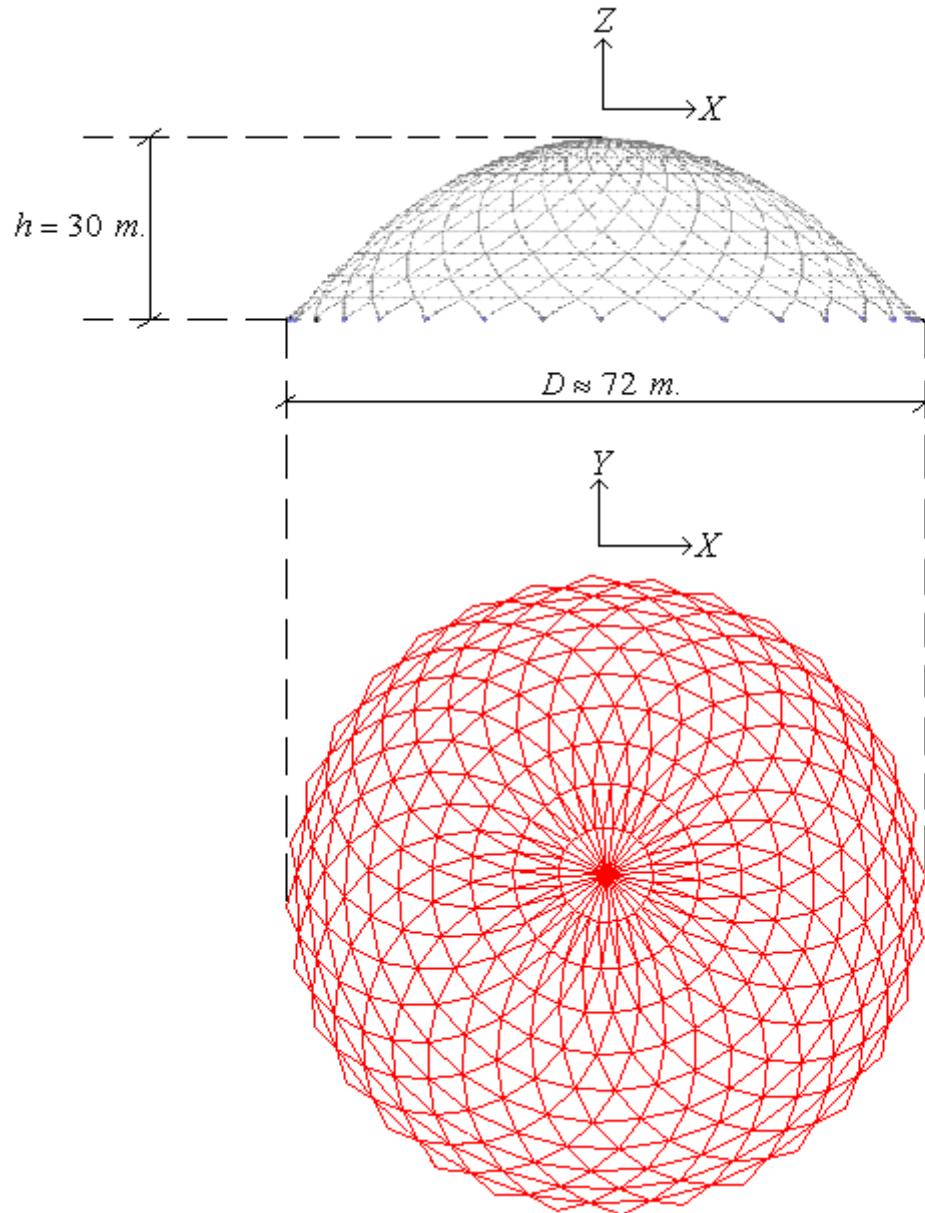


Figure 7.2. Plan view of the lattice-dome

7.3. Modeling the Dome with LUSAS

There are totally 620 members, and some of them form the groups in each other. So that there are 21 different member groups, and these groups have their own properties such as their length and sections...Moreover 353 points exist in this dome structure. And the orders of these coordinates of these points are that:

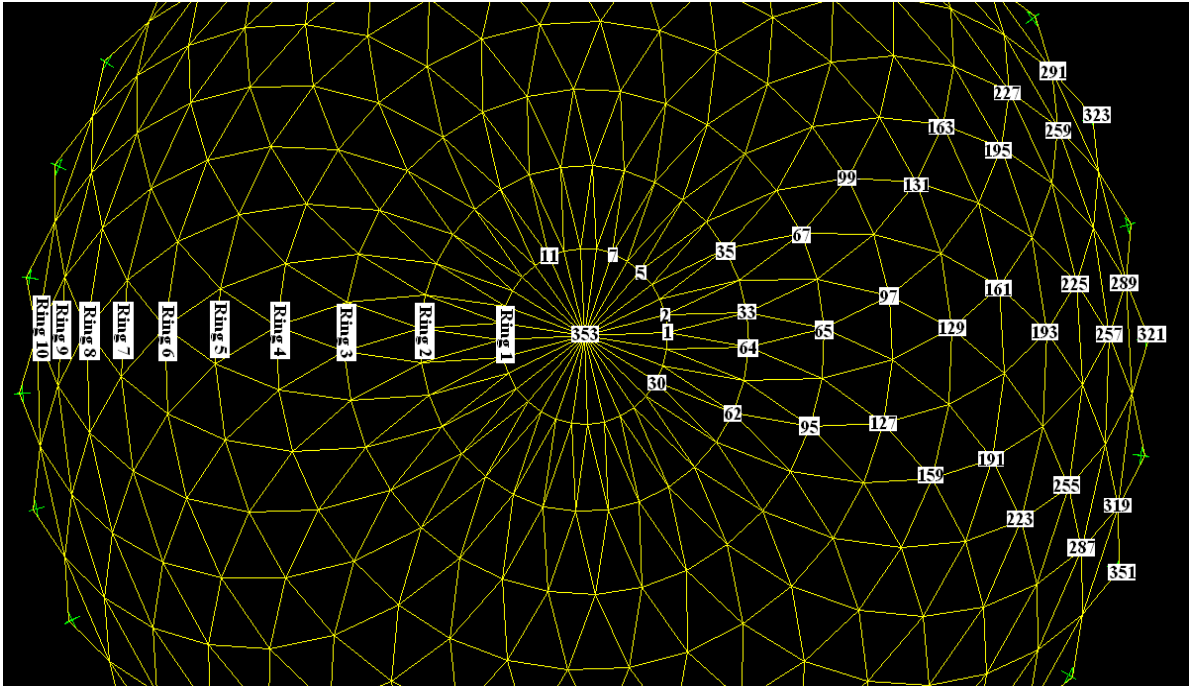


Figure 7.3. Rings and the nodes of the dome structure

Table 7.1. Calculation of nodal coordinates

Ring No.	X-Coordinates	Y-Coordinates
1	$4 \cos \theta_n$	$4 \sin \theta_n$
2	$8 \cos \theta_1 \cos \theta_n$	$8 \cos \theta_{33} \sin \theta_n$
3	$(2.X_{33} - X_1) \cos \theta_n$	$(2.X_{33} - X_1) \sin \theta_n$
4	$(2.X_{65} \cos \theta_{97} - \frac{X_{33}}{\cos \theta_{97}}) \cos \theta_n$	$(2.X_{65} \cos \theta_{97} - \frac{X_{33}}{\cos \theta_{97}}) \sin \theta_n$
5	$(2.X_{97} - X_{65}) \cos \theta_n$	$(2.X_{97} - X_{65}) \sin \theta_n$
6	$(2.X_{129} \cos \theta_{161} - \frac{X_{97}}{\cos \theta_{161}}) \cos \theta_n$	$(2.X_{129} \cos \theta_{161} - \frac{X_{97}}{\cos \theta_{161}}) \sin \theta_n$
7	$(2.X_{161} - X_{129}) \cos \theta_n$	$(2.X_{161} - X_{129}) \sin \theta_n$
8	$(2.X_{193} \cos \theta_{225} - \frac{X_{161}}{\cos \theta_{225}}) \cos \theta_n$	$(2.X_{193} \cos \theta_{225} - \frac{X_{161}}{\cos \theta_{225}}) \sin \theta_n$
9	$(2.X_{225} - X_{193}) \cos \theta_n$	$(2.X_{225} - X_{193}) \sin \theta_n$
10	$(2.X_{257} \cos \theta_{289} - \frac{X_{225}}{\cos \theta_{289}}) \cos \theta_n$	$(2.X_{257} \cos \theta_{289} - \frac{X_{225}}{\cos \theta_{289}}) \sin \theta_n$
11 <i>(for the support points)</i>	$(2.X_{289} - X_{257}) \cos \theta_n$	$(2.X_{289} - X_{257}) \sin \theta_n$
All	Z-Coordinates	
	$30 - \frac{5}{216}(X_n^2 + Y_n^2)$	
$\theta_n = \text{Numerical value of } \theta \text{ angles for each node are supplied in Table 7.2.}$		

Table 7.2. Coordinates of all points of the dome

Node No.	Angle θ	X (m)	Y (m)	Node No.	Angle θ	X (m)	Y (m)
Ring No:1	$Z_1 = 29.62963$ m.			Ring No:7	$Z_7 = 14.48508$ m.		
1	0	39.99(†)	0.00(†)	193	0	61.87956	0
2	11.25	39.91363	0.78036	194	11.25	61.38211	5.05070
3	22.5	39.68601	1.53073	195	22.5	59.90887	9.90732
4	33.75	39.31636	2.22228	196	33.75	57.51646	14.38319
5	45	38.81892	2.82842	197	45	54.29683	18.30634
6	56.25	38.21277	3.32587	198	56.25	50.37368	21.52597
7	67.5	37.52122	3.69551	199	67.5	45.89781	23.91838
8	78.75	36.77085	3.92314	200	78.75	41.04119	25.39162
9	90	35.99049	4	201	90	35.99049	25.88907
10	101.25	35.21012	3.92314	202	101.25	30.93978	25.39162
11	112.5	34.45975	3.69551	203	112.5	26.08316	23.91838
12	123.75	33.76820	3.32587	204	123.75	21.60729	21.52597
13	135	33.16206	2.82842	205	135	17.68414	18.30634
14	146.25	32.66461	2.22228	206	146.25	14.46451	14.38319
15	157.5	32.29497	1.53073	207	157.5	12.07210	9.90732
16	168.75	32.06734	0.78036	208	168.75	10.59886	5.05070
17	180	31.99049	4.9E-16	209	180	10.10141	3.1E-15
18	191.25	32.06734	-0.78036	210	191.25	10.59886	-5.05070
19	202.5	32.29497	-1.53073	211	202.5	12.07210	-9.90732
20	213.75	32.66461	-2.22228	212	213.75	14.46451	-14.38319
21	225	33.16206	-2.82842	213	225	17.68414	-18.30634
22	236.25	33.76820	-3.32587	214	236.25	21.60729	-21.52597
23	247.5	34.45975	-3.69550	215	247.5	26.08316	-23.91838
24	258.75	35.21012	-3.92314	216	258.75	30.93978	-25.39162
25	270	35.99049	-4	217	270	35.99049	-25.88907
26	281.25	36.77085	-3.92314	218	281.25	41.04119	-25.39162
27	292.5	37.52122	-3.69553	219	292.5	45.89781	-23.91838

Table 7.2. Coordinates of all points of the dome (Cont.)

Node No.	Angle θ	X (m)	Y (m)	Node No.	Angle θ	X (m)	Y (m)
28	303.75	38.21277	-3.32587	220	303.75	50.37368	-21.52597
29	315	38.81891	-2.82842	221	315	54.29683	-18.30634
30	326.25	39.31636	-2.22228	222	326.25	57.51646	-14.38319
31	337.5	39.68600	-1.53073	223	337.5	59.90887	-9.90732
32	348.75	39.91363	-0.78036	224	348.75	61.38211	-5.05070
Ring No:2	$Z_2 = 28.53275$ m.			Ring No:8	$Z_8 = 10.72465$ m.		
33	5.625	43.91363	0.78036	225	5.625	64.70799	2.82842
34	16.875	43.60914	2.31109	226	16.875	63.60439	8.37658
35	28.125	43.01188	3.75301	227	28.125	61.43961	13.60283
36	39.375	42.14479	5.05070	228	39.375	58.29683	18.30634
37	50.625	41.04119	6.15430	229	50.625	54.29683	22.30634
38	61.875	39.74350	7.02139	230	61.875	49.59332	25.44912
39	73.125	38.30158	7.61865	231	73.125	44.36707	27.61390
40	84.375	36.77085	7.92314	232	84.375	38.81891	28.71750
41	95.625	35.21012	7.92314	233	95.625	33.16206	28.71750
42	106.88	33.67939	7.61865	234	106.88	27.61390	27.61390
43	118.13	32.23747	7.02139	235	118.13	22.38765	25.44912
44	129.38	30.93978	6.15430	236	129.38	17.68414	22.30634
45	140.63	29.83618	5.05070	237	140.63	13.68414	18.30634
46	151.88	28.96909	3.75301	238	151.88	10.54136	13.60283
47	163.13	28.37183	2.31109	239	163.13	8.37658	8.37658
48	174.38	28.06734	0.78036	240	174.38	7.27298	2.82842
49	185.63	28.06734	-0.78036	241	185.63	7.27298	-2.82842
50	196.88	28.37183	-2.31109	242	196.88	8.37658	-8.37658
51	208.13	28.96909	-3.75301	243	208.13	10.54136	-13.60283
52	219.38	29.83618	-5.05070	244	219.38	13.68414	-18.30634
53	230.63	30.93978	-6.15430	245	230.63	17.68414	-22.30634
54	241.88	32.23747	-7.02139	246	241.88	22.38765	-25.44912

Table 7.2. Coordinates of all points of the dome (Cont.)

Node No.	Angle θ	X (m)	Y (m)	Node No.	Angle θ	X (m)	Y (m)
55	253.13	33.67939	-7.61865	247	253.13	27.61390	-27.61390
56	264.38	35.21012	-7.92314	248	264.38	33.16206	-28.71750
57	275.63	36.77085	-7.92314	249	275.63	38.81891	-28.71750
58	286.88	38.30158	-7.61865	250	286.88	44.36707	-27.61390
59	298.13	39.74350	-7.02139	251	298.13	49.59332	-25.44912
60	309.38	41.04119	-6.15430	252	309.38	54.29683	-22.30634
61	320.63	42.14479	-5.05070	253	320.63	58.29683	-18.30634
62	331.88	43.01188	-3.75301	254	331.88	61.43961	-13.60283
63	343.13	43.60914	-2.31109	255	343.13	63.60439	-8.376586
64	354.38	43.91363	-0.78036	256	354.38	64.70799	-2.828427
Ring No:3	$Z_3 = 26.75151$ m.			Ring No:9	$Z_9 = 6.96422$ m.		
65	0	47.83677	0	257	0	67.53641	0
66	11.25	47.60914	2.31109	258	11.25	66.93027	6.15430
67	22.5	46.93502	4.53337	259	22.5	65.13512	12.07210
68	33.75	45.84031	6.58144	260	33.75	62.21997	17.52597
69	45	44.36707	8.37658	261	45	58.29683	22.30634
70	56.25	42.57193	9.84982	262	56.25	53.51646	26.22948
71	67.5	40.52386	10.94453	263	67.5	48.06259	29.14463
72	78.75	38.30158	11.61865	264	78.75	42.14479	30.93978
73	90	35.99049	11.84628	265	90	35.99049	31.54592
74	101.25	33.67939	11.61865	266	101.25	29.83618	30.93978
75	112.5	31.45711	10.94453	267	112.5	23.91838	29.14463
76	123.75	29.40904	9.84982	268	123.75	18.46451	26.22948
77	135	27.61390	8.37658	269	135	13.68414	22.30634
78	146.25	26.14066	6.58144	270	146.25	9.76100	17.52597
79	157.5	25.04595	4.53337	271	157.5	6.84585	12.07210
80	168.75	24.37183	2.31109	272	168.75	5.05070	6.15430
81	180	24.14420	1.4E-15	273	180	4.44456	3.8E-15

Table 7.2. Coordinates of all points of the dome (Cont.)

Node No.	Angle θ	X (m)	Y (m)	Node No.	Angle θ	X (m)	Y (m)
82	191.25	24.37183	-2.31109	274	191.25	5.05070	-6.15430
83	202.5	25.04595	-4.53337	275	202.5	6.84585	-12.07210
84	213.75	26.14066	-6.58144	276	213.75	9.76100	-17.52597
85	225	27.61390	-8.37658	277	225	13.68414	-22.30634
86	236.25	29.40904	-9.84982	278	236.25	18.46451	-26.22948
87	247.5	31.45711	-10.94477	279	247.5	23.91838	-29.14463
88	258.75	33.67939	-11.61865	280	258.75	29.83618	-30.93978
89	270	35.99049	-11.84628	281	270	35.9904	-31.54592
90	281.25	38.30158	-11.61865	282	281.25	42.14479	-30.93978
91	292.5	40.52386	-10.94453	283	292.5	48.06259	-29.14463
92	303.75	42.57193	-9.84982	284	303.75	53.51646	-26.22948
93	315	44.36707	-8.37658	285	315	58.29683	-22.30634
94	326.25	45.84031	-6.58144	286	326.25	62.21997	-17.52597
95	337.5	46.93502	-4.53337	287	337.5	65.13512	-12.07210
96	348.75	47.60914	-2.31109	288	348.75	66.93027	-6.15430
Ring No:4	$Z_4 = 24.35438$ m.			Ring No:10	$Z_{10} = 3.34829$ m.		
97	5.625	51.53229	1.53073	289	5.625	69.75870	3.32587
98	16.875	50.93502	4.53337	290	16.875	68.46100	9.84982
99	28.125	49.76345	7.36180	291	28.125	65.91549	15.99524
100	39.375	48.06259	9.90732	292	39.375	62.21997	21.52597
101	50.625	45.89781	12.07210	293	50.625	57.51646	26.22948
102	61.875	43.35229	13.77296	294	61.875	51.98573	29.92500
103	73.125	40.52386	14.94453	295	73.125	45.84031	32.47051
104	84.375	37.52122	15.54180	296	84.375	39.31636	33.76821
105	95.625	34.45975	15.54180	297	95.625	32.66461	33.76821
106	106.88	31.45711	14.94453	298	106.88	26.14066	32.47051
107	118.13	28.62868	13.77296	299	118.13	19.99524	29.92500
108	129.38	26.08316	12.07210	300	129.38	14.46451	26.22948

Table 7.2. Coordinates of all points of the dome (Cont.)

Node No.	Angle θ	X (m)	Y (m)	Node No.	Angle θ	X (m)	Y (m)
109	140.63	23.91838	9.90732	301	140.63	9.76100	21.52597
110	151.88	22.21752	7.36180	302	151.88	6.06548	15.99524
111	163.13	21.04595	4.53337	303	163.13	3.51997	9.84982
112	174.38	20.44868	1.53073	304	174.38	2.22227	3.32587
113	185.63	20.44868	-1.53073	305	185.63	2.22227	-3.32587
114	196.88	21.04595	-4.53335	306	196.88	3.51997	-9.84982
115	208.13	22.21752	-7.36180	307	208.13	6.06548	-15.99524
116	219.38	23.91838	-9.90732	308	219.38	9.76100	-21.52597
117	230.63	26.08316	-12.07210	309	230.63	14.46451	-26.22948
118	241.88	28.62868	-13.77296	310	241.88	19.99524	-29.92500
119	253.13	31.45711	-14.94453	311	253.13	26.14066	-32.47051
120	264.38	34.45975	-15.54180	312	264.38	32.66461	-33.76821
121	275.63	37.52122	-15.54180	313	275.63	39.31636	-33.76821
122	286.88	40.52386	-14.94453	314	286.88	45.84031	-32.47051
123	298.13	43.35229	-13.77296	315	298.13	51.98573	-29.92500
124	309.38	45.89781	-12.07210	316	309.38	57.51646	-26.22948
125	320.63	48.06259	-9.90732	317	320.63	62.21997	-21.52597
126	331.88	49.76345	-7.36180	318	331.88	65.91549	-15.99524
127	343.13	50.93502	-4.53337	319	343.13	68.46100	-9.84982
128	354.38	51.53229	-1.53073	320	354.38	69.75870	-3.32587
Ring No:5	$Z_5 = 21.43346$ m.			Ring No:11	$Z_{11} = 0$ m. (<i>Support Points</i>)		
129	0	55.22780	0	321	0	71.98098	0
130	11.25	54.85816	3.75301	322	11.25	71.28943	7.02139
131	22.5	53.76345	7.36180	323	22.5	69.24136	13.77296
132	33.75	51.98573	10.68768	324	33.75	65.91549	19.99524
133	45	49.59332	13.60283	325	45	61.43961	25.44912
134	56.25	46.67817	15.99524	326	56.25	55.98573	29.92500
135	67.5	43.35229	17.77296	327	67.5	49.76345	33.25087

Table 7.2. Coordinates of all points of the dome (Cont.)

Node No.	Angle θ	X (m)	Y (m)	Node No.	Angle θ	X (m)	Y (m)
136	78.75	39.74350	18.86767	328	78.75	43.01188	35.29894
137	90	35.99049	19.23731	329	90	35.99049	35.99049
138	101.25	32.23747	18.86767	330	101.25	28.96909	35.29894
139	112.5	28.62868	17.77296	331	112.5	22.21752	33.25087
140	123.75	25.30280	15.99524	332	123.75	15.99524	29.92500
141	135	22.38765	13.60283	333	135	10.54136	25.44912
142	146.25	19.99524	10.68768	334	146.25	6.06548	19.99524
143	157.5	18.21752	7.36180	335	157.5	2.73961	13.77296
144	168.75	17.12281	3.75301	336	168.75	0.69154	7.02139
145	180	16.75317	2.3E-15	337	180	-1.5E-06	4.4E-15
146	191.25	17.12281	-3.75301	338	191.25	0.69154	-7.02139
147	202.5	18.21752	-7.36180	339	202.5	2.73961	-13.77296
148	213.75	19.99524	-10.68768	340	213.75	6.06548	-19.99524
149	225	22.38765	-13.60283	341	225	10.54136	-25.44912
150	236.25	25.30280	-15.99524	342	236.25	15.99524	-29.92500
151	247.5	28.62868	-17.77296	343	247.5	22.21752	-33.25087
152	258.75	32.23747	-18.86767	344	258.75	28.96909	-35.29894
153	270	35.99049	-19.23731	345	270	35.99049	-35.99049
154	281.25	39.74350	-18.86767	346	281.25	43.01188	-35.29894
155	292.5	43.35229	-17.77296	347	292.5	49.76345	-33.25087
156	303.75	46.67817	-15.99524	348	303.75	55.98573	-29.92500
157	315	49.59332	-13.60283	349	315	61.43961	-25.44912
158	326.25	51.98573	-10.68768	350	326.25	65.91549	-19.99524
159	337.5	53.76345	-7.36180	351	337.5	69.24136	-13.77296
160	348.75	54.85816	-3.75301	352	348.75	71.28943	-7.021396

Table 7.2. Coordinates of all points of the dome (Cont.)

Node No.	Angle θ	X (m)	Y (m)	Node No.	Angle θ	X (m)	Y (m)
Ring No:6	$Z_6 = 18.10101$ m.			Ring No:6	$Z_6 = 18.10101$ m.		
161	5.625	58.55368	2.22228	177	185.63	13.42729	-2.22228
162	16.875	57.68659	6.58144	178	196.88	14.29438	-6.58144
163	28.125	55.98573	10.68768	179	208.13	15.99524	-10.68768
164	39.375	53.51646	14.38319	180	219.38	18.46451	-14.38319
165	50.625	50.37368	17.52597	181	230.63	21.60729	-17.52597
166	61.875	46.67817	19.99524	182	241.88	25.30280	-19.99524
167	73.125	42.57193	21.69610	183	253.13	29.40904	-21.69610
168	84.375	38.21277	22.56319	184	264.38	33.76820	-22.56319
169	95.625	33.76820	22.56319	185	275.63	38.21277	-22.56319
170	106.88	29.40904	21.69610	186	286.88	42.57193	-21.69610
171	118.13	25.30280	19.99524	187	298.13	46.67817	-19.99524
172	129.38	21.60729	17.52597	188	309.38	50.37368	-17.52597
173	140.63	18.46451	14.38319	189	320.63	53.51646	-14.38319
174	151.88	15.99524	10.68768	190	331.88	55.98573	-10.68768
175	163.13	14.29438	6.58144	191	343.13	57.68659	-6.58144
176	174.38	13.42729	2.22228	192	354.38	58.55368	-2.22228
Ring No:0	$Z_0 = 30$ m.			(†) In reality 9 significant digits have been utilized for X and Y values in computer application.			
353	-----	0	0				

To be necessary to explain the modeling briefly that a 3 dimensional nonlinear beam is selected as the element description in LUSAS. The number of mesh divisions is 4. This small value is used for this model. Because the smaller values and the bigger values are tried and it is easily seen that the 4 value is the optimum point for the number of mesh divisions. It means that the results of the analysis are same for the 4 and the bigger values. And in order to go to the exact solution in the smallest time by using the computer and so the 4 value is selected. Moreover the sections of the steel bar elements are assigned. There are totally 21 different sections for the elements. These sections were determined according to the local buckling analysis of the all members. The bar elements are a isotropic material whose the young modulus is 200×10^6 kN/m². About the supports, all of them are assigned as a pinned support. Finally as a loading type, three different cases are used for this dome nonlinear analysis. The first one is vertical load case with snow and dead loads. The second one is about wind load with dead and live loads, and third loading case is combination of earthquake load with dead and live loads. This load cases are appropriate according to TS-500.

7.4. Loading and Constraints

All of the supports are only pinned for this structure. Thus at the bottom of the dome there are totally 32 pinned supports. About the loadings, there are three kinds of load combination for this dome, and the first one consists of the dead load and the snow load as a live load. And the second load combination is constituted from the dead load and wind load as a live load. The third load combination is formed by the dead load and the earthquake load. As to the calculation of these load types, the TDY-2007 was used for the calculation of the equivalent static earthquake load. For the snow and wind forces on the stories (rings) of the dome structure, the TS-498 was used.

7.4.1. Application of TDY-2007 for the Structure

SAP-200 was used in order to get the periods of the modes of the dome structure. According to the analysis at the SAP-2000 package program, the period of the first mode is 0.25 seconds. And so $T_n = 0.25$ sec.

For the first seismic zone, $A_0 = 0.40$

Table 7.3. Effective ground acceleration coefficient

Seismic Zone	A_0
1	0.40
2	0.30
3	0.20
4	0.10

For all of the local site class $T_A < T_n < T_B$

Table 7.4. Spectrum characteristic periods

Local Site Class	T_A (sec.)	T_B (sec.)
Z1	0.10	0.30
Z2	0.15	0.40
Z3	0.15	0.60
Z4	0.20	0.90

For the spectrum coefficient, $S(T) = 2.5$ ($T_A < T_n < T_B$)

For the building importance factor, $I = 1.2$

Table 7.5. Building importance factor

Purpose of Occupancy or Type of Building	Importance Factor (I)
<p>1. Building to be utilized after the earthquake and buildings containing hazardous materials</p> <p>a) Buildings required to be utilized immediately after the earthquake (Hospitals, dispensaries, health wards, fire fighting buildings and facilities, PTT and other communication facilities, transportation stations and terminals, power generation and distribution facilities; governorate, country and municipality administration buildings, first aid and emergency planning stations)</p> <p>b) Buildings containing or storing toxic, explosive and flammable materials, etc.</p>	1.5
<p>2. Intensively and long-term occupied buildings and buildings preserving valuable goods</p> <p>a) Schools, other educational buildings or facilities, dormitories and hostels, military barracks, prisons, etc.</p> <p>b) Museums</p>	1.4
<p>3. Intensively but short-term occupied buildings</p> <p>Sport facilities, cinema, theatre and concert halls, etc.</p>	1.2
<p>4. Other buildings</p> <p>Buildings other than above defined buildings. (Residential and office buildings, hotels, building-like industrial structures, etc.)</p>	1.0

For the spectral acceleration coefficient,

$$A(T) = A_0 I S(T) \quad (7.1)$$

$$A(T) = (0.40) (1.2) (2.5)$$

$$A(T) = 1.2$$

For the structural behavior factor, $R = 5.6$ (from UBC, for the steel ordinary braced frames)

$$R_a(T) = R = 5.6 \quad (T_n > T_A)$$

$$W = \sum (w_i) = \sum (g_i + n q_i), \quad (n=30\%, \text{ since snow load shall be considered as dead load}) \quad (7.2)$$

$$W = 23.99 + 92.45 + 180.31 + 274.41 + 375.43 + 488.49 + 592.54 + 672.84 + 742.48 + \dots + 803.30 + 828.13 = 5074.38 \text{ kN.}$$

$$V_t = W A(T_1) / R_a(T_1) \geq (0.10) A_0 I W \quad (7.3)$$

$$V_t = (5074.38) (1.2) / (5.6) \geq (0.10) (0.40) (1.2) (5074.38)$$

$$V_t = 1087.37 \geq 243.57 \rightarrow \text{Acceptable!}$$

$$V_t = \Delta F_N + \sum(F_i) \quad (7.4)$$

$$\Delta F_N = (0.07) T_1 V_t \leq (0.2) V_t \quad (7.5)$$

$$\Delta F_N = (0.07) (0.25) (1087.37) \leq (0.2) (1087.37)$$

$$\Delta F_N = 19.03 \leq 217.47 \rightarrow \text{Acceptable!}$$

$$F_i = (V_t - \Delta F_N) (w_i H_i / \sum(w_j H_j)) \quad (7.6)$$

$$\begin{aligned} \sum(w_j H_j) &= [(828.13).(3.35)] + [(803.3).(6.96)] + [(742.48).(10.72)] + \\ &\dots[(672.84).(14.49)] + [(592.54).(18.10)] + [(488.49).(21.43)] + \\ &\dots[(375.43).(24.35)] + [(274.41).(26.75)] + [(180.31).(28.53)] + \\ &\dots[(92.45).(29.63)] + [(23.99).(30)] \end{aligned}$$

$$\begin{aligned} \sum(w_j H_j) &= 2774.24 + 5590.97 + 7959.38 + 9749.45 + 10724.97 + 10468.34 + \\ &\dots 9141.72 + 7340.47 + 5144.24 + 2739.29 + 719.70 \end{aligned}$$

$$\sum(w_j H_j) = 72352.77$$

$$F_{10} = (1087.37 - 19.03) [(828.13) (3.35) / (72352.77)]$$

$$F_{10} = 40.96 \text{ kN.}$$

$$F_9 = (1087.37 - 19.03) [(803.3) (6.96) / (72352.77)]$$

$$F_9 = 82.56 \text{ kN.}$$

$$F_8 = (1087.37 - 19.03) [(742.48) (10.72) / (72352.77)]$$

$$F_8 = 117.53 \text{ kN.}$$

$$F_7 = (1087.37 - 19.03) [(672.84) (14.49) / (72352.77)]$$

$$F_7 = 143.96 \text{ kN.}$$

$$F_6 = (1087.37 - 19.03) [(592.54) (18.10) / (72352.77)]$$

$$F_6 = 158.36 \text{ kN.}$$

$$F_5 = (1087.37 - 19.03) [(488.49) (21.43) / (72352.77)]$$

$$F_5 = 154.57 \text{ kN.}$$

$$F_4 = (1087.37 - 19.03) [(375.43) (24.35) / (72352.77)]$$

$$F_4 = 134.98 \text{ kN.}$$

$$F_3 = (1087.37 - 19.03) [(274.41) (26.75) / (72352.77)]$$

$$F_3 = 108.39 \text{ kN.}$$

$$F_2 = (1087.37 - 19.03) [(180.31) (28.53) / (72352.77)]$$

$$F_2 = 75.96 \text{ kN.}$$

$$F_1 = (1087.37 - 19.03) [(92.45) (29.63) / (72352.77)]$$

$$F_1 = 40.45 \text{ kN.}$$

$$F_{0(N)} = (1087.37 - 19.03) [(23.99) (30) / (72352.77)] + 19.03$$

$$F_{0(N)} = 29.66 \text{ kN.}$$

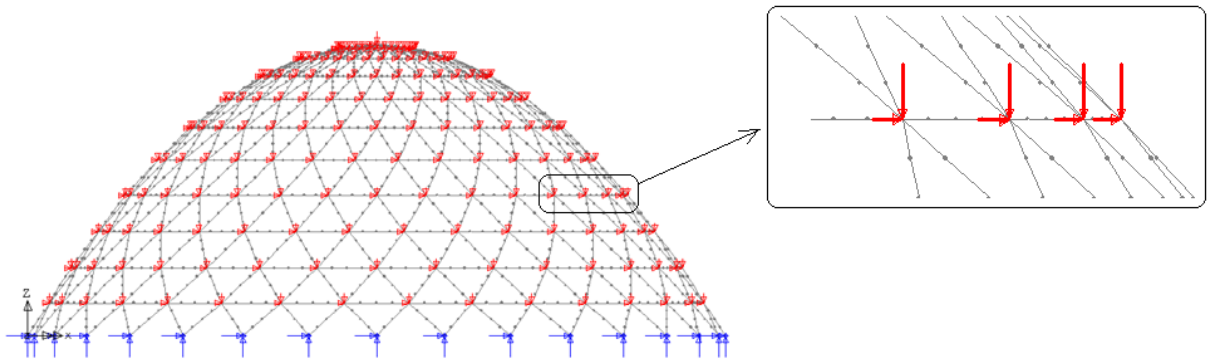


Figure 7.4. Dead and earthquake loads on the points of the dome

7.4.2. Application of TS-498 for the Structure (*For Wind Loads*)

About the Areas of the Points for the Wind and Snow Loads:

The 3-D coordinates of all points of the dome are known. Thus the length of the members which start from a point to another point of the dome structure can be determined easily by using the formula below,

$$L = \sqrt{(x_1 - x_2)^2 + (y_1 - y_2)^2 + (z_1 - z_2)^2} \quad (7.7)$$

Table 7.6. The length and name of the elements

ELEMENTS, E	LENGTH (m)	ELEMENTS, E	LENGTH (m)
From the Top Point to the 1. Ring	4.0171102	6. Ring-Horizontal	4.4445619
1. Ring-Horizontal	0.7841371	From 6. Ring to 7. Ring	5.3921139
From 1. Ring to 2. Ring	4.1476670	7. Ring-Horizontal	5.0751463
2. Ring-Horizontal	1.5607226	From 7. Ring to 8. Ring	5.4900692
From 2. Ring to 3. Ring	4.3786747	8. Ring-Horizontal	5.6568542
3. Ring-Horizontal	2.3222774	From 8. Ring to 9. Ring	5.4900692
From 3. Ring to 4. Ring	4.6632890	9. Ring-Horizontal	6.1840836
4. Ring-Horizontal	3.0614675	From 9. Ring to 10. Ring	5.3921139
From 4. Ring to 5. Ring	4.9529557	10. Ring-Horizontal	6.6517569
5. Ring-Horizontal	3.7711739	From 10. Ring to the Bottom	5.2164261

$$W = c \cdot q, \quad (\text{for the value of coefficient } c, 0.8 + 0.4 \text{ is used.}) \quad (7.8)$$

Table 7.7. The speed and absorption values for wind loads

Height (m)	Speed of the wind (m/sec)	Absorption(Pressure) q (kN/m ²)	Rings
0-8	28	0.5	9,10
9-20	36	0.8	6,7,8
21-100	42	1.1	0,1,2,3,4,5
>100	46	1.3	---

The 3-D coordinates of all points of the dome structure and the angles between the earth surface and the triangular surface which is formed by the points of the dome structure are known. Thus the areas of these triangular surfaces can be determined easily. And of course, the wind loads and the snow loads depend on these areas.

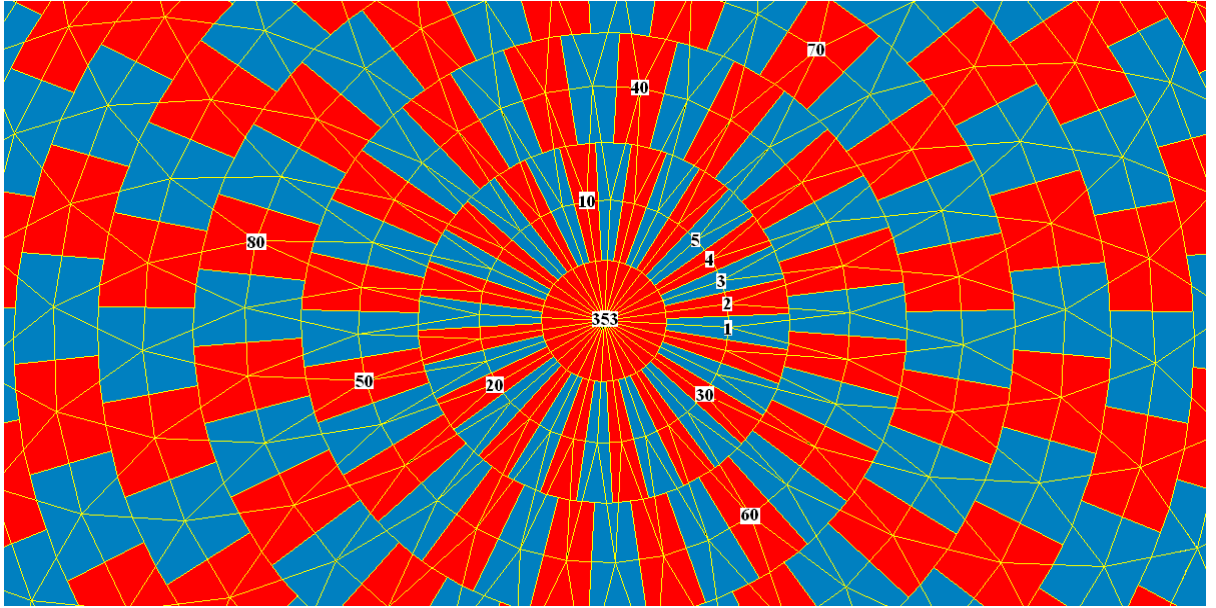


Figure 7.5. Represented areas for all points of the dome

To calculate the load areas, the formulas are that:

For the Point 353:

$$A_{L,353} = 32 \cdot \left(\frac{1}{2} \frac{L_{E1}}{2} \frac{L_{E1}}{2} \sin \theta_2 \right) \quad (7.9)$$

For the Points on the Ring 1:

$$A_{L,n} = \frac{3}{2} \frac{1}{4} L_{E2} \left(\frac{\sqrt{L_{E1}^2 - \frac{L_{E2}^2}{2^2}}}{2} + \frac{L_{E4}}{2} \sqrt{\frac{4L_{E3}^2 - L_{E4}^2}{2^2}} \right) \quad (7.10)$$

For the Points on the Ring 2:

$$A_{L,n} = \frac{3}{2} \frac{1}{4} L_{E4} \left(\frac{\sqrt{L_{E3}^2 - \frac{L_{E4}^2}{2^2}}}{2} + \frac{L_{E6}}{2} \sqrt{\frac{4L_{E5}^2 - L_{E6}^2}{2^2}} \right) + \frac{1}{2} \frac{L_{E1}^2}{2^2} \sin \theta_2 \quad (7.11)$$

For the Points on the Ring 3:

$$A_{L,n} = \frac{3}{2} \frac{1}{4} L_{E6} \left(\frac{\sqrt{L_{E5}^2 - \frac{L_{E6}^2}{2^2}}}{2} + \frac{L_{E8}}{2} \sqrt{\frac{4L_{E7}^2 - L_{E8}^2}{2^2}} + \frac{L_{E4}}{2} \sqrt{\frac{2 \cdot L_{E3}^2 - L_{E4}^2}{2^2}} \right) \quad (7.12)$$

For the Points on the Ring 4:

$$A_{L,n} = \frac{3}{2} \frac{1}{4} L_{E8} \left(\frac{\sqrt{L_{E7}^2 - \frac{L_{E8}^2}{2^2}}}{2} + \frac{L_{E10}}{2} \sqrt{\frac{4L_{E9}^2 - L_{E10}^2}{2^2}} + \frac{L_{E6}}{2} \sqrt{\frac{4L_{E5}^2 - L_{E6}^2}{2^2}} \right) \quad (7.13)$$

For the Points on the Ring 5:

$$A_{L,n} = \frac{3}{2} \frac{1}{4} L_{E10} \left(\frac{\sqrt{L_{E9}^2 - \frac{L_{E10}^2}{2^2}}}{2} + \frac{L_{E12}}{2} \sqrt{\frac{4L_{E11}^2 - L_{E12}^2}{2^2}} + \frac{L_{E8}}{2} \sqrt{\frac{4L_{E7}^2 - L_{E8}^2}{2^2}} \right) \quad (7.14)$$

For the Points on the Ring 6:

$$A_{L,n} = \frac{3}{2} \frac{1}{4} L_{E12} \left(\frac{\sqrt{L_{E11}^2 - \frac{L_{E12}^2}{2^2}}}{2} + \frac{L_{E14}}{2} \sqrt{\frac{4L_{E13}^2 - L_{E14}^2}{2^2}} + \frac{L_{E10}}{2} \sqrt{\frac{4L_{E9}^2 - L_{E10}^2}{2^2}} \right) \quad (7.15)$$

For the Points on the Ring 7:

$$A_{L,n} = \frac{3}{2} \frac{1}{4} L_{E14} \left(\frac{\sqrt{L_{E13}^2 - \frac{L_{E14}^2}{2^2}}}{2} + \frac{L_{E16}}{2} \sqrt{\frac{4L_{E15}^2 - L_{E16}^2}{2^2}} + \frac{L_{E12}}{2} \sqrt{\frac{4L_{E11}^2 - L_{E12}^2}{2^2}} \right) \quad (7.16)$$

For the Points on the Ring 8:

$$A_{L,n} = \frac{3}{2} \frac{1}{4} L_{E16} \left(\frac{\sqrt{L_{E15}^2 - \frac{L_{E16}^2}{2^2}}}{2} + \frac{L_{E18}}{2} \sqrt{\frac{4L_{E17}^2 - L_{E18}^2}{2^2}} + \frac{L_{E14}}{2} \sqrt{\frac{4L_{E13}^2 - L_{E14}^2}{2^2}} \right) \quad (7.17)$$

For the Points on the Ring 9:

$$A_{L,n} = \frac{3}{2} \frac{1}{4} L_{E18} \left(\frac{\sqrt{L_{E17}^2 - \frac{L_{E18}^2}{2^2}}}{2} + \frac{L_{E20}}{2} \sqrt{\frac{4L_{E19}^2 - L_{E20}^2}{2^2}} + \frac{L_{E16}}{2} \sqrt{\frac{4L_{E15}^2 - L_{E16}^2}{2^2}} \right) \quad (7.18)$$

For the Points on the Ring 10:

$$A_{L,n} = \frac{3}{2} \frac{1}{4} L_{E20} \left(\frac{\sqrt{L_{E19}^2 - \frac{L_{E20}^2}{2^2}}}{2} + \frac{L_{E22}}{2} \sqrt{\frac{4L_{E21}^2 - L_{E22}^2}{2^2}} + \frac{L_{E18}}{2} \sqrt{\frac{4L_{E17}^2 - L_{E18}^2}{2^2}} \right) \quad (7.19)$$

To calculate the Wind Forces on each Load Areas:

$$F_{Wind} = A_{Load} \cdot c \cdot q \quad (7.20)$$

Table 7.8. Wind loads for all points of the dome

Points on the (Rings)	Load Areas (m²)	Wind Loads Pressure (kN)	Wind Loads Suction (kN)
353 (0)	6.2964130	5.540843	2.770422
1---32 (1)	3.1459139	2.768404	1.384202
33---64 (2)	6.3873964	5.620909	2.810454
65---96 (3)	9.8337399	8.653691	4.326846
97---128 (4)	13.4986369	11.87880	5.939400
129---160 (5)	17.2553524	15.18471	7.592355
161---192 (6)	20.8715000	13.35776	6.678880
193---224 (7)	24.0524156	15.39355	7.696773
224---256 (8)	26.4883880	16.95257	8.476284
257---288 (9)	27.8968952	11.15876	5.579379
289---320 (10)	28.0694219	11.22777	5.613884

7.4.3. Application of TS-498 for the Structure (For Snow Loads)

Table 7.9. Snow pressures with respect to the altitudes and regions

Altitude <i>m.</i>	Regions			
	I (kN/m^2)	II (kN/m^2)	III (kN/m^2)	IV (kN/m^2)
≤ 200	0.75	0.75	0.75	0.75
300	0.75	0.75	0.75	0.80
400	0.75	0.75	0.75	0.80
500	0.75	0.75	0.75	0.85
600	0.75	0.75	0.80	0.90
700	0.75	0.75	0.85	0.95
800	0.80	0.85	1.25	1.40
900	0.80	0.95	1.30	1.50
1000	0.80	1.05	1.35	1.60
>1000	110% of the loads at the 1000 m. altitude, 115% of the loads at the 1000 m. altitude,			< 1500 m. altitude > 1500 m. altitude

For example;

The regions: IV

The altitude = 950 m.

Then $P_{Snow} = 1.50 kN/m^2$

To calculate the Snow Forces on each Load Areas:

$$F_{Snow} = (A_{Load} m^2)(1.50 kN / m^2) \quad (7.21)$$

Table 7.10. Snow loads for all points of the dome

Points on the (Rings)	Load Areas (m ²)	Snow Loads (kN)
353 (0)	12.5928261	18.889
1---32 (1)	3.1459139	4.719
33---64 (2)	6.3873964	9.581
65---96 (3)	9.8337399	14.751
97---128 (4)	13.4986370	20.248
129---160 (5)	17.2553525	25.883
161---192 (6)	20.8715000	31.307
193---224 (7)	24.0524155	36.079
224---256 (8)	26.4883880	39.733
257---288 (9)	27.8968952	41.845
289---320 (10)	28.0694219	42.104

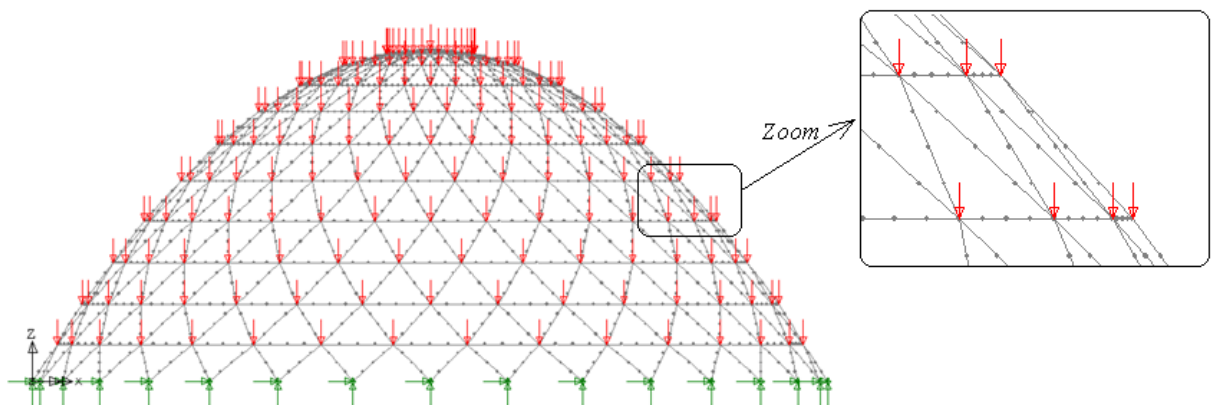


Figure 7.6. Dead and snow loads on the points of the dome

There is a steel plate at the top point of the dome in order to facilitate to get the connections each other of the totally 32 members at the top. Thus the steel mass and weight at the top point of the dome is much more with respect to the other points of the other rings

of the dome. According to the calculations, the weight of the top point is approximately 35.99 kN. as easily seen from the Table 7.11.

To calculate the weight of steel members in terms of the length of the members:

For the Point 353:

$$d_s = 7900 \text{ kg} / \text{m}^3.$$

$$R_{sp} = 0.75 \text{ m.} \quad (\text{At the top point, there is a steel plate whose radius is } R_{sp})$$

$$t_{sp} = 0.20 \text{ m.} \quad (\text{At the top point, there is a steel plate whose thickness is } t_{sp})$$

$$W_s = \frac{\pi R_{sp}^2 t_{sp} d_s g + 32.M_{E1}(L_{E1} - R_{sp}).g}{1000} \quad (7.22)$$

$$W_s = 35.99 \text{ kN.}$$

Table 7.11. Formulas to calculate the steel weights

Ring No.	Node No.	Weight of the Steel Members
0	353	$W_s = \frac{\pi R_{sp}^2 t_{sp} d_s g + 32.M_{E1}(L_{E1} - R_{sp}).g}{1000}$
1	[1, 32]	$W_s = \frac{g \left(\frac{M_{E1}L_{E1}}{2} + M_{E2}L_{E2} + M_{E3}L_{E3} \right)}{1000}$
2	[32, 64]	$W_s = \frac{g(M_{E3}L_{E3} + M_{E4}L_{E4} + M_{E5}L_{E5})}{1000}$
3	[65, 96]	$W_s = \frac{g(M_{E5}L_{E5} + M_{E6}L_{E6} + M_{E7}L_{E7})}{1000}$

Table 7.11. Formulas to calculate the steel weights (Cont.)

Ring No.	Node No.	Weight of the Steel Members
4	[97, 128]	$W_s = \frac{g(M_{E7}L_{E7} + M_{E8}L_{E8} + M_{E9}L_{E9})}{1000}$
5	[129, 160]	$W_s = \frac{g(M_{E9}L_{E9} + M_{E10}L_{E10} + M_{E11}L_{E11})}{1000}$
6	[161, 192]	$W_s = \frac{g(M_{E11}L_{E11} + M_{E12}L_{E12} + M_{E13}L_{E13})}{1000}$
7	[193, 224]	$W_s = \frac{g(M_{E13}L_{E13} + M_{E14}L_{E14} + M_{E15}L_{E15})}{1000}$
8	[225, 256]	$W_s = \frac{g(M_{E15}L_{E15} + M_{E16}L_{E16} + M_{E17}L_{E17})}{1000}$
9	[257, 288]	$W_s = \frac{g(M_{E17}L_{E17} + M_{E18}L_{E18} + M_{E19}L_{E19})}{1000}$
10	[289, 320]	$W_s = \frac{g(M_{E19}L_{E19} + M_{E20}L_{E20} + M_{E21}L_{E21})}{1000}$

To calculate the weight of flexi-glass materials:

$$d_{fgls} = 1.18 \text{ gr / cm}^3, \quad t_{fgls} = 0.01 \text{ m.}$$

$$W_{fgls} = d_{fgls} g A_{L,n} t_{fgls} \quad (7.23)$$

Table 7.12. Total mass and weight for the points due to the materials

Points on the (Rings)	Steel-mass (ton)	W_{Steel} (kN)	W_{flexigl} (kN)	Load Areas (m^2)	Total Vertical Dead Load (kN)
353 (0)	3.669	35.991656	1.4577204	12.5928261	37.4493764
1---32 (1)	0.066	0.6447955	0.3641647	3.1459139	1.0089602
33---64 (2)	0.116	1.1337165	0.7393922	6.3873964	1.8731088
65---96 (3)	0.151	1.4776854	1.1383341	9.8337399	2.6160195
97---128 (4)	0.208	2.0433865	1.5625752	13.4986370	3.6059617
129---160 (5)	0.306	2.9974853	1.9974451	17.2553525	4.9949304
161---192 (6)	0.367	3.6001670	2.4160431	20.8715000	6.0162101
193---224 (7)	0.404	3.9611402	2.7842595	24.0524155	6.7453997
224---256 (8)	0.462	4.5350939	3.0662428	26.4883880	7.6013367
257---288 (9)	0.558	5.4757674	3.2292888	27.8968952	8.7050562
289---320 (10)	0.631	6.1926233	3.2492601	28.0694219	9.4418834

If we want to calculate the cost of the total materials, we should know the amount of the total material which is used for the structure. Thus the total amount of all material is equal to the 32 times with the mass for any point. Because there are equivalent 32 nodes in every ring of the dome structure except the top point of the structure.

Table 7.13. Total weights for the rings due to the materials

Ring Number	Steel-mass (ton)	WSteel (kN)	Flexigl-mass (ton)	Wflexigl (kN)	Total Mass (ton)	Total Vertical Dead Load (kN)
0	3.66887	35.991656	0.148595	1.4577204	3.8175	37.4493764
1	2.10331	20.6334553	1.187897	11.65327038	3.2912	32.2867256
2	3.69816	36.2789296	2.411881	23.66055142	6.1100	59.9394810
3	4.82018	47.2859332	3.713220	36.42668994	8.5334	83.7126231
4	6.66548	65.3883687	5.097085	50.00240695	11.7626	115.3907756
5	9.77773	95.9195291	6.515621	63.91824285	16.2934	159.8377720
6	11.7437	115.205344	7.881078	77.31337925	19.6247	192.5187232
7	12.9212	126.756485	9.082192	89.09630461	22.0033	215.8527900
8	14.7934	145.123006	10.00202	98.11977011	24.7954	243.2427759
9	17.8618	175.224556	10.53387	103.3372413	28.3957	278.5617971
10	20.2002	198.163945	10.59901	103.9763247	30.7992	302.1402694
TOTAL	108.254	1061.971208	67.17247	658.9621	175.4264	1720.93311
Cost	≈ 205000 TL.	-----	≈ 220000 TL.	-----	≈ 425000 TL.	-----

7.4.4. A Single Point Load at the Top Point of the Dome

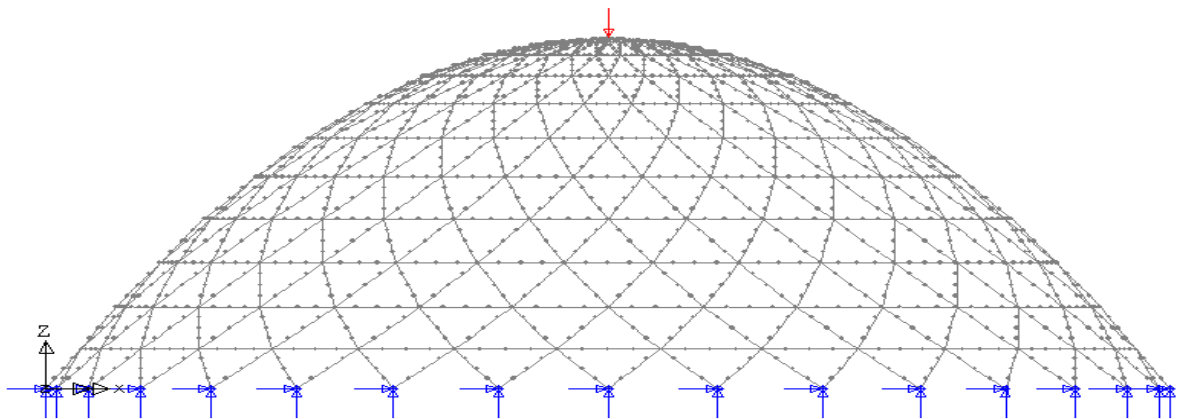


Figure 7.7. Single point load at the top point of the dome

7.5. Nonlinear Solutions for Each Load Case

7.5.1. Nonlinear Behavior of a Critical Point for a Single Point Load at the Top Point

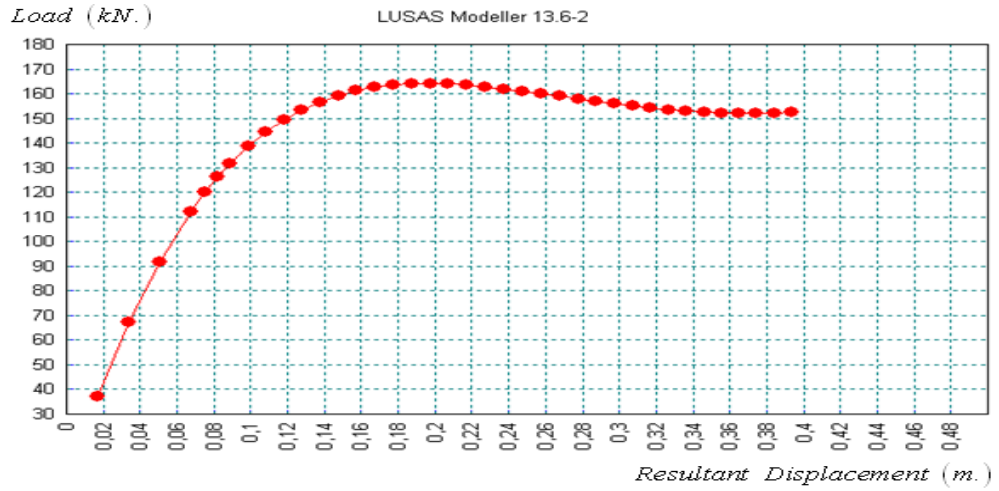


Figure 7.7. Force vs displacement curve under the single point load at the top point

7.5.2. Nonlinear Behavior of a Critical Point for the Dead + Snow Loads

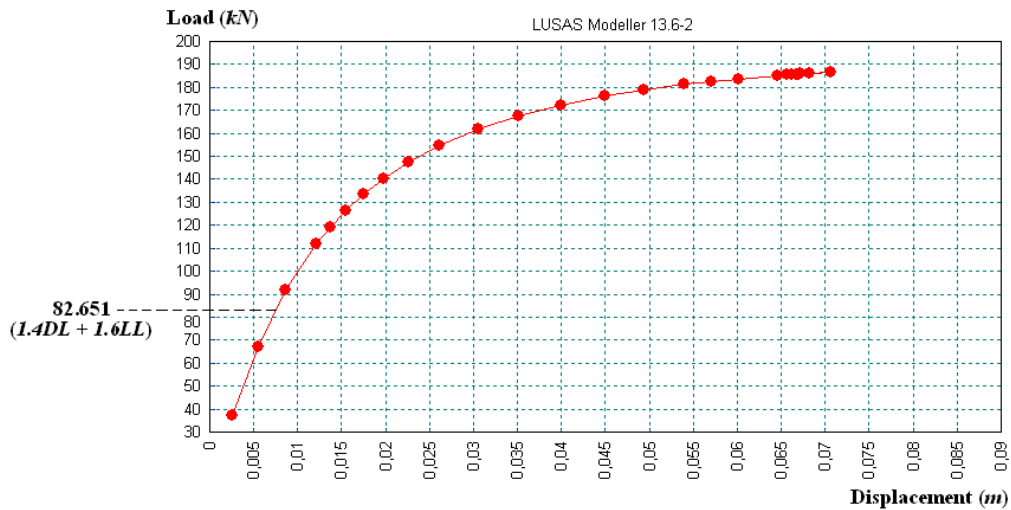


Figure 7.9. Force vs displacement curve under the dead load and the snow load

7.5.3. Nonlinear Behavior of a Critical Point for the Vertical + Earthquake Loads

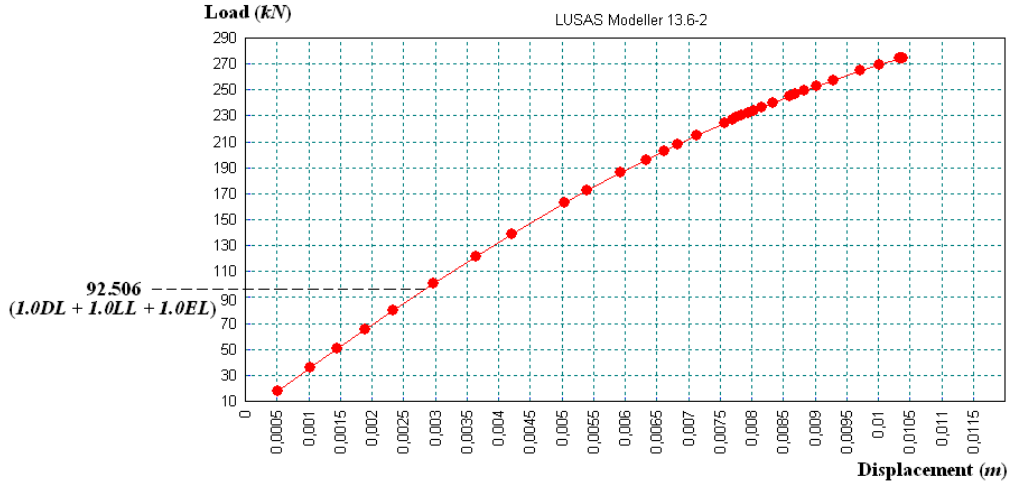


Figure 7.9. Force vs displacement curve under the vertical and earthquake loads

7.5.4. Nonlinear Behavior of a Critical Point for the Vertical + Wind Loads

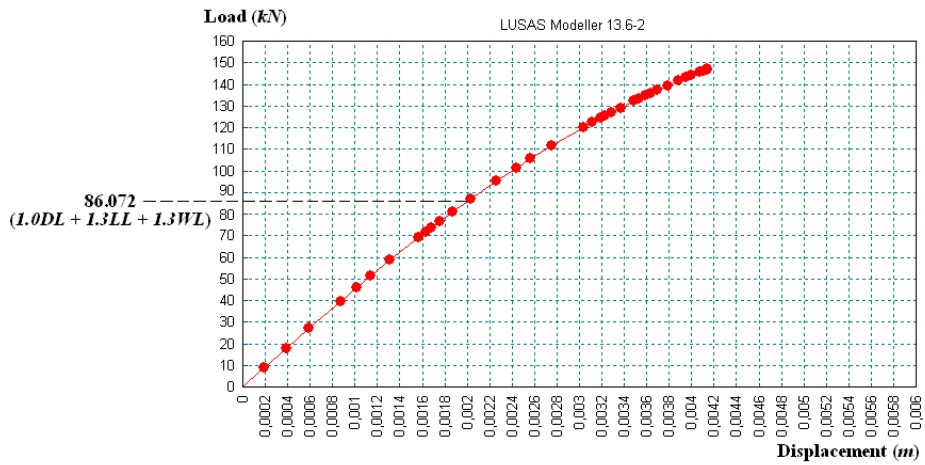


Figure 7.10. Force vs displacement curve under the vertical load and the wind load

7.6. Local Buckling Control

7.6.1. Axial Forces of the Members for a Single Point Load at the Top Point

Table 7.14. Section of the members and critical loads under the single point load

Members	Length (<i>m</i>)	Diameter (<i>mm</i>)	Thickness (<i>mm</i>)	P _{CR} LOAD (<i>kN</i>)	P _{CR} From LUSAS (when P =91.88 <i>kN</i>)	Ratio
353---001	4.017	88.9	4	28.746	25.950 (<i>max.</i>)	9.7%
001---002	0.784	60.3	5	86.855	75.462 (<i>max.</i>)	13.1%
001---033	4.148	76.1	5	33.131	5.794	82.5%
033---034	1.561	76.1	5	89.497	24.700	72.4%
033---065	4.379	88.9	5	64.374	3.608	94.4%
065---066	2.322	88.9	6	103.545	10.378	90%
065---097	4.663	114.3	5	56.926	2.806	95,1%
097---098	3.062	114.3	5	111.697	5.817	94.8%
097---129	4.953	114.3	6	77.664	2.437	96.9%
129---130	3.771	114.3	6	132.060	4.029	96.9%
129---161	5.206	127	8	96.999	2.236	97.7%
161---162	4.444	127	5	134.721	2.984	97.8%
161---193	5.392	133	8	122.723	2.133	98.3%
193---194	5.075	127	5	144.497	2.488	98.3%
193---225	5.490	159	6.3	139.062	2.085	98.5%
225---226	5.657	127	5	166.683	2.180	98.7%
225---257	5.490	159	8	175.624	2.082	98.8%
257---258	6.184	127	5	137.651	1.972	98.6%
257---289	5.392	168.3	10	260.196	2.127	99.2%
289---290	6.652	127	5	120.310	1.530	98.7%
289---321	5.216	168.3	11	295.531	2.256	99.2%

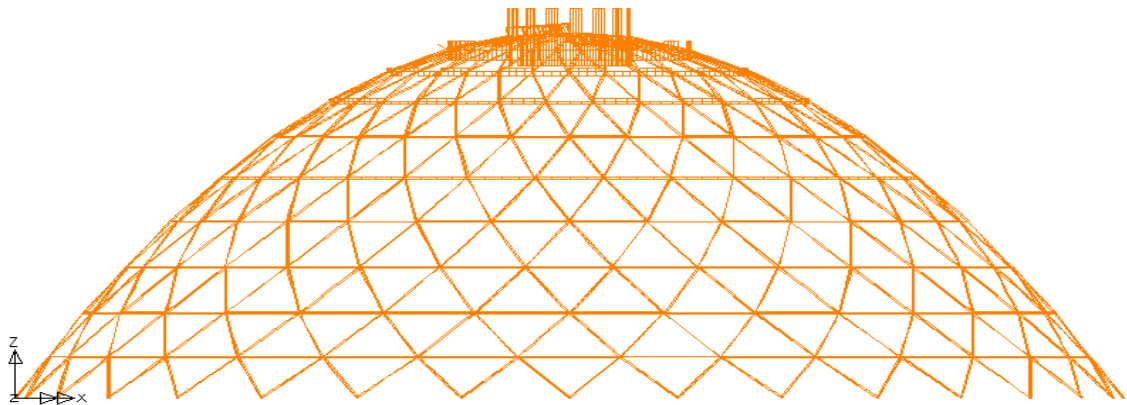


Figure 7.12. Axial force diagrams of the members under the single point load

7.6.2. Axial Forces of the Members for the Dead + Snow Loads

Table 7.15. Section of the members and critical loads under the dead and snow loads

Members	Length (m)	Diameter (mm)	Thickness (mm)	P _{CR} LOAD (kN)	P _{CR} From LUSAS (kN)	Ratio
353---001	4.017	88.9	4	28.746	14.067	51.1%
001---002	0.784	60.3	5	86.855	62.613	27.9%
001---033	4.148	76.1	5	33.131	13.883	58.1%
033---034	1.561	76.1	5	89.497	76.378 (max.)	14.7%
033---065	4.379	88.9	5	64.374	23.816	63%
065---066	2.322	88.9	6	103.545	85.648 (max.)	17.3%
065---097	4.663	114.3	5	56.926	37.434	34.2%
097---098	3.062	114.3	5	111.697	88.256 (max.)	21%
097---129	4.953	114.3	6	77.664	55.150	29%
129---130	3.771	114.3	6	132.060	80.330	39.2%
129---161	5.206	127	8	96.999	76.198	21.4%
161---162	4.444	127	5	134.721	73.754	45.3%
161---193	5.392	133	8	122.723	102.714 (max.)	16.3%

Table 7.15. Section of the members and critical loads under the dead and snow loads (Cont)

Members	Length (m)	Diameter (mm)	Thickness (mm)	P _{CR} LOAD (kN)	P _{CR} From LUSAS (kN)	Ratio
193---194	5.075	127	5	144.497	58.277	59.7%
193---225	5.490	159	6.3	139.062	134.146 (max.)	3.5%
225---226	5.657	127	5	166.683	35.307	78.8%
225---257	5.490	159	8	175.624	171.145 (max.)	2.6%
257---258	6.184	127	5	137.651	12.855	90.7%
257---289	5.392	168.3	10	260.196	214.999 (max.)	17.4%
289---290	6.652	127	5	120.310	29.851	75.2%
289---321	5.216	168.3	11	295.531	268.618 (max.)	9.1%

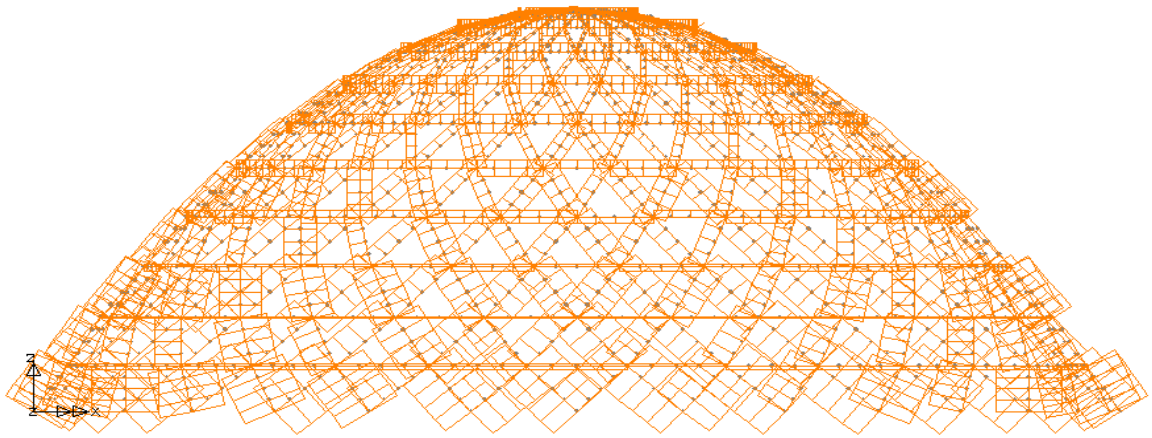


Figure 7.13. Axial force diagrams of the members under the dead and the snow loads

7.6.3. Axial Forces of the Members for the Dead + Earthquake Loads

Table 7.16. Section of the members and critical loads under the dead and earthquake loads

MEMBERS	LENGTH (<i>m</i>)	DIAMETER (<i>mm</i>)	THICKNESS (<i>mm</i>)	P _{CR} LOAD (<i>kN</i>)	P _{CR} From LUSAS (<i>kN</i>)	Ratio
353---001	4.017	88.9	4	28.746	8.159	71.6%
001---002	0.784	60.3	5	86.855	13.436	84.5%
001---033	4.148	88.9	5	33.131	10.968	66.9%
033---034	1.561	76.1	5	89.497	30.509	65.9%
033---065	4.379	114.3	5	64.374	18.906	70.6%
065---066	2.322	88.9	6	103.545	39.505	61.8%
065---097	4.663	114.3	5	56.926	27.623	51.5%
097---098	3.062	114.3	5	111.697	44.645	60%
097---129	4.953	114.3	8	77.664	37.365	51.9%
129---130	3.771	114.3	8	132.060	52.002	60.6%
129---161	5.206	127	8	96.999	48.538	50%
161---162	4.444	127	8	134.721	52.138	61.3%
161---193	5.392	139.7	8	122.723	59.714	51.3%
193---194	5.075	141.3	8	144.497	47.502	67.1%
193---225	5.490	159	6.3	139.062	70.354	49.4%
225---226	5.657	159	8	166.683	41.894	74.9%
225---257	5.490	159	8	175.624	80.864	54%
257---258	6.184	159	8	137.651	32.659	76.3%
257---289	5.392	168.3	10	260.196	91.557	64.8%
289---290	6.652	159	8	120.310	18.920	84.3%
289---321	5.216	168.3	11	295.531	103.886	64.8%

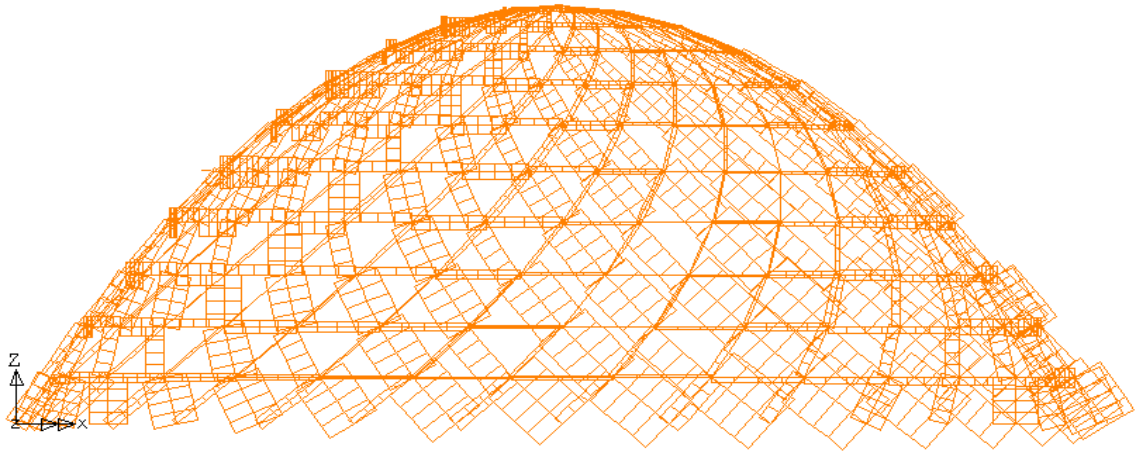


Figure 7.14. Axial force diagrams of the members under the dead and the earthquake loads

7.6.4. Axial Forces of the Members for the Dead + Wind Loads

Table 7.17. Section of the members and critical loads under the dead and wind loads

Members	Length (m)	Diameter (mm)	Thickness (mm)	P _{CR} LOAD (kN)	P _{CR} From LUSAS (kN)	Ratio
353---001	4.017	88.9	4	28.746	17.365	39.6%
001---002	0.784	60.3	5	86.855	22.415	74.2%
001---033	4.148	88.9	5	33.131	23.526 (max.)	29%
033---034	1.561	76.1	5	89.497	45.729	48.9%
033---065	4.379	114.3	5	64.374	40.969 (max.)	36.4%
065---066	2.322	88.9	6	103.545	55.515	46.4%
065---097	4.663	114.3	5	56.926	45.804 (max.)	19.5%
097---098	3.062	114.3	5	111.697	77.025	31%
097---129	4.953	114.3	8	77.664	59.807 (max.)	23%
129---130	3.771	114.3	8	132.060	102.678 (max.)	22.2%
129---161	5.206	127	8	96.999	76.798 (max.)	20.8%

Table 7.17. Section of the members and critical loads under the dead and wind loads (Cont)

Members	Length (<i>m</i>)	Diameter (<i>mm</i>)	Thickness (<i>mm</i>)	P _{CR} LOAD (<i>kN</i>)	P _{CR} From LUSAS (<i>kN</i>)	Ratio
161---162	4.444	127	8	134.721	100.646 (<i>max.</i>)	25.3%
161---193	5.392	139.7	8	122.723	92.423	24.7%
193---194	5.075	141.3	8	144.497	110.709 (<i>max.</i>)	23.4%
193---225	5.490	159	6.3	139.062	108.958	21.6%
225---226	5.657	159	8	166.683	121.179 (<i>max.</i>)	27.3%
225---257	5.490	159	8	175.624	128.469	26.8%
257---258	6.184	159	8	137.651	98.062 (<i>max.</i>)	28.8%
257---289	5.392	168.3	10	260.196	149.906	42.4%
289---290	6.652	159	8	120.310	83.612 (<i>max.</i>)	30.5%
289---321	5.216	168.3	11	295.531	160.526	45.7%

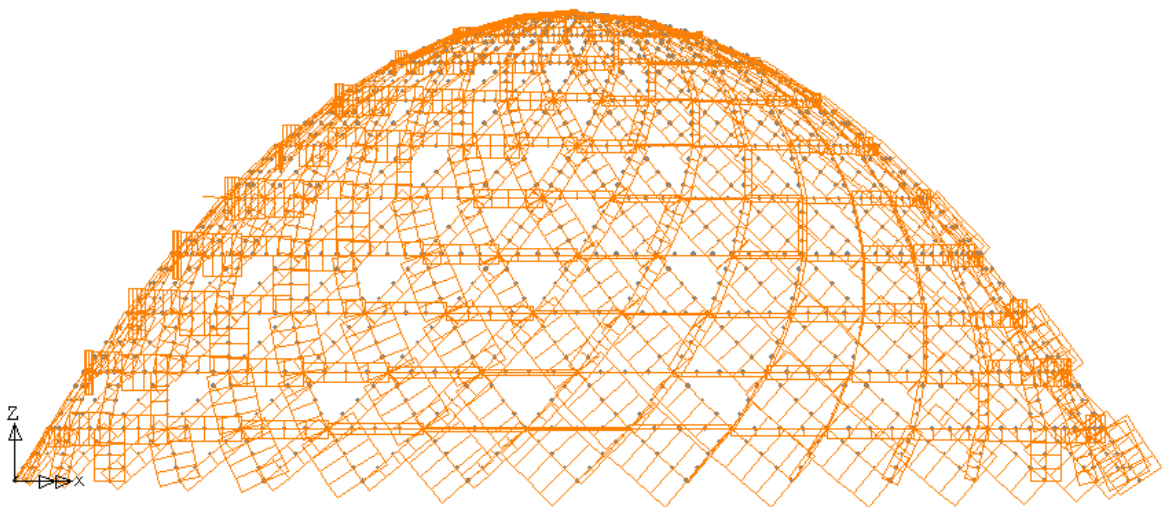


Figure 7.15. Axial force diagrams of the members under the dead and the wind loads

Table 7.18. Sections and properties of the members

ELEMENTS, E	Outer Diameter (mm)	Wall Thickness (mm)	Unit Mass, M (kg/m)	Cross Sectional Area (cm ²)	Moment of Inertia, I (cm ⁴)	Radius of Gyration, i (cm)
From the Top Nodes to the 1. Ring	88.9	4	8.4	10.7	96.3	3.0
1. Ring-Horizontal	60.3	5	6.8	8.7	33.5	2.0
From 1. Ring to 2. Ring	88.9	5	10.3	13.2	116.4	3.0
2. Ring-Horizontal	76.1	5	8.8	11.2	70.9	2.5
From 2. Ring to 3. Ring	114.3	5	13.5	17.2	256.9	3.9
3. Ring-Horizontal	88.9	6	12.3	15.6	134.9	2.9
From 3. Ring to 4. Ring	114.3	5	13.5	17.2	256.9	3.9
4. Ring-Horizontal	114.3	5	13.5	17.2	256.9	3.9
From 4. Ring to 5. Ring	114.3	8	21	26.7	379.5	3.8
5. Ring-Horizontal	114.3	8	21	26.7	379.5	3.8
From 5. Ring to 6. Ring	127	8	23.5	29.9	531.8	4.2
6. Ring-Horizontal	127	8	23.5	29.9	531.8	4.2
From 6. Ring to 7. Ring	139.7	8	26	33.1	720.3	4.7
7. Ring-Horizontal	141.3	8	26.3	33.5	746.8	4.7
From 7. Ring to 8. Ring	159	6.3	23.7	30.2	882.4	5.4
8. Ring-Horizontal	159	8	29.8	38	1084.7	5.3
From 8. Ring to 9. Ring	159	8	29.8	38	1084.7	5.3
9. Ring-Horizontal	159	8	29.8	38	1084.7	5.3
From 9. Ring to 10. Ring	168.3	10	39	49.7	1564	5.6
10. Ring-Horizontal	159	8	29.8	38	1084.7	5.3
From 10. Ring to the Bottom	168.3	11	42.7	54.4	1689.5	5.6

7.7. Surface Cover of the Dome

For this lattice dome, flexi-glass material is selected as the surface coverage of the dome due to some important advantages. Some significant properties are listed below:

- It is a kind of thermoplastic material.
- It is produced generally as a transparent material. Ratio of transparency is equal to the ratio of the transparency of glass material.
- Thickness of the material changes generally from 2 mm. to 40 mm.
- Strength of the material is 6 times better than the strength of the glass material.
- Heat conductivity is 20% times less than the glass material.
- It can be adjusted to some different types of the climate.
- Density = 1.18 gr. / cm³.

But some areas may be weak because of the effect of the wind loads or snow loads. Since the largest areas of these areas are approximately 28 m². In order to decrease this area, it should be divided 4 triangle areas. Therefore its area will decrease to approximately 7 m², and this flexi glass material will be stronger against the loads.

8. CONCLUSIONS AND RECOMMENDATIONS

In light of the overview of this Thesis, the stability of steel dome structures is investigated by considering the nonlinear behavior under some compressive forces. So according to this Thesis, a few concluding remarks and recommendations may be expressed as follows:

- The updated tangent stiffness matrices of bar elements for a two or three dimensional system provide extreme convenience in achieving high speed for iterative nonlinear computations.
- The incremental and iterative procedures such as Newton – Raphson Method, Modified Newton –Raphson Method, and mixed procedures provide very accurate and speedy solutions for a wide range of geometrically and materially nonlinear problems.
- The iterative procedures appear to be very effective and efficient in solving the geometrically nonlinear problems, while the incremental loading procedures contribute themselves ideally suitable for the material nonlinearity. What is more, the results appear to be more exact when iterative solutions are used, while the incremental methods contain accumulative errors. Furthermore, the mixed procedures can produce the most accurate results, and because of this reason most of the computer programs utilize this particular procedure.
- While solving nonlinear test problems and also during the analyses of the space dome, it is observed that the LUSAS package program is a very efficient, user friendly and versatile software.
- The structural behavior of the spherical dome composed of steel pipe sections has been investigated under a variety of load combinations including dead loads, wind loads, snow loads, and statically equivalent earthquake loads. Additionally, it is recommended that the dome should be also analyzed under time history earthquake loads in future studies.
- For stability of the dome structures, the general and local buckling states control the design. The outputs of LUSAS should be compared with the critical loads calculated by mathematical formulas on the slenderness ratio of bar elements.

- While investigating the relative degree of nonlinearity for vertical and horizontal loads, it has been discovered that the degree of nonlinearity under horizontal loads is much smaller.
- The pin support conditions have been used in this Thesis, however the fixed support conditions should be investigated in the future studies. Elevated base ring situation is another option on dome structures that may be considered as an alternate design. Finally, it is also suggested that the effects of temperature changes of the steel structure should be also investigated in future studies.

9. REFERENCES

- Aguilar, R. J., 1967, "Snap-Through Buckling of Framed Triangular Domes", *Journal of the Structural Division*, ASCE, Vol. 93, No. ST2, April, pp. 301 - 318.
- Aguilar, R. J. and T. Huang, 1966, *The Snap-through Buckling of Triangular Lattice Domes Under the Simultaneous Application of Concentrated Loads*, International Conference on Space Structures 1966, Department of Civil Engineering, University of Surrey.
- Aguire - Rameriz, G. and J. T. Oden, 1969, "The Finite Element Technique Applied to Heat Conduction with Temperature Dependent Thermal Conductivity", Winter Meeting ASME, ASME Paper, Los Angeles, California, November.
- Anderson, R. G., B. M. Irons and O. C. Zienkiewicz, 1968, "Vibrations and Stability of Plates Using Finite Elements", *International Journal of Solids and Structures*, Vol. 4, No. 10, October, pp. 1031 - 1055.
- Argyris, J. H., 1959, "Recent Developments of Matrix Theory of Structure", Paper presented at the 10th meeting of the Structures and Materials Panel, Aachen, Germany, September.
- Argyris, J. H., S. Kelsey and H. Kamel, 1964, "Matrix Methods of Structural Analysis A Precis of Recent Developments", *Matrix Methods in Structural Analysis – AGARDograph 72*, Edited by B. Fraeijs de Veubeke, Pergamon Press, Oxford, pp. 1 - 164. (Presented at AGARD Structures and Materials Panel, Paris, July, 1964).
- Argyris, J. H., 1965, "Matrix Analysis of Three - Dimensional Elastic Media, Small and Large Displacements", *AIAA Journal*, Vol. 3, No. 1, January, pp. 45 - 51.
- Argyris, J. H., 1966, "Continua and Discontinua", *Proceedings, Conference on Matrix Methods in Structural Mechanics*, AFFDL - TR - 66 - 80, (Edited by J. S. Przemieniecki *et al*), Wright -Patterson Air Force Base, Ohio, pp. 11 - 189.

- Bakes, W. E. and R. M. Mello, 1969, "Some Applications of Finite Element Shell Analysis to Shell Buckling Prediction", *Proceedings, Second Conference on Matrix Methods in Structural Mechanics*, AFFDL TR 69, Wright -Patterson Air Force Base, Ohio (held October, 1968).
- Brebbia, C. and J. Corner, 1969, "Geometrically Nonlinear Finite Element Analysis", *Journal of the Engineering Mechanics Division*, ASCE, Vol. 95, No. EM2, April, pp.463 - 483.
- Brooks, S. H., 1959, "A Comparison of Maximum Seeking Methods", *Journal of Operations Research*, Vol. 7, pp. 430 - 457.
- Brown, J. E., J. M. Hutt and A. E. Salama, 1968, "Finite Element Solution to Dynamic Stability of Bars", *AIAA Journal*, Vol. 6, No. 7, July, pp. 1423 - 1425.
- Buchert, K. P., 1966, *Buckling Considerations in the Design and Construction of doubly curved space structures*, International Conference on Space Structures 1966, Department of Civil Engineering, University of Surrey.
- Carpenter, W. C., J. F. Ely and C. R. Bramer, 1966, *The Joint Instability of Latticed structures Under Generalized Loads*, International Conference on Space Structures 1966, Department of Civil Engineering, University of Surrey.
- Conner, J. J., A. M. Logcher and S. C. Chan, 1968, "Nonlinear Elastic Analysis of Elastic Framed Structures", *Journal of the Structural Division*, ASCE, Vol. 94, No. ST6, June, pp. 1525 - 1546.
- Dong, R. G., K. S. Pister and R. S. Dunham, 1968, "Mechanical Characterization of Nonlinear Viscoelastic Solids for Iterative Solution of Boundary Value Problems", *Report No. 68 - 11, Structural Engineering Laboratory*, University of California, Berkeley.
- Felippa, C. A., 1966, "Refined Finite Element Analysis of Linear and Nonlinear Two Dimensional Structures", *Ph.D. Dissertation*, University of California, Berkeley.
- Gallagher, R. H. and J. Padlog, 1963, "Discrete Element Approach to Structural Instability Analysis", *AIAA Journal*, Vol. 1, No. 6, June, pp. 1437 - 1439.

- Gallagher, R. H., 1966, "The Development and Evulation of Matrix Methods of Thin Shell Analysis", *Ph.D. Dissertation*, University of New York at Buffalo.
- Gallagher, R. H., R. A. Gellatly, J. Padlog and R. H. Mallett, 1967, "Discrete Element Procedure for Thin Shell Instability Analysis", *AIAA Journal*, Vol. 5, No. 1, January.
- Goldberg, J. E. and R. M. Richard, 1963, "Analysis of Non - Linear Structures", *Journal of the Structural Division*, ASCE, Vol. 89, No. ST4, August, pp. 333 - 351.
- Greene, B. C., 1960, "Buckling Loads for Columns of Variable Section, Structural Analysis Research Memorandum No. 12, The Boeing Co.", Aerospace Division, Seattle, June.
- Hartz, B. J., 1965, "Matrix Formulation of Structural Stability Problems", *Journal of the Structural Division*, ASCE, Vol. 91, No. ST6, December.
- Hensley, R.C. and J. J. Azar, 1968, "Computer Analysis of Nonlinear Truss – Structures", *Journal of the Structural Division*, ASCE, Vol. 94, No. ST6, June, pp. 1427 - 1439.
- Hicks, G. W., 1967, "Finite - Element Elastic Buckling Analysis", *Journal of the Structural Division*, ASCE, Vol. 93, No. ST6, December, pp. 71 - 86.
- Hrennikoff, A., 1941, "Solutions of Problems of Elasticity by the Framework Method", *Journal of Applied Mechanics*, Vol. 8, pp. A169 - A1175.
- Hutt, J. M., 1968, "Dynamic Stability of Plates by Finite Elements", *Ph.D. Dissertation*, Oklahoma State University, Stillwater.
- Johnson, D. and D. M. Brotton, 1966, "Finite Deflection Analysis for Space Structures", *Space Structures, Proceedings of the International Conference on Space Structures*, University of Surey, Blackwell Scientific Publishers, Oxford.
- Kapur, K. K., 1965, "Buckling of Thin Plates Using the Direct Stiffness Method", *Ph.D. Dissertation*, University of Washington, Seattle, June.
- Kapur, K. K. and B. J. Hartz, 1966, "Stability of Plates Using the Finite Element Method", *Journal of the Engineering Mechanics Division*, ASCE, Vol. 92, No. EM2, April.

- Kawai, T. and H. Ohtsubo, 1969, "A Method of Solution of the Complicated Buckling Problems of Elastic Plates with Combined Use of the Rayleigh - Ritz Procedure and the Finite Element Method", *Proceedings, Second Conference on Matrix Methods in Structural Mechanics*, AFFDL TR - 69, Wright - Patterson Air Force Base, Ohio (held October, 1968).
- Kawai, T., 1969, "Finite Element Analysis of the Geometrically Nonlinear Problems", *Proceedings, Japan - U. S. Seminar on Matrix Methods in Structural Analysis and Design*, Tokyo.
- Loo, H., 1966, "The Design and Construction of Three Reticulated Steel Domes", *International Conference on Space Structures*, Department of Civil Engineering, University of Surrey.
- Lee, S. L., F. S. Manuel and E. C. Roscow, 1968, "Large Deflections and Stability of Elastic Frames", *Journal of the Engineering Mechanics Division*, ASCE, Vol. 94., no. EM2, April, pp. 521- 547.
- Livesley, R. K., 1964, "Matrix Methods of Structural Analysis", *Pergamon Press*, Oxford, pp. 241 - 247.
- Mallett, R. H. and L. Berke, 1966, "Automated Method for the Large Deflection and Instability Analysis of Three - Dimensional Truss and Frame Assemblies", *Technical Report, AFFDL - TR - 66 - 102*, Wright - Patterson Air Force Base, Ohio.
- Mallett, R. H. and P. V. Marcal, 1968, "Finite Element Analysis of Nonlinear Structures", *Journal of the Structural Division*, ASCE, Vol.94, No. ST9, September, pp. 2081 – 2105. (see also Discussion by J. T Oden, Vol. 95, No. ST6, 1969)
- Martin, H. C., 1966, "Large Deflection and Stability Analysis by the Direct Stiffness Method", *NASA Tech. Rept.*, 32 - 931.
- Martin, H. C., 1966, "On the Derivation of Stiffness Matrices for the Analysis of Large Deflection and Stability Problems", *Proceedings, Conf. on Matrix Methods in Structural Mechanics*, (Edited by J. S. Pizemieniecki *et al*), AFFDL - TR - 66 - 80, Wright - Patterson Air Force Base, Ohio.

- McMinn, S. J., 1962, "Matrices for Structural Analysis", John Wiley and Sons, New York.
- McCormic, C. W., 1966, "*The Comparison of a Digital Computer Analysis with full-scale Tests of a Space Structure*", International Conference on Space Structures 1966, Department of Civil Engineering, University of Surrey.
- Murray, D. W., 1967, "Large Deflection Analysis of Plates", *Ph. D. Dissertation*, University of California, Berkeley.
- Murray, D. W. and E. L. Wilson, 1969, "Finite Element Post Buckling Analysis of Thin Elastic Plates", *Proceedings, Second Conference on Matrix Methods in Structural Mechanics; AFFDL TR - 69*, Wright - Patterson Air Force Base, Ohio. (held October, 1968)
- Murray, D. W. and E. L. Wilson, 1969, "Finite Element Large Deflection Analysis of Plates", *Journal of the Engineering Mechanics Division*, ASCE, Vol. 95, No. EM1, February, pp. 143 - 165.
- Navaratna, D. R., T. H. H. Pian, and E. A. Witmer, 1967, "Analysis of Elastic Stability of Shells of Revolution by the Finite Element Method", *Proceedings, AIAA / ASME 8th Structures, Structural Dynamics, and Materials Conference*, Palm Springs, Florida, March, pp. 175 - 186.
- Navaratna, D. R., 1967, "Analysis of Elastic Stability of Shells of Revolution by the Finite Element Method", *Proceedings, AIAA / ASME 8th Structures, Structural Dynamics, and Materials Conference*, Palm Springs, California, March, pp. 175 - 183.
- Novozhilov, V. V., 1953, *Foundations of the Nonlinear Theory of Elasticity*, Graylock Press, Rochester, N.Y., 1953.
- Naylor, D. J., G. N. Pande, B. Simpson, and R. Tabb, 1981, *Finite Elements in Geotechnical Engineering*, Pineridge Press Ltd. , 91 West Cross Lane, Swansea, U. K.
- Oden, J. T., 1966, "Calculation of Geometric Stiffness Matrices for Complex Structures", 3 *AIAA Journal*, Vol. 4, No. 8, pp. 1480 - 1482.

- Oden, J. T. and G. Ramirez, 1969, "Formulation of General Discrete Models of Thermomechanical Behavior of Materials with Memory, it International Journal of Solids and Structures", (to appear).
- Oden, J. T., 1967, "Linear and Nonlinear Analysis by Conjugate Analogy", *Journal of the Structural Division*, ASCE, Vol. 93, No. ST4, August, pp. 27 - 45.
- Oden, J. T. and A. Neighbors, 1966, "Network - Topological Formulation of Analyses of Geometrically and Materially Non - Linear Space Frames", *Space Structures, Proceedings of the International Conference on Space Structures*, University of Surrey, Blackwell Scientific Publishers, Oxford.
- Oden, J. T., 1967, "Numerical Formulation of a Class of Problems in Nonlinear Viscoelasticity", *Advances in the Astronautical Sciences*, 24, June.
- Oden, J. T., 1969, "On a Generalization of the Finite Element Concept and its Application to a class of Problems in Nonlinear Viscoelasticity", *Developments in Theoretical and Applied Mechanics*, Vol. IV, Pergamon Press, London, pp. 581 - 593.
- Oden, J. T. and D. A. Kross, 1969, "Analysis of General Coupled Thermoelasticity Problems by the Finite Element Method", *Proceedings, Second Conference on Matrix Methods in Structural Mechanics*, AFFDL TR 69, Wright - Patterson Air Force Base, Ohio (held October, 1968).
- Oden, J. T., 1969, "Finite Element Analysis of Nonlinear Problems in the Dynamical Theory of Coupled Thermoelasticity", *Nuclear Engineering and Design*, Amsterdam, July.
- Oden, J. T., 1969, "A General Theory of Finite Elements; Applications", *International Journal of Numerical Methods in Engineering*, Vol. 1, No. 3.
- Oden, J. T. and D. Somogyi, 1969, "Finite Element Applications in Fluid Dynamics", *Journal of the Engineering Mechanics Division*, ASCE, Vol. 95, No. EM3, June, pp.821 826.
- Oden, J. T. and D. M. Rigsby and D. Cornett, 1969, "On the Numerical Solution of a Class of Problems in a Linear First Strain Gradient Theory of Elasticity", *International Journal for Numerical Methods in Engineering*.

- Oden, J. T., 1969, "On a Generalization of the Finite Element Concept and its Application to a class of Problems in Nonlinear Viscoelasticity", *Developments in Theoretical and Applied Mechanics*, Vol. IV, Pergamon Press, London, pp. 581 - 593.
- Ortega, M. A., 1969, "Application of the Stiffness Method to Large Deflections of Columns with Initial Imperfections", *Structural Analysis Search Memorandum No.17, The Boeing Co., Aerospace Division*, Seattle.
- Poppleton, E. D., 1961, "Note on the Matrix Analysis of Nonlinear Structures", *Technical Note, Toronto University Institute of Aerophysics*, No. 46, March.
- Poskitt, T. J., 1967, "Numerical Solution of Nonlinear Structures", *Journal of the Structural Division, ASCE*, Vol. 93, No. ST4, August, pp. 69 - 94.
- Prasad, H. S. S., 1969, "Discussion of Nonlinear Analysis of Elastic Framed Structures", *Journal of Structural Division, ASCE*, Vol. 95, No. ST3, March, pp. 517 - 519.
- Przemieniecki, J. S., R. M. Bader, W. F. Bozich, J. R. Johnson and W. J. Mykytow, 1966, (Editors), *Proceedings of Conference on Matrix Methods in Structural Mechanics*, AFFDL - TR - 66 - 80, Wright - Patterson Air Force Base, Ohio.
- Przemieniecki, J. S., 1967, "Stability Analysis of Complex Structures Using Discrete Element Techniques, Symposium on Structural Stability and Optimization", *Royal Aeronautical Society and Loughborough University of Technology*, England.
- Przemieniecki, J. S. and D. M. Purdy, 1968, "Large Deflection and Stability Analysis of Two - Dimensional Truss and Frame Structures", *Technical Report AFFDL - TR - 68 38*, Wright - Patterson Air Force Base, Ohio.
- Renton, J. D., 1962, "Stability of Space Frames by Computer Analogy", *Journal of the Structural Division, ASCE*, Vol. 88, No. ST4, August, pp. 81 - 103.
- Saafan, S. A., 1963, "Nonlinear Behavior of Structural Plane Frames", *Journal of the Structural Division, ASCE*, Vol. 89, No. ST4, August, pp. 451 - 459.
- Simo, J., 1991, "Nonlinear Stability of the Time - Discrete Variational Problem of Evolution in Nonlinear Heat Conduction Plasticity and Viscoplasticity", *Comp. Methods in Applied Mechanics and Engineering*, 88.1, pp. 111 -131.

- Stricklin, J. A., W. E. Haisler, H. R. MacDougall and F. J. Stebbins, 1968, "Nonlinear Analysis of Shells of Revolution by the Matrix Displacement Method", *Proceedings 6th AIAA Aerospace Sciences Meeting (AIAA Paper 68 - 177)*, New York, January.
- Stricklin, J. A., J. C. DeAndrade, F. J. Stebbins and A. J. Cwiertny, 1969, "Linear and Nonlinear Analysis of Shells of Revolution with Asymmetric Stiffness Properties", *Proceedings, Second Conference on Matrix Methods of Structural Mechanics, AFFDL TR 69*, Wright - Patterson Air Force Base, Ohio, (held October, 1968) .
- Tezcan, S. S. and B. Ovunc, 1966, "An Iteration Method for the Nonlinear Buckling of Framed Structures", *Space Structures, Proceedings of the International Conference on Space Structures*, University of Surrey, Blackwell Scientific Publications, London.
- Tezcan, S. S., 1967, "Nonlinear Analysis of Thin Plates by the Framework Method", *AIAA Journal*, Vol. 5, No. 10, pp. 1890 - 1892.
- Tezcan, S. S. and B. C. Mahapatra, 1969, "Tangent Stiffness Matrix for Space Frame Members", *Journal of the Structural Division*, ASCE, Vol. 95, No. ST6, June, pp. 1257 - 1270.
- Thompson, J. M. T. and A. C. Walker, 1968, "The Nonlinear Perturbation Analysis of Discrete Structural Systems", *International Journal of Solids and Structures*, Vol. 4, No.8, September, pp. 757 - 767.
- Thompson, J. M. T. and A. C. Walker, 1969, "A General Theory for the Branching Analysis of Discrete Structural Systems", *International Journal of Solids and Structures*, Vol. 5, No. 4, April, pp. 281 - 288.
- Timoshenko, S. P. and J. M. Gere, 1961, "Theory of Elastic Stability", McGraw – Hill Book Company, Inc New York, Toronto, London 1961 p 300 – 305.
- Turner, M. J., 1959, "The Direct Stiffness Method of Structural Analysis", *Paper presented at the 10th meeting of the Structures and Materials Panel*, Aac'lien, Germany, September.

- Turner, M. J., E. H. Dill, H. C. Martin and R. J. Melosh, 1960, "Large Deflections of Structures Subjected to Heating and External Loads", *Journal of Aerospace Sciences*, Vol. 27, pp. 97 - 102, 127.
- Turner, M. J., H. C. Martin and B. C. Weikel, 1964, "Further Development and Applications of the Stiffness Method", *Matrix Methods in Structural Analysis – AGARDograph 72*, (Edited by Fraeijs de Veubeke) , Pergamon Press, Oxford, pp. 203 - 266 (Presented at AGARD Structures and Materials Panel, Paris, July 1964) .
- Valliappan, S., 1968, "Nonlinear Stress Analysis of Two Dimensional Problems with Special Reference to Rock and Soil Mechanics", *Ph.D. Dissertation*, University of Wales, Swansea.
- Walker, A. C. and D. G. Hall, 1968, *An Analysis of the Large Deflections of Beams Using the Rayleigh - Ritz Finite Element Method*, Aeronautical Quarterly, November, pp. 357 - 367.
- Walker, A. C., 1969, "A Nonlinear Finite Element Analysis of Shallow Circular Arches", *International Journal of Solids and Structures*, Vol. 5, No. 2, February, pp.97-107
- Wilson, E. L., 1960, "Matrix Analysis of Nonlinear Structures", *Proceedings, Second. ASCE Conference on Electronic Computation*, Pittsburg, Pa.
- Wissmann, J. W., 1966, "Nonlinear Structural Analysis, Tensor Formulation", *Proceedings, Conference on Matrix Methods in Structural Mechanics*, (Edited by J. S. Priemieniecki *et al*, AFFDL TR - 66 - 80, Wright - Patterson Air Force Base, Ohio.
- Yaghmai, S., 1968, "Incremental Analysis of Large Deformations in Mechanics of Solids with Applications to Axisymmetric Shells of Revolution", *Ph.D. Dissertation*, University of California, Berkeley.
- Yao, F. C., 1968, "Analysis of Shells by the Finite Element Displacement Method", *Ph.D. Thesis*, Massachusetts Institute of Technology, Cambridge, January.
- Zarghamee, M. S. and J. M. Shah, 1968, "Stability of Space Frames", *Journal of the Engineering Mechanics Division*, ASCE, Vol. 94, No. EM2, April, pp. 371 - 384.